DOI: 10.14750/ME.2019.010

Sucker Rod Pumping Analysis Based on Measured Electrical Parameters

PhD Thesis

Ádám Koncz
Ms in Petroleum Engineering

University of Miskolc, Petroleum Engineering Department

Mikoviny Sámuel Doctoral School of Earth Sciences
Head of the doctoral school: Prof. Dr. Mihály Dobróka, professor

Fluid production and transporting research section
Head of the section: Prof. Dr. László Tihanyi, professor emeritus

Integrated petroleum and natural gas production systems topic
Head of the topic: Prof. Dr. Gábor Takács, professor emeritus

Advisor: ***Prof. Dr. Gábor Takács, professor emeritus***

Miskolc, 2018

DOI: 10.14750/ME.2019.010

CONTENTS

DOI: 10.14750/ME.2019.010

ADVISOR'S FOREWORD

The great majority of sucker-rod pumped installations are driven by AC induction-type electric motors all over the world. Despite their long usage and the results of cumulated experience, the exact behavior of these machines at the very specific kind of loading conditions that exist in a rod pumped installation is still not fully known. The topic of this PhD Thesis investigates all those performance parameters of AC induction motors that determine their operating conditions under regular use.

The selection of the topic is appropriate today because mature fields containing rod pumped wells create serious problems for operators, especially in Hungary where the average life of the oilfields is well over 40 years. The interesting and important research of the author surely will help increase the life of sucker-rod pumping installations.

The author of this Thesis successfully utilized his electrical engineering knowledge (having previously obtained a BS degree in Electrical Engineering) to investigate the behavior of the AC electric motor driving a pumping unit. This type of interdisciplinary research is not very common in the international practice and the promising new results can change the overall thinking on the motor's role in the sucker rod pumping system.

The Thesis is properly constructed and clearly proves the candidate's skills in scientific research and publication. Several of the novel methods and calculation models developed by the author can be considered as new scientific achievements in the discipline of artificial lifting of oil wells.

The candidate has fulfilled the requirements for the PhD degree. He is the author or co-author of five conference articles (one in the Hungarian language and four in English) in the Thesis' topic. He held nine conference presentations in the topic on different conferences, among them the biggest Hungarian petroleum industry conference. He is author of one international journal article and one regional journal article.

Budapest, April 7, 2018.

Prof. Dr. Gábor Takács
Petroleum Engineering Department
University of Miskolc

DOI: 10.14750/ME.2019.010

ACKNOWLEDGMENTS

Doing research and publishing results is not an easy job and can never be learned independently. The success depends on the instructor, on the motivation, on the topic selection, on the research institute's facilities and on many other things which can be not summarized shortly. I hope that all parts were given in my case which makes me possible to finish my PhD studies.

First of all, would like to express my gratitude to Prof. Dr. Gábor Takács for providing me the opportunity to do PhD work. His valuable knowledge and experience made me able to conduct the research work. He showed me how to write articles and helped me to find out the direction in which to look. He corrected all my poor English texts unbelievably fast with really useful comments. I could never finish my PhD studies without his contribution.

I heartily thank to the Department of Electrical and Electronic Engineering especially Dr. Csaba Blága for lending me the necessary instruments and Sándor Molnár who worked many hours on the equipped measurement system.

I would like to thank the MOL Nyrt.'s upstream department (sorry for the name, but it is really hard to follow on the good department name) to allow me to test my hardware and theory on their wells. Special thanks to Gábor Takács and Bence Mallár who helped me with the field measurements.

I would like to thank Mr. László Kis for his friendship of many years and for his cooperation in publishing our results.

Special thanks are due to my family, too, because this long journey took place not only in the workplace.

The research was carried out in the framework of the GINOP-2.3.2-15-2016- 00010 "Development of enhanced engineering methods with the aim at utilization of subterranean energy resources" project of the Research Institute of Applied Earth Sciences of the University of Miskolc in the framework of the Széchenyi 2020 Plan, funded by the European Union, co-financed by the European Structural and Investment Funds.

DOI: 10.14750/ME.2019.010

1 INTRODUCTION AND THE TOPIC'S IMPORTANCE

Sucker rod pumping is the leading artificial lifting method in the world. More than 75% of the world's artificial lifted wells are operated using beam pump units (SPE, 2015.). The popularity of the system is not new because ever since artificial lift exists the sucker rod pumping system has been the most widely used method in the history (Beckwith, 2014.). Rod pumping is a mature and well-known production method and the long history of rod pumping provided enough time for petroleum (and other mechanical) engineers to invent and optimize the technology. However, there are always new ways to improve the existing system. This Thesis is about a new approach to improve rod pumping supervision techniques. The research conducted combines electrical and petroleum engineering aspects to develop new methods for rod pump analysis.

The understanding of the lifting system components is necessary for the scientific analysis. Chapter 2. describes the electric motors used in sucker rod pumping units. The construction and working theory is explained as well. The importance of the equivalent circuit based motor models is discussed in details and new parameter estimation methods are presented. A new high-slip motor speed-efficiency characteristics determination is presented. The efficiency determination is based on empirical correlations. The equivalent circuit parameter determination is and up-to-date research goal in electrical engineering. The problem is widely examined in the literature but there are some border areas as well where the existing methods do not produce reliable results. A new parameter estimation method was invented especially for high-slip motors.

The actual rod pumping technological and supervision overview can be found in Chapter 3. The pumping system's components are presented as well. The chapter focuses on the necessary information only since there are good books available about sucker rod pumps like Sucker-Rod Pumping Handbook written by (Takács, 2015.). The production supervising techniques are the dominant part of the chapter because the original objective of the research work was to invent new techniques in the field of producing well supervision. A new method is published in this section for sucker rod pumping units partial efficiency determination. The partial efficiencies play an important role in the system analysis and optimization hence the results are important. A reversed torque calculation method is presented as well which makes possible to infer the dynamometer diagram based on electrical measurements only.

New data acquisition system had to be invented to be able to conduct the planed research. The author made both the hardware and software development. The development procedure is presented in Chapter 4. The source code of the software parts can be found in the Appendices.

Chapter 5. presents the field measurements and data analysis on a real well. More wells were analyzed to prove and improve the proposed techniques.

The new scientific achievements are summarized in Chapter 6. so that section is the essence of the research conducted.

1.1 RESEARCH GOALS AND RESEARCH CONDUCTED

Previous authors (Gibbs & Miller, 1997.) suggested to perform research in the electrical motor – sucker rod pumping system. The research direction was clear from the beginning based on the author's previous experience: to investigate the sucker rod pumping system from the motor's view.

The Thesis' structure represents the research techniques as well. The work has started in 2012 with literature research. The aims and goals were determined in that period of the investigation. It was clear from the beginning that there is no measurement system available on the market that could fit the research budget and the needed functions. So, the measurement system hardware development was started in the early stages of the scientific work parallel to the basic theoretical research. The detailed literature research is mostly presented at the beginnings of the given chapters and the author's results can be found in the latter sections.

The electrical motors used in sucker rod pumping service were analyzed first and the available solutions for motor modeling were exposed. The special motors used in the petroleum industry and the lack of information about the motors resulted in the improvement of flexible motor equivalent circuit parameter determination solutions. The flexibility of the optimization procedures played an important role because the data on the motors available in existing oil fields is greatly limited. New parameter determination software was coded and tested by the author based on the CPSO-S optimization algorithm. The improved flexible system can be used to produce the motor's appropriate characteristics. Surprisingly, the research gave a new, simple motor efficiency correlation for NEMA D or high-slip motors. Such findings were not expected before, but the developed empirical correlation gives a good opportunity to extend the sucker rod pumping efficiency calculations into new dimensions.

The efficiency of the sucker rod pumping system is normally described using dynamometer cards. The input data is normally the measured polished rod load and any needed information should be determined using the pumping unit geometry and manufacturer data. The torque analysis is a crucial task of the analysis because it gives information about the counterbalancing efficiency in the system. The available solutions were tested to check if they remained a good selection as well when the torque calculation direction is inversed i.e. the different torque components are inferred from the motor torque. The torque calculation analysis describes the selected models and presents the modifications for the reversed calculation.

The self-developed measurement system with the software development was a definite section of the research. The data processing software had to be fitted to the given problem and finally a system was developed which was able to make the necessary measurements and calculation. The final result, the inferred dynamometer data were checked with real dynamometer measurement recorded in the same time. The results are collected in the last section of the Thesis.

The research techniques included all the conventional scientific solutions like:

- literature research to identify the opportunities, then

DOI: 10.14750/ME.2019.010

- theory development and measurement system development to be able to prove the assumptions, and finally
- the data validation using the conventional techniques.

The scientific achievements were continuously published throughout the research work. The results include:

- an own measurement system development (hardware selection, Voltage sensor development);
- a new data acquisition and processing algorithm coded by author and fitted for the given purposes;
- several field measurements which resulted over 1.5 Gb raw data;
- a new empirical correlation for high-slip motor's efficiency determination;
- several Matlab programs for existing motor parameter optimization algorithm development;
- new algorithms which are about 1500 lines long.

Finally, the determined goal, the inferring the dynamometer diagram based only on electrical measurement was realized. The research can follow up in more general programming to be able to use the methods developed as a daily routine in everyday engineering practice.

The author hopes that the presented methods, theory and validation will be accepted to fulfill the requirements of the PhD program.

2 INDUCTION MOTORS USED IN SUCKER ROD PUMPING

Most of the beam pumping units are equipped with electrical prime movers which usually means NEMA-D high-slip induction motors. The understanding of the basic construction of the asynchronous motors is necessary for the further research.

"The induction motor must rank alongside the screw thread as one of mankind's best inventions" because "something like one-third of all the electricity generated being converted back to mechanical energy in induction motors" (Hughes, 2006). The induction motors are the dominating energy converters in the industry. The most important advantages of asynchronous motors are the following (Puranen, 2006):

- simple, robust structure;
- excellent durability;
- good efficiency when operated at the motor's nominal load;
- good availability and standardized construction (dimensions, fixing points, power characteristic, etc.);
- low price.

But there are some disadvantages as well (Puranen, 2006):

- the speed control of induction machines is complicated, frequency converters are needed which are expensive;
- the power factor lags always because of the impedance of the motor;
- their efficiency is low when operating under small loads.

2.1 INDUCTION MOTOR'S GENERAL CONSTRUCTION

Electric motors have normally two main parts: stator and rotor. The rotor is the rotating part - built on the motor's main shaft - where the torque is created, and the stator is responsible for the energy flow into the rotor.

The stator develops the rotating magnetic field inside the stator's air gap in case of induction motors. The magnetic field generation is the task of the three-phase (for low power motors sometimes only one-phase) winding system (Uray & Dr. Szabó, 1998). The coils are placed in the core of the stator and they have an angle to each other which angle fits to the electric network's phase number – in case of three phase systems the angle is 120° for two-pole (one pole pair) motors. The number of poles determines the magnetic field's rotating speed (the synchronous speed) according to Equation 1. (Uray & Dr. Szabó, 1998):

$$n_0 = 60 \cdot \frac{f}{p}$$ *Equation 1.*

Where:

n_0 synchronous speed [1/min or commonly referred as rpm]

f	frequency of the electric network
p	number of pole pairs.

The number of poles depends on the motor's coil structure as it can be seen in Figure 1. The motor in the figure has 4-poles as it has 6 different windings. The current flows through the coils and each coil will generate its own magnetic field. Thanks to the sinusoidal power source the magnetic flux will change with the current flowing in the coils.

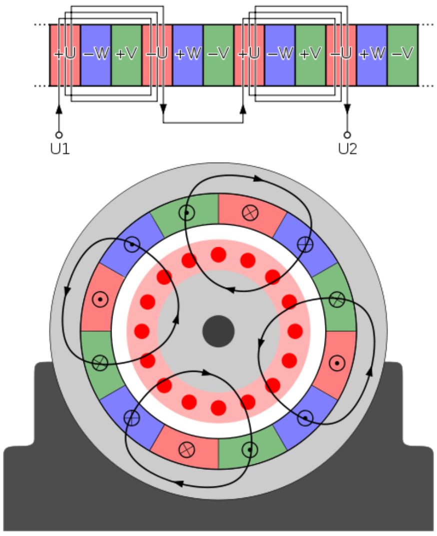

Figure 1. Magnetic circles in 4-pole induction motor (Wikipedia, 2017.)

The basic physical behavior of the magnetic field states that only one magnetic field can exist in the same time and same place. There exists only one resultant magnetic field generated by all coils' magnetic fields and that resultant magnetic field rotates with the synchronous speed. If we increase the number of coils the "current path" will be increased as well and the synchronous speed will be divided by the number of coil pairs. The universal industrial motors have normally 2-4-6 poles or sometimes more. The conventional trend is an increasing cost with increasing pole numbers because the construction of the core will be more complex resulting in more expensive production. The motors used in sucker rod pumping operation have normally 6 poles (Takács, 2015.) having a synchronous speed of 1,000 rpm in case of 50 Hz electric distribution system and 1,200 rpm for US electric systems (60 Hz). However other motor types can be found in the oil fields as well.

The rotating magnetic field induces voltage in the rotor and the potential difference will generate current in the squirrel cage. The interaction between the rotating magnetic field and the squirrel cage's magnetic field generates torque. If the rotor speed and the rotating magnetic field's speed are equal, then no interaction will happen between them and there will be no torque generated. That phenomenon happens at the synchronous speed. The stator current will reach its minimum level in that point because the electric power will be used only to maintain the magnetic flux. It is clear from the previous explanation that the rotor never rotates - without an extra energy source - at the synchronous speed. The rotor speed delays in relation to the synchronous speed and the delay – referred as slip - is an important parameter for describing the motor features. The slip's definition is the following (Uray & Dr. Szabó, 1998):

$$s = \frac{n_0 - n}{n_0} \qquad \textit{Equation 2.}$$

Where:

n	rotor speed [1/min or commonly referred as rpm]
s	motor slip
n_0	synchronous speed [1/min or commonly referred as rpm]

The normal nominal slip values for industry motors change between 1-5% (NEMA, 2017.) however the high-slip motors are better choice for sucker rod pumping (Durham & Lockerd, 1988.).

2.2 INDUCTION MOTOR'S STANDARDIZED CHARACTERISTICS

The induction motors used in the industry are nowadays standardized (NEMA, 2017.). The NEMA MG 10-2017 contains the most important standardized features of medium sized asynchronous motors. The standard focuses on energy efficiency however it contains important information on the torque characteristics of induction motors. The typical speed-torque characteristics of different NEMA design type motors can be seen in Figure 2.

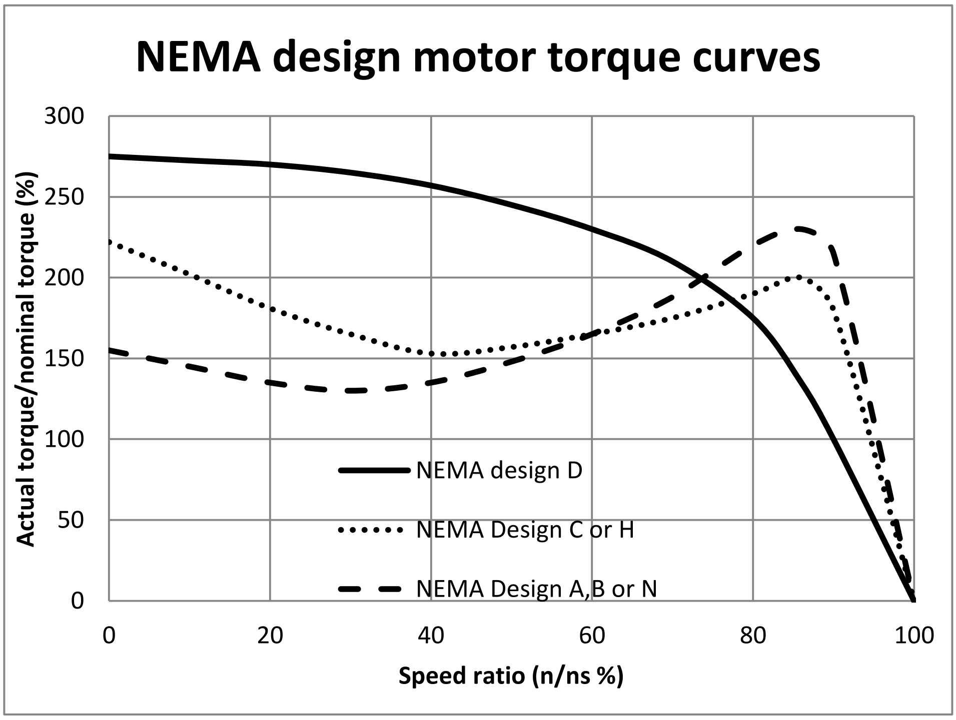

Figure 2. NEMA motor classification speed-torque characteristics (NEMA, 2017.)

The conventional industry-standard motors are normally NEMA B design motors. They have low starting- and pull-up torque and a higher (175-300% of the nominal torque) breakdown torque. Those data are vital for industrial applications because the drive design is unimaginable without information about the motor's torque capacity. Their maximum slip is 5% and they have 6-8 times greater starting current compared to the nominal current. The high starting current needs sometimes additional element into the electric network. The NEMA B motor's efficiency is medium or high (NEMA, 2017.). Their speed-torque, speed-current and speed-efficiency characteristics are steep close to the nominal operational speed hence a small change in the speed causes high changes in the efficiency and stator current.

NEMA D motors are widely used in conventional (no VFD/VSD motor drive or smart controllers) sucker rod pumping operations because of their better behavior under cyclic loading (Durham & Lockerd, 1988.).

2.3 Induction motor's efficiency

The efficiency of the induction motor plays an important role in the operation. The understanding of the losses is necessary because the motor modeling is normally based on accurate modeling of the losses. The losses occurring in induction motors are normally classified into the following groups (Uray & Dr. Szabó, 1998):

- wiring losses (Joule heating in the copper wires);
- core (iron) losses;
- magnetic losses;
- rotor losses (Joule heating in the rotor);
- mechanical losses (friction and drag).

The first three losses occur in the stator and they are stator-related losses. The Joule heating depends on the stator current and wire material, diameter. The iron losses are a result of the Eddy currents in the stator's core. The iron core is built from steel laminates to reduce Eddy current losses. The laminated composition eliminates any current flow between two iron disks and the total losses are reduced because of that special construction. The magnetic losses are the result of the magnetic flux dissipation in the air gap. They can be reduced by maintaining a smaller air gap. The power which is being transferred through the air gap is the air gap power.

The remaining two losses occur in the rotor and in the rotating parts of the system. The rotor heat losses are normally low because the rotor winding (the squirrel cage) is built from big-diameter conductors. The friction and drag is relatively higher for small motors but can be neglected for standard industry motors. The models – discussed in more detail in Chapter 2.4 – try to describe the motor behavior by modeling the losses occurring in the motor.

The mechanical power available at the motor shaft is the following considering all losses (Uray & Dr. Szabó, 1998):

$$P_{mech} = 3 \cdot U_f \cdot I_f \cdot \cos\varphi - P_{stator} - P_{rotor} - P_{friction} = P_{ag}(1-s) - P_{friction} \quad \textit{Equation 3.}$$

Where:

P_{mech}	mechanical power [W]
U_f	phase Voltage of the electric network [V]
I_f	phase current [A]
$\cos\varphi$	power factor
P_{stator}	stator losses [W]
P_{rotor}	rotor losses [W]
P_{ag}	air gap power [W]
$P_{friction}$	friction losses [W]

The electric power depends on the motor's connection configuration to the network: it can be either Wye or Delta connection. The electric network provides three times larger power to the motor in Delta configuration, the preferred way used in the industry.

Electrical motors used in sucker rod pumping services are 3-pole asynchronous motors. Their conventional nominal efficiency is above 90% based on the manufacturer's information. However, this efficiency value is valid only at nominal conditions. The motors in sucker rod pumping service operate under cyclic loads that significantly reduce their efficiency. A typical asynchronous motor's power- and efficiency performance is shown in Figure 3.

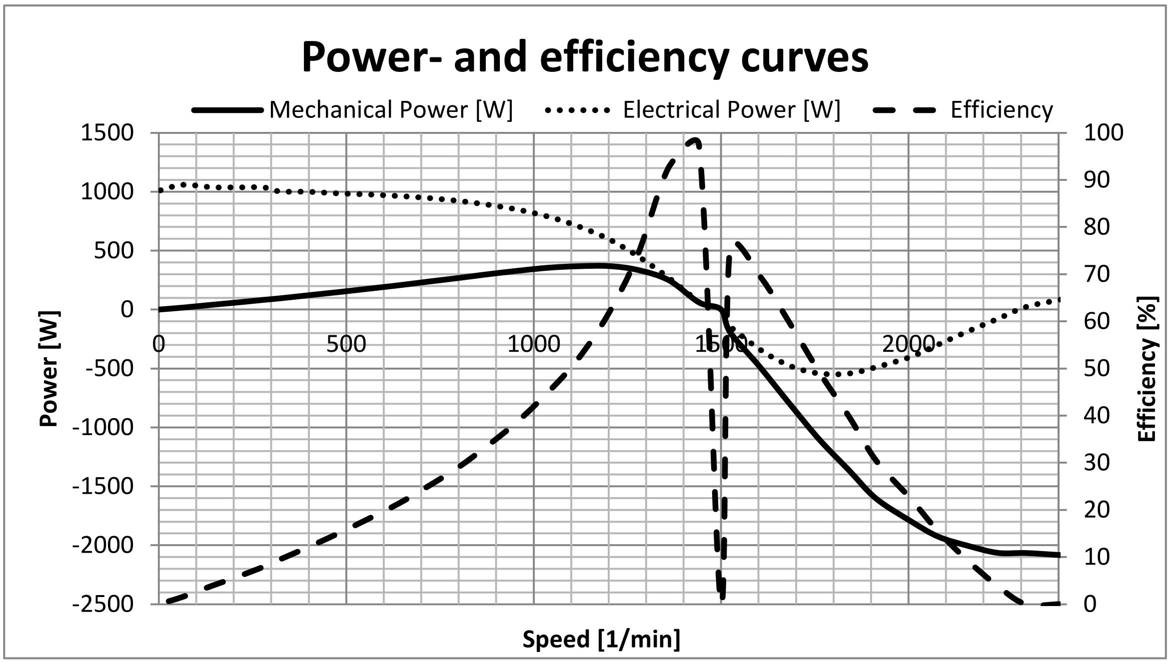

Figure 3. Asynchronous motor's efficiency characteristic (the author's measurement)

The performance curves shown in Figure 3. were measured on a small asynchronous motor but all induction motor's curves' shapes are similar. The curves are valid for a 2-pole squirrel cage motor so its synchronous speed at 50 Hz electrical system is 1500 1/min. The efficiency curve is steep that means small changes in the shaft velocity causes significant changes in the efficiency. The cyclic loading of the sucker rod pumping unit forces the motor's shaft to accelerate and decelerate. The motor can reach and exceed the synchronous speed as well; moreover, the motor is normally operated in generating brake mode for properly balanced units. The steep efficiency curve results in a drastic efficiency decrease in speeds between the nominal – and synchronous speeds. This is the reason why oversized motors perform badly on sucker rod pumping units. The importance of proper motor sizing was firstly recognized by (Kilgore & Tripp, 1991.) based on the system efficiency measurements.

The industry's answer to the cyclic loading was the use of high-slip asynchronous motors. High-slip motors don't have as steep efficiency- and power curves as the conventional industry standard NEMA B motors. Hence they react on the changing load with speed reduction rather than with higher current. The continuously changing load causes smaller reductions in the efficiency for NEMA D motors than in NEMA B motors and the overall load conditions in the pumping system are better when NEMA D motors are used. Moreover, the NEMA standard mentions oil-well pumping as one of the most important applications of the NEMA D motors. However, the asynchronous motor's mechanical power is proportional to the slip:

$$P_{motor} = (1 - s) \cdot P_a \qquad \textit{Equation 4.}$$

Where:

P_{motor}	motor's mechanical power available at its shaft [kW or Hp]
s	motor slip
P_a	air-gap power [kW or Hp]

The conventional NEMA B motors have higher efficiency at their nominal parameters than high-slip NEMA D motors used in sucker rod pumping. However, the reaction on the cyclic loading makes NEMA D motors more energy-efficient for sucker rod pumping (Podio, et al., 1994.).

2.3.1 New empirical correlation for high-slip motor's efficiency determination

The induction motor's speed-efficiency relationship is important when one wants to determine the average efficiency of a motor working on cyclic loading. This chapter deals with an easy solution to estimate the high-slip motors' efficiency curves. The proposed solution for the speed-efficiency characteristic generation is based on an empirical analysis. There are several available solutions in the literature to determine the induction motor's efficiency however they have normally high computation demand and need information that are normally not available at field conditions (Haque, 1993). The advantage of the following method is its simplicity and the fast calculation procedure which makes the method perfect for sucker rod pumping system efficiency analysis performed in the field.

The NEMA standard clarifies as a general rule-of-thumb that the higher power induction motors have normally higher efficiency than the smaller ones (NEMA, 2017.). It seems to be straightforward to find a correlation between the efficiency and the motor power. Such a correlation could help generate the full speed-efficiency characteristics based only on the motor's nameplate power and efficiency. The direct comparison of motors having different nominal speed can be misleading. The induction motor's speed-efficiency curve is steep in the nominal range (or between the nominal and synchronous speed) and a small change in the speed could cause big differences in the efficiency and power as well. So as the nominal slip differs for the different size NEMA D motors the motor's power should be analyzed at a reference speed for all motors. Hence the research methodology was to find a reference speed and reference power for each asynchronous motor at which the correlation can be developed. The speed-power curve of an induction motor is steep and almost linear between the nominal speed and synchronous speed, so it can be approximated using a linear function. If the reference speed is forced to be in that speed range the needed power value can be calculated using simple rational calculation. Experience has shown that in case of 3-pole pair motors and 60 Hz network frequency the reference speed can be set for n=1,150 1/min (so a slip of 0.0417).

The speed-efficiency curves of 28 high-slip motors were analyzed using the reference speed theory in this work. An oil industry motor manufacturer (Sargent Electric Co.) provided motor data for research purposes. The full speed-efficiency, speed-power, speed-current characteristics were measured in the lab of the manufacturer. Those 28 motors cover the manufacturer's product line in high-slip motors. The correlation was developed based on the motors' maximal efficiency. The final empirical correlation for the high-slip induction motor's maximal efficiency, developed by the present author, is the following:

$$\eta_{max} = 2.6141 \cdot ln(P_{ref}) + 60.567 \qquad \textit{Equation 5.}$$

Where:

η_{max}	motor's maximal efficiency
P_{ref}	motor power at the reference speed [W]

The reliability of the correlation for the given 28 motors is summarized in Table 1. The calculated parameters in the table refer to efficiency percentage. The results show that the correlated maximal efficiency values are good approximations of the real data.

Table 1. Statistical data of the developed correlation for NEMA D motors maximal efficiency in case of the investigated 28 motors

Average absolute error [efficiency %]	1.86
Standard deviation [efficiency %]	2.26
Median [efficiency %]	-0.01

The maximal efficiency value is very important but not enough to produce the full speed characteristics. The efficiency curve could be produced using a linear function between the synchronous speed and the maximal efficiency speed – the easy linear function works well for the run-up region i.e. from motor starting till the maximal efficiency point - but the real motor curves do not follow that simple curvature in the operational region of oversized motors. The simple linear function would underestimate the efficiency close to the maximal efficiency speed. The decision was made to improve the correlation using empirical solutions between a given efficiency-decrement and the rotational speed.

The maximal efficiency point-synchronous speed-efficiency region was divided into two subsections. The data analysis has shown that the speed-efficiency characteristics can be reconstructed using a given efficiency reduction. 16% reduction in efficiency was found at a speed of 1164 rpm for the investigated motors and a 50% reduction at a speed of 1187. The statistical data of the correlations can be found in Table 2.

Table 2. Statistical data of the developed correlation for NEMA D motors efficiency reduction

Parameter	16% efficiency reduction point	50% efficiency reduction point
Average absolute error [in RPM]	8.18	3.75
Standard deviation [in RPM]	11.4	4.67
Median [RPM]	1164.37	1187.83

The steps of the full speed characteristic development are shown in Figure 4.

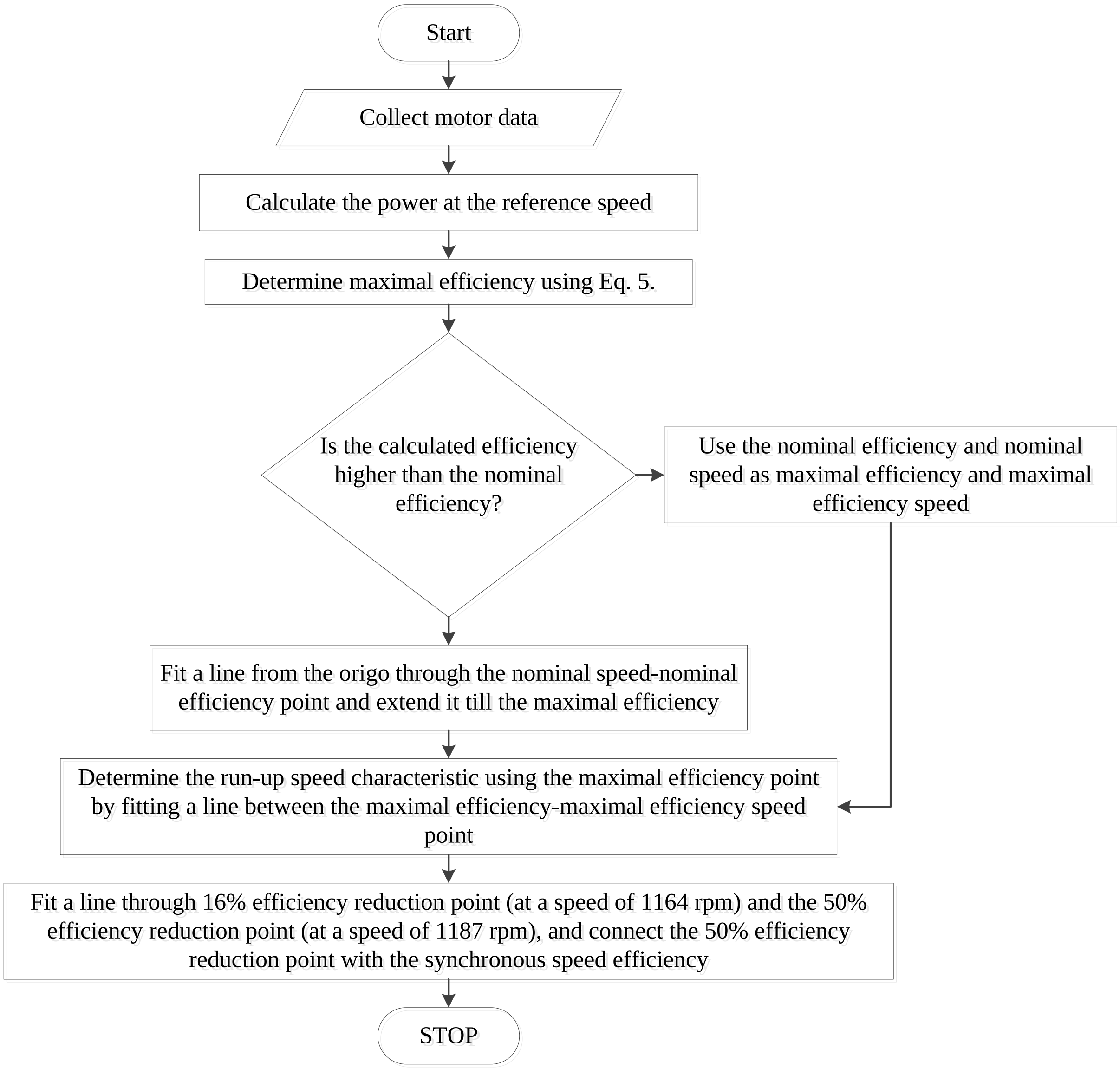

Figure 4. Full-speed efficiency characteristic determination process

Figure 5. shows the calculation results for a 15 kW high-slip motor. The good correlation between the measured and calculated values shows the effectiveness of the process. The method is compared in the figure with the conventional, easy approximation where the nominal efficiency is connected with the starting- and synchronous point.

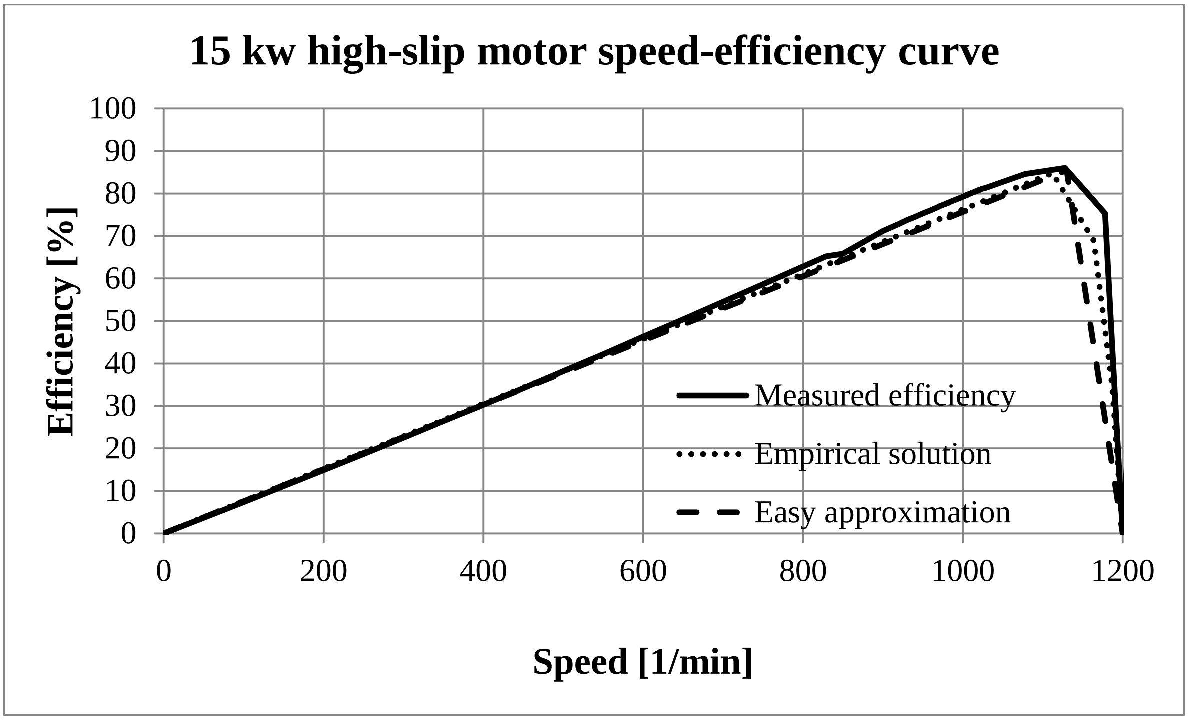

Figure 5. 15 kW high-slip induction motor speed-efficiency characteristic

2.4 MODELING THE OPERATION OF ASYNCHRONOUS MOTORS

Many researchers reported on special calculation processes in the sucker rod pumping system if the performance curves of the prime mover are known. One of these sources states that the actual load conditions can be inferred from electrical measurements (Wilamowsky & Kaynak, 2000.) and the use of dynamometer cards can be avoided. Some authors (Podio, et al., 1994.) recommend electrical measurements to improve the pumping efficiency. Others (Gibbs & Miller, 1997.) suggest measuring the motor speed and calculating power consumption and electrical performance based on those measurements. The main conclusions of these papers are: electrical or speed measurement has many advantages; the most important is the cost efficiency, but the motor performance curves are difficult to obtain. Manufacturers seldom publish reliable curves and the measurement of performance curves for every installed motor is difficult and expensive. The key issue of any new measurement method is the appropriate motor model.

Modeling the behavior of an asynchronous motor is a crucial and up-to-date task not only in the petroleum industry but in other industries as well. Many researchers were working on the overall best calculation method however the high number of available solutions show that the problem is still not completely solved (Pedra, 2008.) (Lindenmeyer, et al., 2001.). There are available solutions in the widely used engineering software MatLab as well. The MatLab adopted as an add-in the solution of (Pedra & Córcoles, 2004.) to estimate the induction motor’s parameters.

The electric machines are normally modeled using their equivalent circuits. An equivalent circuit is a simplified connection of basic electrical components (resistors, capacitors, inductances) which gives almost the same answer to Voltage and/or frequency changes as the original machine (Graf, 1999.). It is not always an easy task to find the best available equivalent circuit. The equivalent circuits normally neglect some parameters and have always their constraints in usage. The equivalent circuits normally neglect the following (Kral, et al., 2009.):

- they were developed basically for three-phase systems;
- the power source and the motor are totally symmetrical;
- only sinusoidal waveform is assumed and no harmonics;
- any kind of non-linearity is neglected;
- the friction losses are normally not included.

If one wants to describe the operation of a given machine the only task is to determine the unknown parameters in the equivalent circuit and using basic electric calculations the needed data can be obtained.

(Lindenmeyer, et al., 2001.) gave a good overview about equivalent circuit parameter estimation methods. Their classification differentiates five different groups of the parameter estimation methods:

- Parameter estimation from motor construction data: the most accurate and most costly solution. Data are normally not available for such analysis especially not for old or existing motor installations.
- Parameter estimation based on steady-state motor models: these solutions apply a kind of numerical optimization to find the equivalent circuit's parameters. Their most important advantage is that there is no need for expensive measurements but the accuracy is limited. The overall calculation accuracy depends on the accuracy of the manufacturer data. The common features of such methods are that the authors try to use only the commonly available catalog- and nameplate data of the motors.
- Frequency-domain parameter estimation: an accurate solution but it needs stand-still conditions i.e. the motor should be stopped and special equipment is needed. Motor operators seldom apply this solution.
- Time-domain parameter estimation: time-domain measurements are needed and the motor model should be simplified. This solution is not widely used.
- Real-time parameter estimation: the solution is normally applied in modern, smart motor controllers. The method is becoming far more widespread wherever complete and smart motor control equipment is needed. This parameter estimation type generates the motor model in real time and it is accurate. Such types of motor controllers are used only in high quality electric drives.

The parameter estimation based on steady state model fits our purposes best because the limited data and measurement opportunities leave only that opportunity to model the motor's behavior. The information sources at field site are limited so the easiest solution should be preferred. The steady-state model assumes constant values for the parameters or only the slip can influence the actual values of the parameters. The steady-state model can be used for transitional analysis according to (Lindenmeyer, et al., 2001.). Other authors also confirmed that the constant value equivalent circuit can be used for NEMA D motors as well (Stefopoulos & Mliopoulos, 2007.).

The literature deals with many available solutions to determine the equivalent circuit's parameters however the parameter estimation processes developed for conventional asynchronous motors have several common features. The problem formulation is always the same: provide the physical values of the elements in the equivalent circuit; although the equivalent circuits used are not always the same. Most of the processes try to apply only manufacturer published data set for calculation but (Lindenmeyer, et al., 2001.) deals the opportunity to use any number of measured data as initial values. All authors use numerical optimization solutions (for example fsolve (Pedra & Córcoles, 2004.)), Solnp from Mathworks Matlab program (Lindenmeyer, et al., 2001.), PSO - particle swarm optimization (Sakhtivel, et al., 2010.), etc.). They formulate some kind of objective function(s) for the different optimization routines and then minimize those functions. The initial data are chosen to create the necessary number of equations for the given number of unknowns in the equivalent circuit. Not all parameters in the equivalent circuit are handled as independent parameters; (Pedra & Córcoles, 2004.) have proved that the stator resistance has less influence on the model's accuracy – it is obvious to use the stator resistance as a simple function of the rotor resistance. Many references (Lindenmeyer, et al., 2001.), (Pedra & Córcoles, 2004.) suggest that the rotor inductance and the stator inductance are proportional to each other. The number of unknowns can be reduced by using those assumptions and the necessary input data can be reduced as well.

2.4.1 Modeling the motor using its equivalent circuit

Many different equivalent circuits can be developed for the parameter estimation method. The equivalent circuits can model one cage or double cage rotors as well. Double cage rotors are used to create higher starting torque and to achieve better torque characteristics. The magnetic saturation can be included as well (Lindenmeyer, et al., 2001.). The one cage motor model can be seen in Figure 6. R_s is the stator's Ohmic resistance and X_s the stator's magnetizing inductance. The values with the subscript "r" are for the rotor resistance and for the rotor inductance. X_m represents the core inductances.

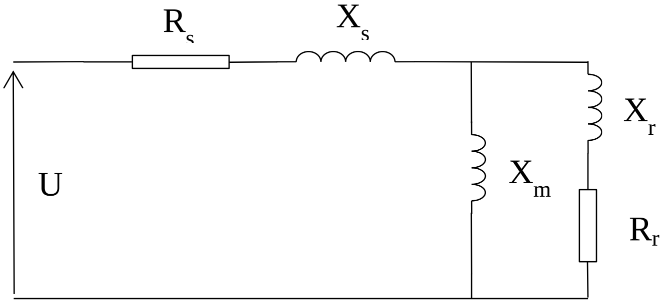

Figure 6. Single-cage motor model

Previous research (Pedra & Córcoles, 2004.) has shown that the single cage motor model cannot simulate the starting conditions of the induction motors. The double cage motor model has the advantage that it can provide reliable starting and operating parameters. The steady-state equivalent circuit suggested by (Pedra & Córcoles, 2004.) is shown in Figure 7. The stator-related parameters are the same as for the single cage case the difference can be found only in the rotor branch. The subscript “1” represents the inner cage and subscript “2” the outer cage. The useful mechanical work is included in the cage resistances which values depend on the actual slip. The core losses, mechanical losses, friction losses are neglected so any approximation of the parameters will have some inaccuracy but still they can be used for studying the operational conditions of the pumping system (Lindenmeyer, et al., 2001.).

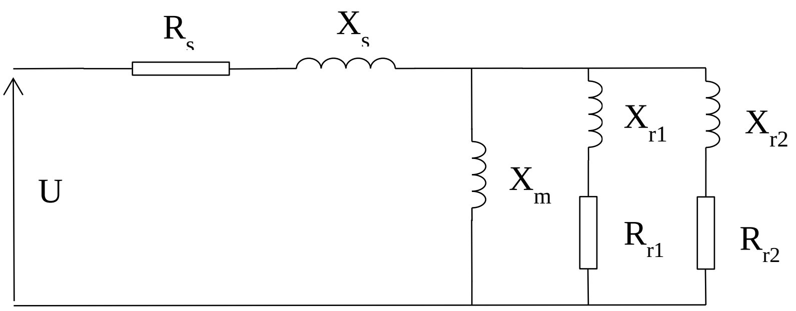

Figure 7. Double-cage equivalent circuit of induction motors (Pedra, 2008.)

The initial data used in previous studies include the manufacturer-supplied data and/or other, measured data. In case of the motor model shown in Figure 7. the number of unknown parameters is seven but according to the previous simplifications there are only five independent parameters (Pedra & Córcoles, 2004.). In order to achieve a well-defined equation system, one should ensure at least five independent inputs in the seven-parameter equivalent circuit after reducing the number of the independent variables. The common input data in the literature are the following:

- full load power,
- nominal voltage,
- nominal efficiency,
- nominal power factor,
- starting current,
- starting torque,
- breakdown torque,
- nominal speed,
- rated frequency,
- according to (Pedra & Córcoles, 2004.), the reactive electrical power.

The breakdown torque plays an important role in the parameter estimation processes because it assigns the maximal point of the speed-torque characteristics and the curve changes its slope at that point. The breakdown slip can be easily calculated for single cage model and it is a strong boundary for those motor models. The breakdown slip can be calculated for the double-cage model as well, however the calculation is not so easy in this case but it can be used as a boundary condition for the numerical optimization method. But the breakdown torque's use for high slip (or NEMA D) motors is impossible because NEMA D motors produce normally their maximal torque at the start so the breakdown torque cannot be used as a limiting factor for the optimization procedure. So, if one wants to determine the NEMA D motor's parameters the available solutions will not work because of the lack of the breakdown torque. Other limiting factors should be found.

The parameter estimation methods based on manufacturer data suffer from other problems as well. The manufacturer data are not always accurate measurement results. They are sometimes rounded, and the measurement conditions are important as well (Kral, et al., 2009.). Any model built from those data will suffer from errors, but they can be tolerated for the most common use of the motor models.

2.4.2 Parameter estimation for NEMA D or high-slip motors

The previous sections showed that breakdown torque is important for the conventional parameter estimation processes however if one wants to develop a robust and stable motor model for high slip motors the breakdown torque should be replaced with other data. The alternative solutions are limited because there is no opportunity to stop the production and measure the necessary motor data. A method should be found where the needed data can be obtained directly from the manufacturer or can be measured at field conditions as well.

The available dataset is limited. Previous works include all reliable, easily accessible data for the motor parameter estimation. Motors working in sucker rod pumping service may be driven by the load above the synchronous speed on well-balanced beam pump units. The magnetizing current can be measured very simply, and the use of exact measured data can improve the effectiveness of the optimization procedure. The magnetizing current can help to improve the robustness of any algorithm because it is assumed in that case that no current is flowing through the rotor cages. The uncertainty which comes from the breakdown slip calculation can be avoided using the magnetizing current. The magnetizing current is a measured data, so its accuracy depends on the measurement system. The input data used for the equipped optimization algorithm are the following:

- nominal voltage, frequency;
- full load power, nominal power factor and the reactive electrical power;
- magnetizing current;
- starting current and torque.

The calculation process presented in this section is based on (Pedra & Córcoles, 2004.) solution but some modifications were applied to fit the method for NEMA D motors. The equivalent circuit presented in Figure 7. is applied. MatLab fsolve is the core optimization algorithm. Since numerical methods are very sensitive for the starting values the algorithm's efficiency can be improved using initial values as accurate as possible. The single cage motor model can be used to improve the initial data accuracy for the double cage model (Pedra & Córcoles, 2004.). The single cage motor model shown in Figure 6. will be used to produce the initial data for the double cage model.

The double cage initial data set is based on the single cage calculation results. (Pedra & Córcoles, 2004.) recommend to use the k_r (constant multiplication factor between the stator- and rotor resistances) and k_x (constant multiplication factor between the stator- and rotor reactance) values as concrete numbers. The practical calculations have shown that the appropriate selection of k_r and k_x values is very important for the creation of the high slip motor model. The other modifications in the input data selection were previously presented. The objective function formulation for single cage calculation is the following:

$$F(R_r, X_m, X_s, s) = \begin{Bmatrix} P_{nameplate} - P_{calculated_{sfl}} \\ Q_{nameplate} - Q_{calculated_{sfl}} \\ I_{magnetezing} - I_{calculated_{magnetizing}} \end{Bmatrix} = 0 \qquad \textit{Equation 5.}$$

Where:

R_r	rotor resistance [Ω]
X_m	magnetizing reactance [Ω]
X_s	stator reactance [Ω]
$P_{nameplate}$	nameplate power [kW or Hp]
$P_{calculated_{sfl}}$	calculated power at the nominal slip [kW or Hp]
$Q_{nameplate}$	nameplate reactive power [kVAr]
$Q_{calculated_{sfl}}$	calculated reactive power at the nominal slip [kVAr]
$I_{magnetizing}$	magnetizing current at the synchronous speed [A]
$I_{calculated_{magnetizing}}$	calculated magnetizing current [A]

The objective function formulation for double cage calculation is the following:

$$F(R_{r1}, R_{r2}, X_m, X_s, X_{r1}, s) = \begin{Bmatrix} \dfrac{P_{nameplate} - P_{calculated_{sfl}}}{P_{nameplate}} \\ \dfrac{Q_{nameplate} - Q_{calculated_{sfl}}}{Q_{nameplate}} \\ \dfrac{I_{magnetizing} - I_{calculated_{magnetizing}}}{I_{magnetizing}} \\ \dfrac{I_{start} - I_{calculated_{start}}}{I_{magnetizing}} \\ \dfrac{M_{start} - M_{calculated_{start}}}{M_{start}} \end{Bmatrix} = 0 \qquad \textit{Equation 6.}$$

Where:

R_{r1}	inner cage rotor resistance [Ω]
R_{r2}	outer cage rotor resistance [Ω]
X_{r1}	inner cage rotor reactance [Ω]
I_{start}	starting current at nominal Voltage [A]

$I_{calculated_{start}}$ calculated starting current [A]
M_{start} starting torque [Nm or in-lbs]
$M_{calculated_{start}}$ calculated starting torque [Nm or in-lbs]

Matlab fsolve algorithm is proposed to solve the system of nonlinear equations. Calculation errors can reach very high levels if not using the best combination of k_x and k_r values. Table 3. shows the combination of k_x and k_r values and the error of the objective function with the estimated parameters (calculated for a 25 kW high slip motor).

Table 3. Residual errors using different k_r-k_x combination

k_r	0,2	0,2	0,2	0,2	0,8	0,8	0,8	0,8	0,8	1,4	1,4	1,4	1,4	1,4
k_x	0,2	0,6	1	1,4	0,2	0,6	1	1,4	1,8	0,2	0,6	1	1,4	1,8
objective function result	1,02	1,20	1,05	1,13	1,17	1,41	1,31	1,33	1,31	2,14	1,73	1,45	1,37	1,36

The reason behind this phenomenon is found after analyzing the construction of high slip motors. To achieve a high starting (locked-rotor) torque and not too steep speed-torque characteristics close to the synchronous speed (the normal operational area), a special conductor bar construction is needed. The special construction gives k_r and k_x ratios different from normal industrial motors. The flowchart of the calculation process is shown in Figure 8.

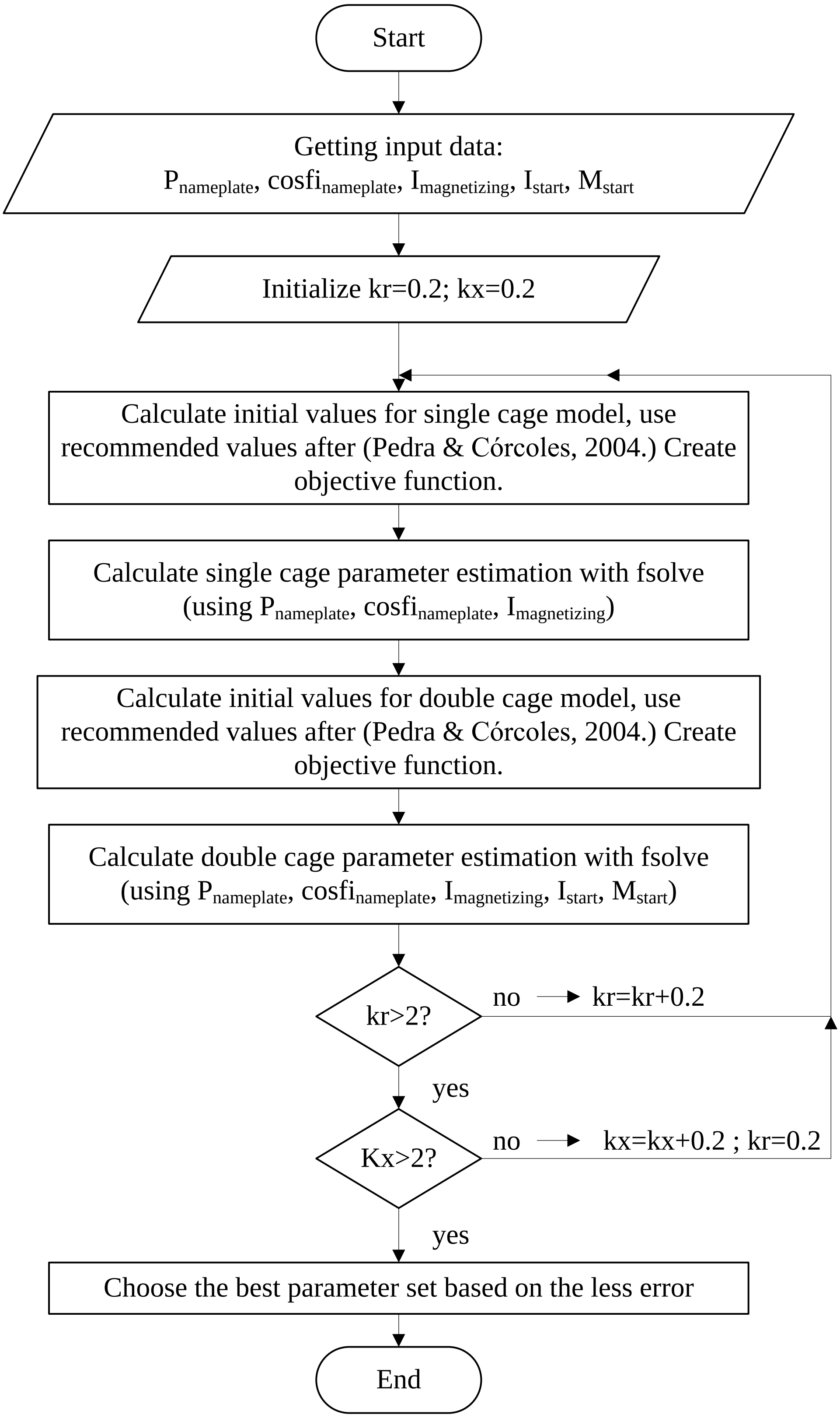

Figure 8. Flowchart of the improved method

The calculation method just presented was tested with 9 high slip motors of different characteristics. The average torque residual error was 0.20. One speed-torque performance curve for a given motor is shown in Figure 9. The error of the calculation is acceptable in the operational range (speeds above 800 [1/min]).

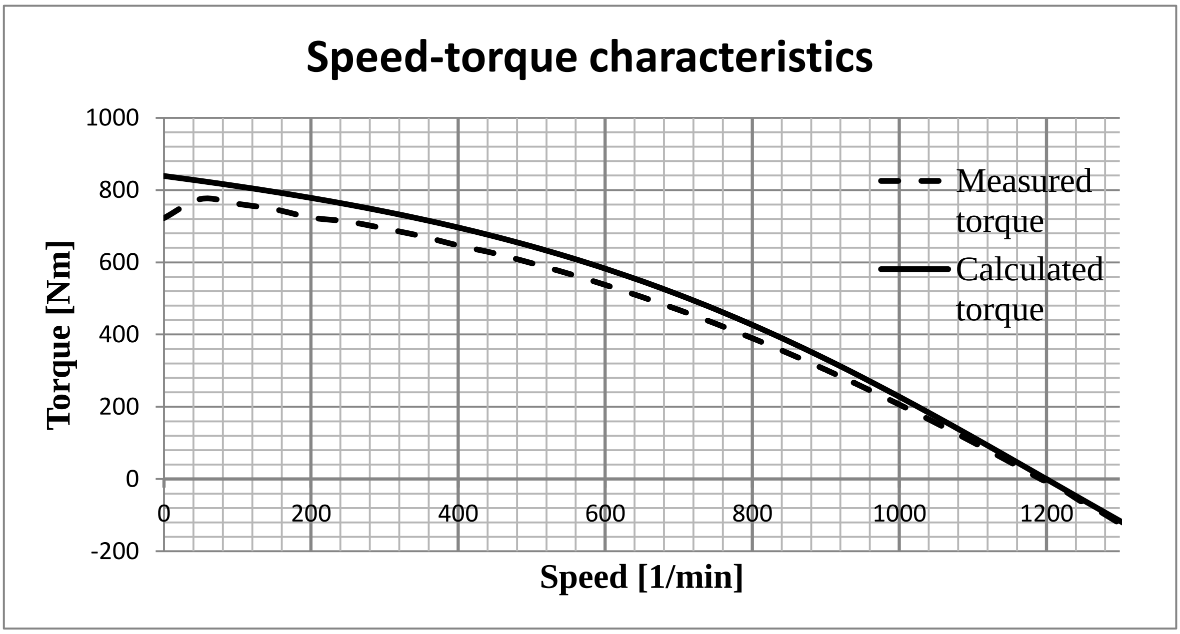

Figure 9. Speed-torque characteristics of a 12 kW high slip motor

The results prove the effectiveness of the improved method. The parameters just estimated, and the calculated speed-torque characteristics are ready to further use in the sucker rod pumped well inspection. The source code developed by the author can be found in MatLab form in the Appendices.

There are weaknesses of the proposed method as well. The speed-torque characteristics can be prepared highly accurately but the speed-current characteristics are not as accurate. The production of the speed-current characteristics is always a more complicated task (Pedra & Córcoles, 2004.) because the assumptions used to develop the equivalent circuit, the computational difficulties by the numerical optimization and the possibility that the solution found is only a local minimum in the multi-dimensional space increase the calculation errors. The speed-efficiency characteristics is a bit more complicated to achieve than the speed-current curve because in the speed-efficiency characteristic all losses (including friction losses etc.) should be included which were generally neglected by the equivalent circuit development.

DOI: 10.14750/ME.2019.010

2.4.3 PARAMETER ESTIMATION FOR HIGH SLIP MOTORS USING CPSO-S ALGORITHM

The method described in the previous section is a reliable and robust solution to find the motor's speed-torque performance curves. However, those characteristics are not sufficient to perform a full system analysis. We need to find additional performance curves like the speed-current and speed-efficiency as well. The research done with the MatLab fsolve algorithm showed that more freedom is needed to build a more uniform and useful algorithm. The numerical optimization's core code is hard to modify in the fsolve algorithm and the opportunity to fit the code for our purposes was limited. Moreover, Matlab is not generally used software in oilfield applications.

Other optimization methods were tested, and the choice was the Particle Swarm Optimization (PSO) firstly invented by (Eberhardt & Kennedy, 1995.). The most dominant selection criterion was its relatively easy coding, the high number of available modifications and the extensive literature backgorund. The optimization procedure is relatively new and gives excellent freedom to the programmer while the research background is extensive, and many useful papers and other works are available on the topic. The PSO's convergence is proven (van den Bergh, 2001.) and it is suitable for multidimensional optimization problems. Other authors used the PSO algorithm to determine the motor's equivalent circuit parameters as well (Bayoumi, 2010.) (Sakhtivel, et al., 2010.) etc. however they used their results for other purposes.

(van den Bergh, 2001.) gives a comprehensive review about the PSO algorithms and ongoing researches. The PSO is normally characterized using the inventors' description in the original paper: it is modeled as bird flocking or fish schooling (Eberhardt & Kennedy, 1995.). The PSO method uses a "population of particles, where each particle represents a potential solution to an optimization problem" (van den Bergh, 2001.). The population is randomly generated, and the swarm's new position update depends on the actual fitness to the searched value. There are four important definitions which are the particle's feature:

- current position of the particle: a vector, whose size depends on the optimization's dimension;
- current velocity: a vector containing the modification of the actual position's value, its dimension is the same as the current position's size;
- personal best position: the particle's best position, where already found solution was the best.
- the last important definition is the global best position. The global best position is the best position from the personal best positions of all particles.

The population size depends on the given problem and the dimension of the problem. The population size is normally about 20 (Clerc & Kennedy, 2002.) but can be smaller and higher as well. Higher population number can be better for multidimensional problems (Bayoumi, 2010.) as the induction motor parameter estimation. The algorithm's robustness and vitality are maintained due to the randomized part of the new velocities.

The optimization is started with the generation of the population. Then the actual position's evaluation is the next step. The velocities are generated using the best positions while a randomized part is responsible to ensure the good convergence. The velocity is updated using the following equation (van den Bergh, 2001.):

$$v_{i,j}(t+1) = v_{i,j}(t) + c_1 r_{1,j}(t)\left[y_{i.j}(t) - x_{i,j}(t)\right] + c_2 r_{2,j}(t)[\hat{y}_j(t) - x_{i,j}(t)] \qquad \textit{Equation 7.}$$

Where:

$v_{i,j}(t+1)$	particle's new velocity
$v_{i,j}(t)$	particle's previous velocity
c_1, c_2	acceleration constants
r_1, r_2	uniform pseudo-random numbers to achieve the algorithm's freshness
y_i	particle's best position
$x_{i,j}(t)$	particle's previous position
$\hat{y}_i$	swarm's overall best position

The randomized part is used to prevent the sticking of the optimization algorithm at a local minimum. The particle's new position can be calculated using the following equation (van den Bergh, 2001.):

$$x_i(t+1) = x_i(t) + v_i(t+1) \qquad \textit{Equation 8.}$$

Where:

$x_i(t+1)$	particle's new position

The number of iteration depends on the dimension of the given problem and the convergence speed. The iteration number has a great influence on the final solution however after reaching a limit number the accuracy cannot be improved according to the present author's experiences and as usual for optimization algorithms. The original PSO's pseudo code can be seen in Figure 10., after (van den Bergh, 2001.).

```
Create and initialize an n-dimensional PSO (initialize the numberparticles pcs. swarms): S
Repeat:
    For each particle i=1..numberparticles
        If f(S.x_i)<f(S.y_i)
            Then S.y_i=S.x_i
        if f(S.y_i)<f(S.y_best)
            Then S.y_best=S.y_i
    End for
    Update the particle's position using Eq. 7. and 8.
Stop when reached the desired iteration number
```

Figure 10. Original PSO pseudo code after (van den Bergh, 2001.)

The original PSO works well on basic functions (van den Bergh, 2001.) however it was not able to solve the multidimensional optimization problem of the asynchronous machine's equivalent circuit.

There are available modifications of the original algorithm which are pretty good explained in the work of (van den Bergh, 2001.). The choice was a slightly modified CPSO-S (cooperative PSO-split) because it is a novel PSO modification for complex multidimensional problems (van den Bergh, 2001.). The difference from the original PSO is that a context vector is used to store the overall best positions of each dimension. The CPSO-S algorithm's pseudo code is shown in Figure 11. after (van den Bergh, 2001.).

```
Define a context vector b(j,z)
Create and initialize n one-dimensional PSO (initialize the numberparticles pcs. swarms): S
Repeat:
    For each swarm i=1..n
        For each particle j=1..numberparticles
            If f(b(j,P_j,x_i)< f(b(j,P_j,y_i)
                Then P_j.y_i=P_j.x_i
            if f(b(j,P_j,y_i)< f(b(j,P_j,y_best)
                Then P_j,y_best = P_j,y_i
        End for
        Update the particle's position using Eq. 8. and 9.
    End for
Stop when reached the desired iteration number
```

Figure 11. CPSO-S pseudo code after (van den Bergh, 2001.)

Some small differences can be found in the velocity calculation as well. The CPSO-S uses an inertia-weighted update equation:

$$v_{i,j}(t+1) = wv_{i,j}(t) + c_1 r_{1,j}(t)\big[y_{i.j}(t) - x_{i,j}(t)\big] + c_2 r_{2,j}(t)[\hat{y}_j(t) - x_{i,j}(t)] \qquad \textit{Equation 9.}$$

Where:

w inertia weight

The just coded CPSO-S program was tested on the conventional optimization test functions, like the Mátyás-function, Rosenbrock-function etc. and the convergence was found optimal with the factors suggested by (van den Bergh, 2001.). The factors used for the coding were the following:

- w inertia weight: 0.72
- c1, c2 acceleration constants: 1.49
- the minimal and maximal velocity is reduced to ±0.57
- particle number: 50

The software developed by the author for the optimization algorithm gives enormously high freedom for the optimization problem solution. Several data sets could be tested, and the core section could be adjusted to the induction motor's parameter estimation. There is no need for single cage optimization rerun because the developed algorithm is robust and finds the parameters without any help. There are other authors

(Sakhtivel, et al., 2010.) in the literature who used the PSO for parameter estimation however only for on-line parameter estimation however their solution does not fit to our problems.

Problems occurring in the sucker rod pumping system analysis need different parameter estimation procedure: the data available are always limited but restricted field measurements can be carried out. There is no need for an overall-best and physically fully possible equivalent circuit parameter set. The important characteristics are only the torque-speed and current-speed (or mainly current-torque) when one wants to infer the dynamometer diagram for current measurements, as described later in Chapter 5. The efficiency-speed characteristics would be an interesting one however it is not easy to produce it (Pedra, 2008.). The aim of this parameter estimation procedure is to produce the input data for the method described in Chapter 5.

The optimization problems have only one overall best solution if the problem is well-defined. If the problem is not well-defined so we use fewer constraints than the number of unknowns, the optimization algorithm can find more solutions. The (error) function to be minimized is the following:

$$F(R_{r1}, R_{r2}, X_m, X_s, X_{r1}, s) = \left\{ \begin{matrix} \left(\dfrac{P_{nameplate} - P_{calculated_{sfl}}}{P_{nameplate}}\right)^2 \\ \left(\dfrac{I_{magnetizing} - I_{calculated_{magnetizing}}}{I_{magnetizing}}\right)^2 \\ \left(\dfrac{I_{start} - I_{calculated_{start}}}{I_{magnetizing}}\right)^2 \\ \left(\dfrac{I_{nameplate} - I_{calculated_{nameplate}}}{I_{nameplate}}\right)^2 \end{matrix} \right\} = 0 \qquad \textit{Equation 10.}$$

Where:

$I_{nameplate}$	nameplate current at nominal Voltage [A]
$I_{calculated_{nameplate}}$	calculated nameplate current [A]

The convergence speed is normally increased in the under defined cases because there can be more mathematically correct solutions. The method presented in this chapter will be used at field conditions using limited computational capacity computers such as laptops. If the mathematically good solutions properly describe the needed behavior of the model, then the smaller computational demand is really advantageous. The result in our case is that only the rated speed and power should be available on the motor's nameplate because any other necessary parameters can be measured at the pumping unit.

The magnetizing and starting current can be measured at the pumping unit when starting the unit and operating it at normal conditions. The measured starting current will not be the locked-rotor nameplate current which is conventionally used for parameter estimations. The actual starting current depends on the transient phenomenon, on the load, on the network and others. However, the starting current works as a limitation constraint in

DOI: 10.14750/ME.2019.010

the optimization and only the starting current is included in the error function from the running-up region of the characteristics, as can be seen in Eq. 10. The operational range is over-represented in the error function and causes a better motor modeling in the operational region. Hence the starting current's value is only forcing the starting conditions into the better modelling and it is less important than the other data close to the operation range. According to present author's experience it can be assumed that the first current value using 10 Hz sampling rate (so the first 0.1 sec of the starting procedure) can be used as starting current for the optimization.

The algorithm's flowchart is presented in Figure 12. The parameter estimation determines the values of the equivalent circuit depicted in Figure 7. The model applies (Pedra & Córcoles, 2004.) recommendation: the k_r (constant multiplication factor between the stator- and rotor resistances) and k_x (constant multiplication factor between the stator- and rotor reactance) values are used in the same meaning as in Chapter 2.4.2. The different k_r and k_x values guarantee that the algorithm always finds the function's minimum point. The different k_r and k_x values mean different data set to be evaluated and the result is more program runs which makes it possible to find minimum points of the objective function. The number of program runs were reduced as compared to the previous chapter: the starting number of k_r and k_x values are different and the step differences as well.

There are some limitations to keep the parameters within the conventional equivalent circuit parameter ranges:

- the outer cage's resistance is always bigger than the inner cage resistance (Pedra & Córcoles, 2004.)
- the inner cage's leakage reactance is always bigger than the outer one (Pedra & Córcoles, 2004.)
- all parameters can only be positive numbers
- there is an upper limit to the parameters: 5000 Ω.

DOI: 10.14750/ME.2019.010

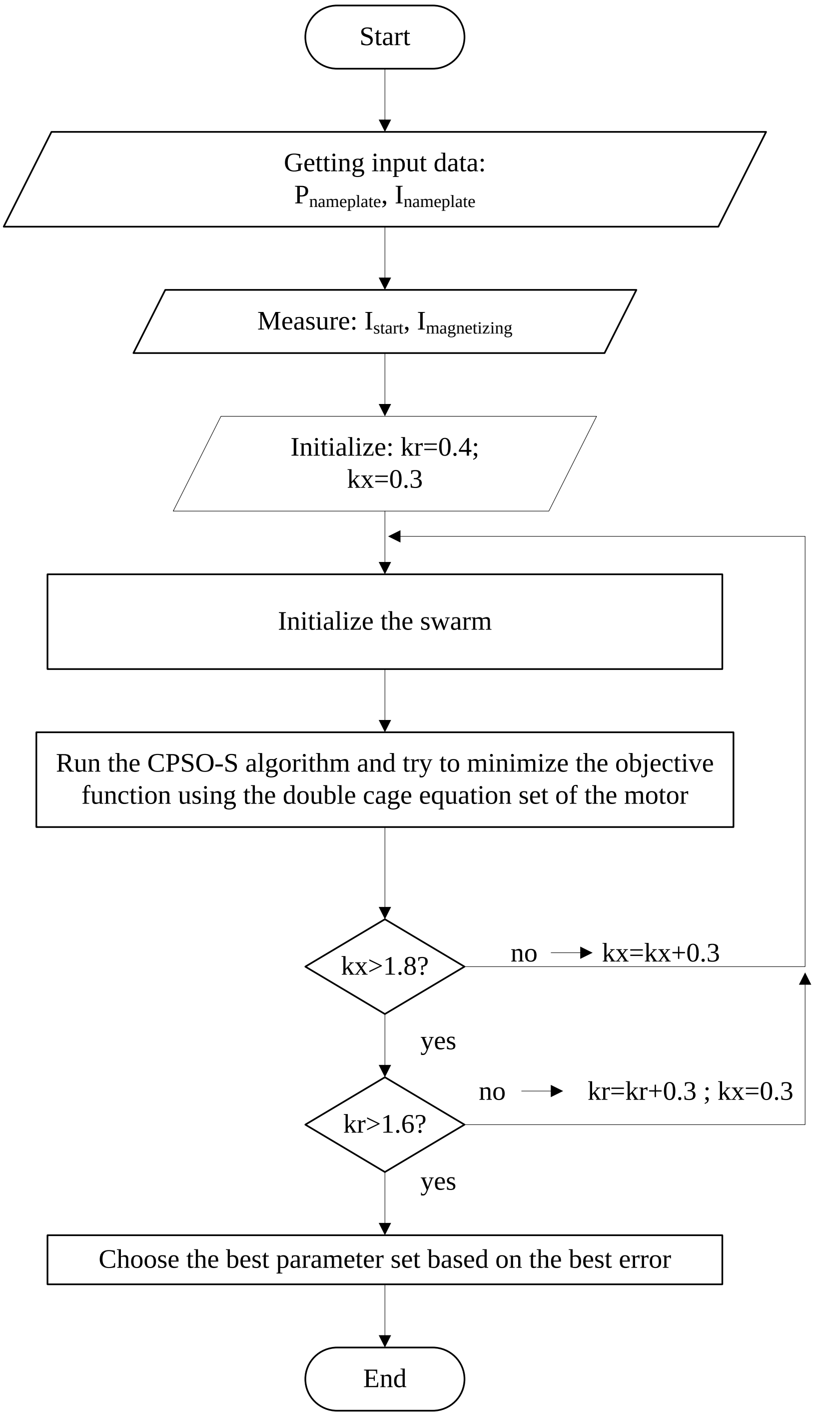

Figure 12. CPSO-S optimization diagram flowchart

Figure 13. shows an example calculation result for a known motor characteristic, where the measured and calculated data are shown. The calculation was performed using the proposed method.

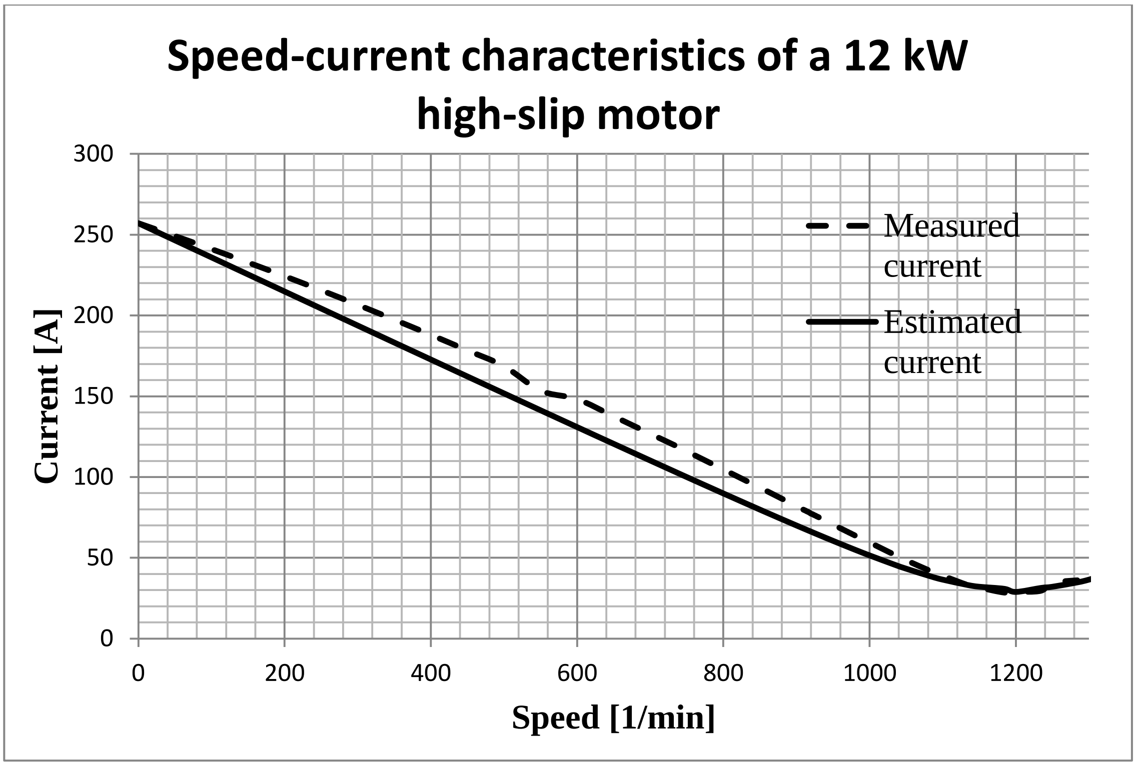

Figure 13. Speed-current characteristic of a 12 kW high-slip motor with the measured and estimated current

The current characteristics shows an excellent fit. The difference between the measured and estimated values comes probably from the non-linearity and weaknesses of the equivalent circuit. The 3 error functions out of the 4 functions in the objective function ensure the good current behavior description. On the other hand, the torque characteristic is taken into account only through the nominal mechanical power in the objective function. The only one restriction creates excellent torque estimation close to the nominal range, but the starting conditions can be modeled poorer as Figure 14 shows.

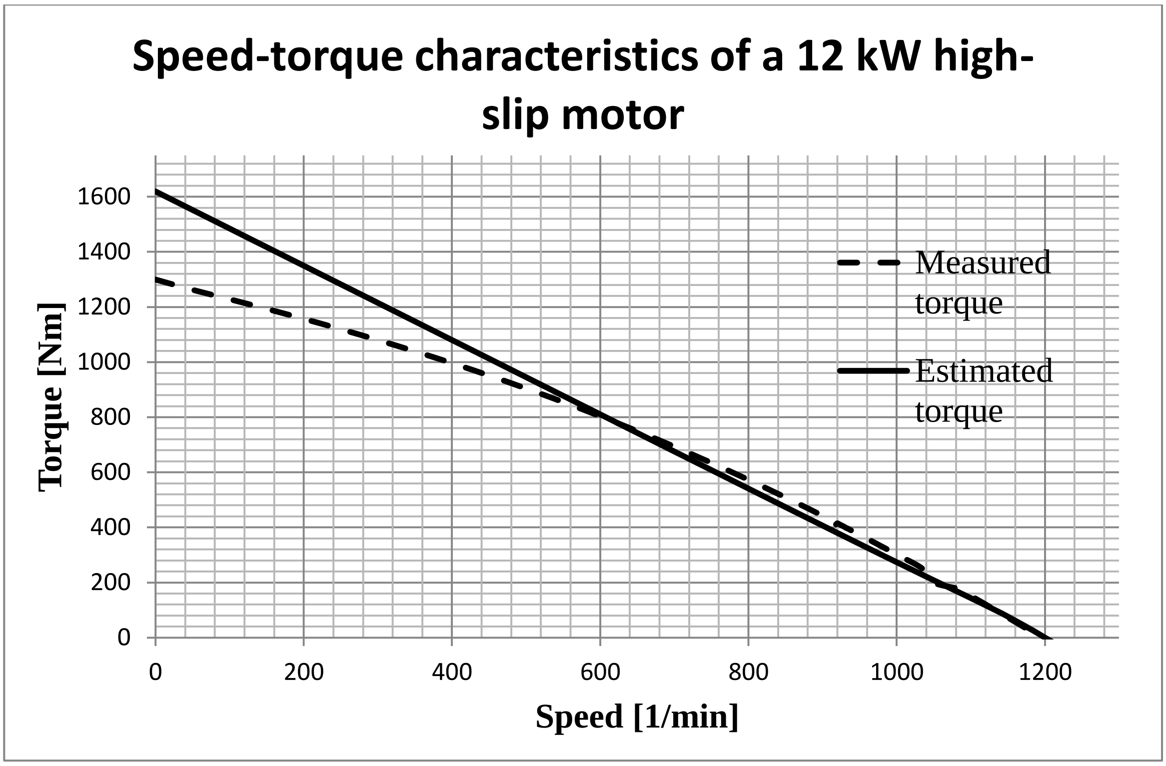

Figure 14. Speed-torque characteristic of a 12 kW high-slip motor with the measured and estimated torque

The method was tested on the same 28 high-slip motor performance curves as in Chapter 2.3.1. The full speed-efficiency, speed-power, speed-current characteristics were measured in the lab of the manufacturer. Those 28 motors cover the manufacturer's product line in high-slip motors. The test results for the objective function are summarized in Table 4. The table contains all runs of the 28 motors for the different k_r and k_x values. The table contains 28x30, so 840 different optimization solution results.

Table 4. Statistical data of the developed method

Average minimum value of the objective function	0.00143
Standard deviation of the objective function	0.53
Average objective function's value	0.31673

The results indicate that the optimization process stack at local minimums in 10-20% of the cases. This phenomenon is corrected using the different k_r and k_x value runs which helps the algorithm to find different solutions. The algorithm always found a minimum 2-3 good solutions in case of all 28 motors, which is the key to the good average minimum value. The robustness and accuracy of the proposed solution is proven through the data shown in Table 4.

The method can be generalized to be used an all motors by modifying the objective function's formulation and can be adjusted to cases where more data are available about the motors (like breakdown torque in case of normal NEM B motors).

DOI: 10.14750/ME.2019.010

3 SUCKER ROD PUMPING ANALYSIS – AN OVERVIEW

The supervision and production optimization are a crucial task in every oil production system. Only the cost-effective production can extend the life of existing mature oil fields. Not only should the surface technology be monitored from time to time but the well inflow parameters as well. When speaking about sucker rod pumped wells the following parameters should be known by the production engineer to find comprehensive and reliable solutions:

- information related to the reservoir – producing well system:
  1. flowing bottomhole pressure (FBHP),
  2. static reservoir pressure (SBHP),
  3. well data (depth, perforation, etc.),
  4. production rate,
  5. produced fluid composition (water cut, gas-oil ratio, etc.);
- information about the production system:
  6. loads in the polished rod (PRL),
  7. counterbalancing efficiency,
  8. subsurface system's operation (valve conditions, plunger-barrel condition),
  9. presence of gas- or sand related problems,
  10. surface system's condition (bearings, gear reducer, V-belts, etc.),
  11. prime mover's load.

There are some data from the list which needs a cooperation between different disciplines (drilling & workover: 3, reservoir analysis: 5) and some data can be measured or calculated directly by the production engineer (1 and 2; 6-11). The continuous supervision of an operating sucker rod pumped well is always needed. The data are needed for the proper maintenance as well. The system efficiency and cost conditions can be evaluated using the previously mentioned data.

The production engineer has many conventional opportunities to improve system efficiency and to optimize production:

- production rate can be modified by the stroke length and the pumping speed. The flowing bottomhole pressure will change with the production rate. The bottomhole pressure can be calculated based on acoustic measurements;
- pump-off conditions can be prevented using pump-off controllers;
- loads in the surface system can be optimized by proper counterbalancing. Loads are measured normally by dynamometers;

- the surface gathering system has an important effect on the pressures in the well, so production can be manipulated through modifications in the gathering system.

There are some unconventional solutions for production supervision and optimization. The most important equipment are smart rod pump controllers and the variable frequency drive units. They are really useful and clever solutions, but they are expensive. The big number of sucker rod pumped wells mentioned in Chapter 1. can be misleading because the majority of the sucker rod pumped wells are stripper wells, especially in the US. Such wells produce only 10 bpd or less. It can be assumed that the situation is similar worldwide and most of the sucker rod pumped wells produce low daily rates. This recognition makes it important to find cost-effective solutions for supervising beam pumped wells.

The main goal of this Thesis is to find new scientific ways for supervising sucker rod pumped wells. This chapter deals with the conventional solutions but first it will demonstrate the important parts of the surface system to better understand the model described later.

3.1 THE SUCKER ROD PUMPING SYSTEM

The sucker rod pumping system is a well-known and mature technology. There are lots of really good and detailed technical books available for example (Takács, 2015.) and thousands of papers. This chapter will focus only on the necessary information for the later discussion; otherwise a good guideline can be found in (Rowlan & McCoy, 2007.). The sucker rod pumping surface system can be seen in Figure 15. after (Kis, 2013.).

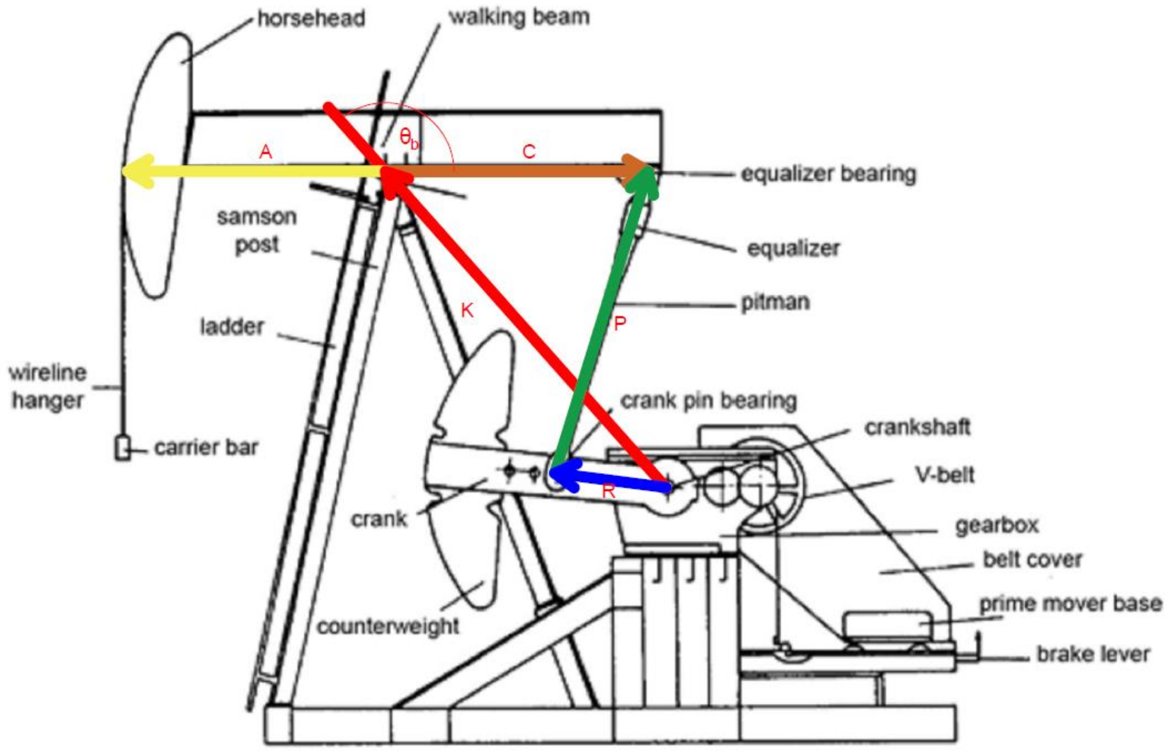

Figure 15. Sucker rod pumping unit surface system after (Kis, 2013.) and (Svinos, 1983.)

The basic invention of the system goes back to the 19th century (Beckwith, 2014.). The first wells were drilled using cable tool equipment, and the walking beam made possible to lift and release the drillstring. The pioneer oil-well drillers used to build a special wooden "rig" to drill each well and this system was not easy to move. However, the wood equipment was well-suited for moving a plunger in a barrel to lift the oil like it did with the drill bit. Nowadays the basic equipment is highly developed, but the working principle remains the same: the walking beam moves via a rod string the plunger and by using simple one-way valves the plunger lifts the oil. The system needs an alternating movement at the wellhead to move the rod string. Steam engine was used to move the system in the past but modern engine- and motor techniques spread at the beginning of the 20th century. Today the dominant prime mover is an electric motor. A complex energy conversation system is needed to convert the electrical energy to alternating movement ready for usage at the wellhead. The conventional construction and nomenclature of a sucker rod pumping unit is described in the followings.

The modern prime mover can be a high-speed induction motor or gas engine but the dominating one is the 3-pole pair high slip asynchronous motor for conventional systems (Takács, 2015.). The energy is transferred to the gearbox through V-belts. There is an increase in torque and a reduction of the speed because of the different diameters of the V-belt sheaves. Those sheaves can be replaced to adjust the system for the required speed. A big torque increment and speed reduction occurs in the gearbox where the power is transferred normally through three shafts, and the common transmission ratio is about 30:1 (Takács, 2015.). The crank equipped with massive iron counterweights is connected to the crankshaft. The counterweights have a very significant effect on the efficiency of the pumping system. The use of counterweights allowed the developers to use smaller prime movers and gearboxes because the counterweights act as a kinetic energy storage system and “smooth” the loads acting on the gearbox. A pitman transfers the power to the walking beam. A so called “horsehead” can be found at the end of the walking beam and the polished rod is connected to the horsehead by a wireline hanger. The shape of the horsehead makes it possible to move the polished rod only in the needed vertical direction. The polished rod is continued in the rod string down to the plunger. The pump is a positive displacement pump and its operation is based on the relative movement of the plunger and the barrel.

The mechanical equipment just described contains many parts which should be optimized very well to fully utilize the potential in the system. Poor operating conditions can lead to very low efficiencies, but a system operated according to the recommendations can reach an overall efficiency of about 60% (Podio, et al., 1994.). Continuous system analysis and maintenance is needed to reach the possible highest efficiency and simultaneously keep costs as low as possible. The following chapters deal with the conventional supervising techniques and the novel solutions as well.

3.2 PRODUCTION SUPERVISION TECHNIQUES

The need for production supervision techniques goes back to the beginning of the 20th century. The first dynamometer surveys to analyze oil wells were taken in the 1920’s (Takács, 2015.). The supervision techniques can be classified according to (Giangacomo & Hill, 1999.) in three big groups:

1. fluid level measurements (“well shooting” or acoustic measurements),
2. dynamometry,
3. electrical power based analysis.

The measurements mentioned previously can be combined as well. It is suggested by the author of this Thesis extending the 3rd group not only for the “old” power and counterbalance measurements but for the smart solutions as well. The conventional data acquisition system uses dynamometer surveys only that includes “well shooting”, and may include an electrical survey (Takács, 2015.). The operational parameters can be determined from the dynacard and some information is received about the motor’s operation if an electrical survey is performed as well. The counterbalancing of the unit can be checked using electrical measurements. The dynamic or static fluid level can be measured in the annulus so one can get information on the well’s and reservoir’s condition.

Other types of data collection may be attained using smart well controllers equipped with remote monitoring or control facilities. This modern type of data acquisition gives a lot of informative data on the well and the reservoir. But smart well controllers are expensive, complicated and are not cost effective for stripper wells.

3.2.1 Acoustic measurements

FBHP determination is a crucial task when one wants to check the inflow performance of hydrocarbon wells. Well sounding is a good and accurate solution to determine the liquid level in the annulus. In theory, the FBHP can be easily calculated based on the liquid level and the average density of the fluid in the annulus. The need for liquid level determination was always a common demand of production engineers since oil is produced. The first application of the acoustic measurements goes back into the 30s (McCoy, et al., 2002.).

The operating principle of the acoustic measurements is simple and straightforward. An intensive sound wave is generated at the wellhead and the reflected waves in the annulus are recorded. The sound waves will be reflected from restrictions in the annular area (collars) and from the liquid level as well. If the sound velocity in the given gas is known or we can determine the number of collars, then the liquid level can be determined.

The first measurement systems used explosives to create a strong enough sound wave (McCoy, et al., 2002.). The use of such materials is dangerous when flammable hydrocarbon gases and oxygen is present. Other solution had to be invented to eliminate the danger of the explosions. High pressure gas (nitrogen or CO_2) was used to create sound waves and the so called "gas gun" was invented. The gas gun is a simple and safe piece of equipment to produce high energy waves and it can be adjusted for the given wellhead pressure. The operation of gas guns is based on two different methods (McCoy, et al., 2002.):

- creating a compression gas pulse: the gas gun has gas storage facility (chamber) that can be filled with working gas up to a given pressure limit. The pressure limit is based on the gas gun's type and on the wellhead pressure. Normal charging pressure is 100 psi above the wellhead pressure (McCoy, et al., 1985.). Then the pressure is released suddenly into the annulus creating a high energy sound wave pulse.
- creating a rarefaction gas pulse: this measurement method is used for high pressure wells. Sucker rod pumped wells seldom meet that criterion. The gas gun's chamber is empty during the installation. Then the high WHP is released suddenly into the chamber and the fast expansion creates sound waves.

The reflection is recorded using a microphone. The measured sound signals vs. time are plotted on a paper or on a digital chart and the liquid level can be calculated based on the collar's reflection or based on the sound velocity in the given gas. A typical acoustic survey can be seen in Figure 16.

DOI: 10.14750/ME.2019.010

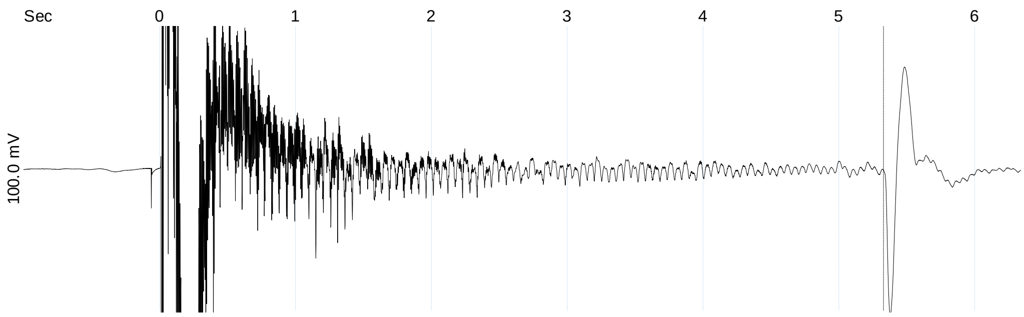

Figure 16. Acoustic measurement diagram (exported from Echometer's TWM software)

The evaluation of similar surveys presented in Figure 16. was a complicated task before the introduction of modern computer software. The small peaks in the signal had to be counted by the operator and the fluid level had to be calculated using the average length of tubing joints. When the method based on the sound velocity was chosen special charts (McCoy, 1974.) had to be used to calculate the actual sound velocity in the given natural gas. Reading of those charts increased the evaluator's effect on the measurement accuracy. The charts were provided by the producer of the measurement system. Moreover, the bottomhole pressure calculation was based on similar charts (McCoy, 1969.) hence the evaluator's knowledge specified the calculation accuracy. Those systems have been used (or sometimes are still in use) for decades until the widespread use of the computer-based measurement systems which are easy to use.

The computer-based measurement systems highly increased the bottomhole pressure's calculation accuracy. An analog-digital converter converts the microphone's analog signal into digital data. The digital data can be filtered and modified as needed. Modern well analyzer software calculates automatically the collars' reflections and the sound velocity for known gas composition, pressure and temperature. The operator's only task is to approve the computer's calculation. Calculation accuracy is improved based on additional physical phenomena that could never be used for paper records (McCoy, et al., 2002.). The reflected sound wave's frequency depends on the distance traveled and on other parameters as well. But this physical phenomenon clearly indicates that the collars' reflections have different frequency content than the reflection from the liquid level. The algorithm can be coded more robustly after applying low-pass or high-pass filters. The automatic liquid level determination can be used successfully in about 95% of the wells (McCoy, et al., 2002.).

Although the well-sounding technique is widely used in the industry, but it has some disadvantages as well. There are about 5% of the wells where the well-trained operator's responsibility is increased. Those wells include foamy liquid levels, highly gaseous liquid columns in the annulus, paraffin deposition on the collars and other non-conventional conditions which make the measurement complicated. Special tricks can be used in such wells like application of downhole markers or shutting in the annulus vent line to increase the bottomhole pressure to reduce the gaseous liquid column's height, or applying anti-foaming agents.

3.2.2 DYNAMOMETRY

The basic idea of dynamometer measurements is to determine the loads in the sucker rod string or more accurately to determine the loads at the plunger. The common solution is to measure the loads at the polished rod and to convert them to a pump dynamometer card. The evolution of such equipment was started in the 1920's. Today dynamometry means a computer-based detailed analysis system to check pump efficiency, valve conditions and power flow in the system. There are existing systems directly measuring the downhole pump cards, but they are unpractical and expensive solutions. The discussion will be on the conventional surface dynamometers in the following. Such system is shown in Figure 17.

Figure 17. Dynamometer system (Echometer, 2017.)

There are two basic versions of surface dynamometers: the mechanical one and the electronic one. The mechanical solution was used in the past but lately the industry switched to electronic devices although the mechanical one is still in use. Normally the mechanical dynamometers have a fluid-filled reservoir and the sensor is placed between the polished rod and the carrier bar. The load is converted into pressure signals and those pressure signals are plotted versus the time or polished rod position. One kind (horseshoe transducer, No. 4. in Figure 17.) of the electronic devices operates on the same principle only the paper register was changed into resistor gauges and electronic devices. The gauges create a voltage signal proportional to the load and the signals are measured and analyzed using a computer-based data acquisition system. The other solution uses a clamp-on (No. 5. in Figure 17.) load transducer connected to the polished rod. New systems contain wireless sensors making measurements easier (Echometer, 2017.) but at an elevated price.

The working principle of the clamp-on transducer is based on Hooke's law. The polished rod is under continuously changing load and that load causes an elongation in the rod's steel material. The elongation will be measured using the clamp-on transducer and the load can be calculated. This measurement principle has some disadvantages:

- there is some production uncertainty in the polished rod's material. The lack of information may cause higher errors;
- the neutral point can never be measured (but it does not exist normally in the polished rod);
- a polished rod position transducer is needed to build up the load versus position dynacard;
- the polished rod's surface is hard, and the installation of the transducer may be complicated.

The result of the above effects is a limited accuracy of ±7% (Echometer, 2017.). This inaccuracy is relatively high compared to the horseshoe transducers. On the other hand, there are some advantages of using such systems:

- the transducer can be installed relatively quickly;
- there is no need to stop the production during the measurement;
- the measurement is a non-intrusive one, so it does not change the position of the plunger in the barrel.

The clamp-on transducer can be recommended for fast tests where the accuracy does not play an important role.

Horseshoe transducers normally use a hydraulic fluid and a pressure sensor, or resistor gauges. The pressure can be measured accurately. The advantages of the horseshoe transducer are the following:

- the direct measurement of the load makes it more accurate than the clamp-on transducer;
- the neutral point is known because it can be set by hydraulic cylinders.

However, there are some disadvantages as well:

- a special, previously installed spacer is needed. If this is not installed in the system, the position of the plunger in the barrel will be modified because of the height of the sensor. The spacer means an additional cost as well;
- when measuring without the previously installed spacer, the production must be stopped for installing the transducer;
- a polished rod position transducer is needed to build up the load versus position dynacard.

The system does not consist only of the sensors because there is additional equipment as well. The most important is the data acquisition system. System accuracy highly depends on the proper analog/digital conversation and on the algorithm's calculation accuracy.

DOI: 10.14750/ME.2019.010

3.2.3 Computer based solutions

This chapter discusses the prime mover’s power analysis and the new, novel techniques developed by the author to make the sucker rod pumping system’s analysis cheaper and more effective. The importance of the electrical measurements was recognized relatively late because of the slow development in measurement technology. Echometer Inc. is one of the two biggest producers of dynamometer equipment on the market. The first white papers on the importance of the continuous motor power measurement (Podio, et al., 1994.) were published only in the 90’s by Echometer. The first computer-based, high sampling rate data acquisition systems made it possible to perform a thorough analysis of the pumping system. Older pumping analysis systems measured the prime mover’s current as well, but the measured data were not good enough to perform a full analysis on the system. The continuous current- and power measurement opened new possibilities in the sucker rod pumping optimization. Not only the counterbalance effect could be examined but the system’s efficiency conditions as well. There was only a small step from these comprehensive measurements to build a system that not only measures but controls the well’s operation. So, the smart rod pump controller’s invention was near.

The objective of all smart rod pump control systems is the same: to achieve the highest production rate with the lowest production costs. The development of such systems began in the 70s and 80s with easy pump-off and timer controllers (Neely, et al., 1989.). The early types of controllers could control the running time and later to detect no-flow conditions. Then the availability of microcomputers allowed developers to include more functions in rod pump controllers. Today’s smart well management systems are offered as comprehensive systems with remote monitoring facility, liquid flow measurement (Lufkin Industries Inc., 2015.) using the pump as a flow meter and are equipped with other important and practical parts. Figure 18. shows a modular rod pump controller that can be mounted on normal sucker rod pumping units.

Figure 18. CAC 880 Rod Pump Controller (eProduction Solutions Inc., 2014.)

The rod pump controller’s main control elements can be seen in Figure 18: LCD display, touch panel and the housing. Every important sucker rod pumping unit manufacturer and service company offers their own smart well management or control systems.

The number of available smart well management systems is increasing every day, but they have many common features which are collected in the following list (Lufkin Industries Inc., 2015.), (eProduction Solutions Inc., 2014.):

- online recording of dynamometer surveys
- overload-, fluid pound- and pump-off detection
- automatic control of the operation
- timer facility
- HMI interface where every important parameter can be read out
- early failure detection
- data storage facility
- the controllers can be operated with Hall-sensors and other sensors
- optional: remote control facility
- optional: variable frequency drive for better optimization.

The advantages just listed show that smart rod pump controllers can be adjusted for any given system. Producers stress the advantages only but there are some disadvantages as well. Normally each system should be adopted for the given unit which is not always easy and is normally performed by the controller's manufacturer. Such systems are relatively expensive when compared to common dynamometer surveys. Manufacturers claim that investment costs are paid back through the enhanced production rates and lower workover costs. The use of smart rod pump controllers is probably advantageous for wells with quite high production rates. However, high investment costs are unreasonable for stripper wells or for wells close to abandonment. The solution for that category is a low-cost monitoring or only periodical monitoring system that provides good information about the well's condition. Those systems are the conventional dynamometer measurement packages or other promising, cost effective methods presented in this Thesis.

3.3 ENERGY EFFICIENCY OF SUCKER ROD PUMPING

Normally, the sucker rod pumping system's energy source is electric power and its useful work is the potential- and pressure energy increment of the fluid lifted. During the energy conversation, there are energy losses at several places in the system. Those losses can be classified as follows (Takács, 2010.):

- prime mover's losses
- surface mechanical losses
  - power transmission chain's losses (V-belt, gearbox, pumping unit)
- subsurface losses
  - losses in the pump
  - frictional pressure losses in the tubing

Figure 19. shows the occurrences of the different losses in the sucker rod pumping system. The overall system efficiency can be calculated as the product of the constituent efficiencies:

$$\eta_{system} = \eta_{motor} \cdot \eta_{surface} \cdot \eta_{lifting} = \frac{P_{useful}}{P_{in}} \qquad \textit{Equation 11.}$$

Where:

η_{system}:	overall system efficiency
η_{motor}:	prime mover's efficiency
$\eta_{surface}$:	surface power transmission chain's efficiency
$\eta_{lifting}$:	fluid lifting efficiency
P_{useful}:	useful power [kW or Hp]
P_{in}:	system's power demand [kW or Hp]

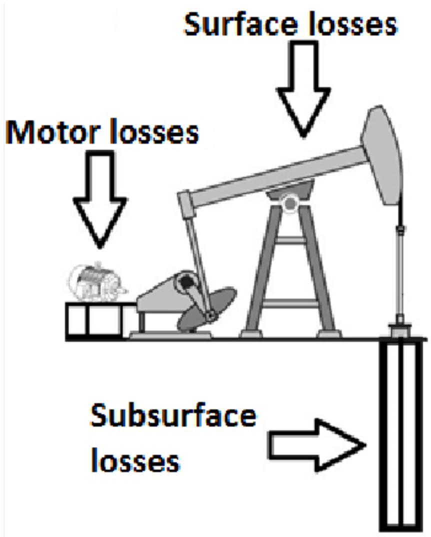

Figure 19. Losses in the sucker rod pumping system

The lifting efficiency is normally the most important component for properly designed and operated systems. The overall efficiency is the product of the different efficiencies so if one wants to achieve the best efficiency all efficiencies should be kept at an acceptable level. For example, if two efficiencies are close to 100% and the third one is only 30% the result of multiplication will give us a number close to 30%. It means that system optimization should consider all effects and the whole system should be analyzed together. The literature deals with many solutions to increase the lifting efficiency but the motor- and surface part is not so much elaborated. The motor- and surface efficiency is usually assumed to be high. We want to change this idea in this Thesis because the electrical motor's efficiency is above 90% close to its nominal load only. However, motors are seldom operated in this region because of the cyclic loads generated by the sucker rod pumping system and the general motor oversizing tendencies.

The surface system's efficiency and the lifting efficiency will be discussed more detailed in the following chapters while the electrical motor's efficiency analysis can be found in Chapter 2.3.

3.3.1 Surface system's efficiency

The surface system converts the electrical motor's low torque, high speed mechanical power into high torque, low speed alternating power available at the wellhead. The first step in this conversation is the V-belt drive between the electrical motor's small-diameter sheave and the gearbox's bigger sheave.

The V-belt drive is a widely used transmission system to convert speed and torque. It has many advantages (NSWC, 2011.):

- V-belt drives are cheap, quiet and require little maintenance,
- they can convert speed up to a ratio of 10:1,
- they are not sensitive for momentary load fluctuations,
- they require less tension than other belt drives.

The efficiency conditions of such drives are not fully understood today although manufacturers publish some useful information on efficiency of V-belt drives. The complexity of the problem depends on the working principle of the V-belt drives: they are friction driven. The efficiency depends on the following factors:

- slip (diameter of sheave) and tension of the belt
- environmental conditions (temperature, humidity, ventilation, etc.).

There is no publication available from sucker rod pumping unit manufacturers on the efficiency of V-belt drives used in their systems. Other industry manufacturers, however, have published interesting papers like (Bigler & Heston, 2013.) who analyzed the effect of belt tension on system efficiency. They found that the tension has a significant effect on the belt drive's efficiency. They conducted long-term measurements as well. The drive efficiency was about 95% for proper tension conditions (up to 70% of the nominal tension value). The efficiency drops rapidly in case of inefficient tension (70% of the nominal value) based on the extrapolated data. These tests were conducted with small motors and sheaves. Other authors (Hubble, 2011.) say that larger sheaves have lower losses. Considering these test results for sucker rod pumping units it can be said that the most probable efficiency value for properly maintained systems is about 95%.

The gearbox is the next equipment in the power flow that should be examined. There are much more data available on gearboxes than on V-belt drives. The efficiency of the gearbox depends mostly on the actual load and the age of the unit assuming normal operational conditions (the housing is filled with the recommended lubricant; the gearbox is not overloaded). The efficiency of the gearbox is above 85% according to (Takács, 2015.). There are smaller frictional losses in the walking beam's main bearing, crank pin bearing and in the equalizer bearing. The overall surface system efficiency is between 60-75% (Kilgore & Tripp, 1991.) or other authors reported a bit higher values (Takács, 2010.). The surface system's efficiency can be calculated using the following equation:

DOI: 10.14750/ME.2019.010

$$\eta_{surface} = \frac{PRHP}{P_{motor}} \qquad \textit{Equation 12.}$$

Where:

$\eta_{surface}$:	surface power transmission chain's efficiency
P_{motor}:	mechanical power at the prime mover's shaft [kW or Hp]
$PRHP$	polished rod horsepower [kW or Hp]

The motor's mechanical power can be calculated if the motor's characteristic curves are known. The polished rod horsepower can be calculated from dynamometer measurements. If the motor's characteristic curves are not known, then the surface efficiency is hard to find and it should be calculated indirectly.

3.3.2 LIFTING EFFICIENCY

The lifting efficiency is related to the subsurface system's hydraulic work. The input power for this subsystem is the polished rod horsepower and the useful power is the power used to lift the fluid. In mathematical form:

$$\eta_{lifting} = \frac{P_{hydraulic}}{PRHP} \qquad \textit{Equation 13.}$$

Where:

$\eta_{lifting}$:	fluid lifting efficiency
$P_{hydraulic}$:	useful work performed by the pump [kW or Hp]

The following terms are included in the lifting efficiency:

- the power that is needed to lift the rod string;
- the frictional losses of the rod string;
- the fluid's frictional pressure losses;
- the filling efficiency of the barrel (fluid pounding, gas lock, etc.);
- leakage between the plunger and barrel.

The lifting efficiency is probably the most important item for the production engineer because its parameters can be easily affected by changing the operational parameters. The available publications in the literature concentrate mostly on the lifting efficiency's optimization (Takács, 2015.), (Gault, 1987.). The frictional losses depend on the well geometry and on the pumping rate which can be selected by the production engineer. The filling efficiency should be kept as high as possible to prevent not only the poor system efficiency but any damage to the system.

There are two basic calculation methods to calculate the pump's useful work. The difference between the different calculations is the effect of the annulus pressure on the pump intake pressure. The annular pressure can be neglected for wells where the casing vent line is open to the atmosphere because the hydrostatic pressure of the gas column is minimal. Equation 14. can be used for such cases:

$$P_{hydraulic} = \frac{9.81}{86400} \cdot Q \cdot L \cdot \gamma \qquad \textit{Equation 14./a}$$

Where:

$P_{hydraulic}$:	useful work performed by the pump [kW]
Q	production rate [m^3/day]
L	dynamic liquid level [m]
γ	specific gravity of the produced fluid [-]

In Imperial units:

$$P_{hydraulic} = 7.36 \cdot 10^{-6} \cdot Q \cdot L \cdot \gamma \qquad \textit{Equation 14./b}$$

Where:

$P_{hydraulic}$:	useful work performed by the pump [Hp]
Q	production rate [bpd]
L	dynamic liquid level [ft]
γ	specific gravity of the produced fluid [-]

The annular pressure can never be neglected for wells having substantial pressures at the casing head. Equation 15. gives the hydraulic power for such wells:

$$P_{hydraulic} = \frac{9.81}{86400} \cdot Q \cdot L_{pset} \cdot \gamma - \frac{100}{86400} \cdot Q \cdot PIP \qquad \textit{Equation 15./a}$$

Where:

$P_{hydraulic}$:	useful work performed by the pump [kW]
PIP	pump intake pressure [bar]
L_{pset}	pump setting depth [m]

In Imperial units:

$$P_{hydraulic} = 1.7 \cdot 10^{-5} \cdot Q \cdot (0.433 \cdot \gamma \cdot L_{pset} - PIP) \qquad \textit{Equation 15./b}$$

Where:

$P_{hydraulic}$:	useful work performed by the pump [Hp]
PIP	pump intake pressure [psi]
L_{pset}	pump setting depth [ft]

More information should be available to use Eq. 15. The pump intake pressure should be measured or calculated. The calculation of the pump intake pressure is not always easy (gassy liquid column, paraffin deposits, etc.). The production rate should be measured accurately as well. A high lifting efficiency is a proper sign of a system operated in a proper way. The common acceptable lifting efficiencies vary between 50-90% (Gault, 1987.), (Kilgore & Tripp, 1991.). Wells having lower lifting efficiencies should be checked.

3.3.3 *NEW METHOD FOR THE DETERMINATION OF THE PARTIAL EFFICIENCIES OF THE SUCKER ROD PUMPING SYSTEM*

The determination of the partial efficiencies is a very important task for the production engineer. Knowing all partial efficiencies is the only way to improve the overall pumping efficiency because that knowledge gives a clear overview about the potential production optimization solutions. However, only a few papers can be found about that topic in the literature (Takács, 2010.). The followings should be analyzed to determine all partial efficiencies:

- prime mover's electrical power;
- production rate;
- rotational speed and torque of the prime mover and gearbox shafts;
- dynamometer measurement at the polished rod.

The high number of measuring points makes it impossible to analyze routinely the partial efficiencies and only a few authors (Kilgore & Tripp, 1991.) did it in the past. The biggest challenge is normally the rotational speed measurement of the different shafts at field conditions.

This chapter deals with a new, empirical correlation for sucker rod pumping partial efficiency determination in case of NEMA D prime movers. Only the nameplate data of the prime mover and the analysis of the dynamometer card will be used.

The first task is to calculate or measure the efficiency of the induction motor. The best solution would be to use an overall-best parameter efficiency method and then all characteristics could be generated using the equivalent circuit, as discussed earlier. However, the efficiency characteristic is the most complicated and most inaccurate one from the performance curves developed by the equivalent circuit (Pedra & Córcoles, 2004.). The author recommends using the empirical correlation presented in Chapter 2.3.1. for the efficiency determination instead of the solutions based on parameter estimation. If one knows the motor's speed-torque characteristic the actual rotational speed of the motor's shaft can be calculated from the dynamometer measurement. The motor's speed-torque curve can be calculated using the method described in Chapter 2.4.2. There are available solutions to deal with inversed torque calculation process for sucker rod pumping units as discussed more detailed in the later section of this Thesis. The motor's speed can be inferred when the transmission ratio in the pumping system is known. However, the belt drive's slip and efficiency should be still assumed but according to Chapter 3.3.1 the overall belt-drive efficiency should be higher than 95% for proper tension. The flowchart of the proposed method is given in Figure 20.

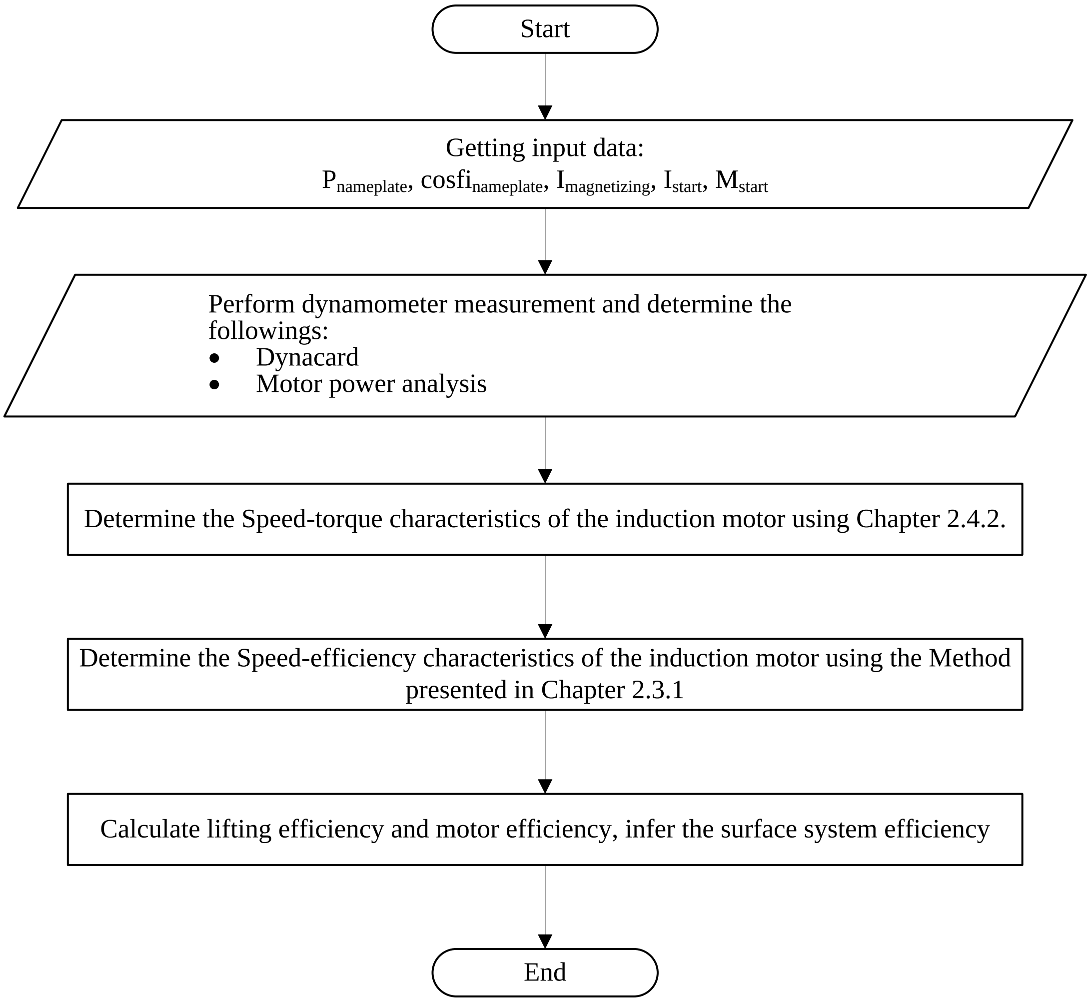

Figure 20. Flowchart of the partial efficiency calculation

The lifting efficiency can be easily calculated using the well data and the dynamometer diagram. The useful hydraulic work can be calculated using Equation 14. and the PRHP by integrating the area of the dynamometer card. The easiest solution to perform numerical integration is the trapezoidal rule. The only unknown remaining parameter is the surface efficiency.

The method was tested using a C-320D-256-100 conventional pumping unit. The surface system was equipped with a Toshiba 30 Hp NEMA D prime mover. The motor nameplate data and the dynamometer analysis were used to determine the partial efficiencies. The motor data and well data are shown in Table 5 and Table 6. respectively.

Table 5. Case study motor data

Motor manufacturer and type:		Toshiba 0306DOOD11A-P	
Power:	30 HP / 22.37 kW	Power factor:	0.82
Voltage:	230/460/796	Nominal speed:	1140 1/min
Frequency:	60 Hz	Nominal efficiency:	86.7 %
Starting current:	209.6 A	Nominal current:	39 A

The motor is a conventional NEMA D motor driven from conventional electric network i.e. no inverter or intelligent control is used. The well is a normal middle-deep oil well with moderate liquid rate.

Table 6. Case study well data

Perforation:	1951 m	Fluid specific gravity:	1
Pump setting depth:	1559 m	Average motor power consumption from electrical survey:	8.2 kW
Production rate:	13.83 m^3/day	PRHP:	3.151 kW
WOR:	69 %	Pumping rate:	8.6 SPM
		Dynamic liquid level:	954.3 m

The motor's torque-speed characteristics was determined according to Chapter 2.4.2. Then the motor's efficiency was calculated over the pumping cycle using the method described in Chapter 2.3.1. When the actual motor efficiency was known Eq. 11. could be applied to the system' partial efficiency determination. The results are summarized in Table 7.

Table 7. Calculation results of the proposed method

$\eta_{lifting}$	η_{motor}	$\eta_{surface}$	η_{system}
0.473	0.5014	0.7665	0.182

The motor was oversized, and that has greatly reduced the system's overall efficiency. The nominal efficiency of the motor was 86.7% however the actual efficiency was only about 50%. The oversized motor greatly reduces the system's overall efficiency. The lifting efficiency is almost acceptable for such an average depth well and according to the results the surface system should be revised. The proposed method can be used for easy and fast part-efficiency determination in field conditions as well.

DOI: 10.14750/ME.2019.010

3.4 TORQUE CONDITIONS IN THE SURFACE SYSTEM

Torque conditions in the surface system play an important role in the operation of sucker rod pumping since optimal pumping efficiency can be reached only in case of proper counterbalancing. The loads on the gear reducer are the result of different torque types acting in the system. The individual torque components are normally determined from the dynamometer card (Takács, 2015.). It is necessary to understand the origin of the different torque types acting in the system for later analysis.

The net torque acting on the gearbox can be calculated in the following way (Takács, 2015.):

$$M_{gearbox} = M_r(\theta) + M_{CB}(\theta) + M_{ia}(\theta) + M_{ir}(\theta)$$ *Equation 16.*

Where:

$M_{gearbox}$	gearbox torque [Nm or in-lbs.]
θ	crank angle [° or rad], measured from the uppermost position of the cranks
$M_r(\theta)$	polished rod torque [Nm or in-lbs.]
$M_{CB}(\theta)$	counterbalance torque [Nm or in-lbs.]
$M_{ia}(\theta)$	articulating torque [Nm or in-lbs.]
$M_{ir}(\theta)$	rotary inertial torque [Nm or in-lbs.]

The net gearbox torque is a result of four different torques whose actual values depend on the crank angle, so the actual crank angle is needed for any torque calculation. The polished rod torque is the direct result of the polished rod load. The polished rod load consists of three basic loads: the rod weight, the fluid load and the dynamic forces. The rod weight and the dynamic forces act always while the fluid load acts only in the upstroke. The polished rod torque can be calculated using the following equation:

$$M_r(\theta) = TF(\theta) \cdot [F(\theta) - SU]$$ *Equation 17.*

Where:

$TF(\theta)$	torque factor [m or in]
$F(\theta)$	polished rod load [N or lbs.]
SU	structural unbalance [N or lbs.]

The torque factor is a special property of the pumping unit. It means an imaginary lever arm which is used to convert the rod load into rod torque. The multiplication of the torque factor and rod load gives the polished rod torque. The torque factor is a function of the crank angle and it is published by the pumping unit manufacturers for every 15° crank angle (Takács, 2015.). The calculation of the torque factor is possible when all geometrical parameters of the given pumping unit are known. The measurement of the needed parameters is easy and can be done at field conditions as well.

The polished rod load is measured normally by a dynamometer survey. The structural unbalance is a pumping unit specific variable and it depends on the pumping unit's construction. "It is defined as the force required at the polished rod to keep the walking beam in a horizontal position with the pitmans disconnected from the cranks"

(Takács, 2015.). It can be positive and negative as well. The SU is provided by the pumping unit's manufacturer as well but it is hard to obtain in old installations.

The rotating counterweights create a sinusoidally changing torque. The counterweights are used to smooth the alternatingly changing polished rod torque to reduce the gearbox' loads. The counterbalance torque can be calculated if the center of gravity of the counterweights and the length of the lever are known. The counterweights can be positioned on the crank using a phase angle for non-conventional pumping units. The counterbalance torque can be calculated using the following equation:

$$M_{CB}(\theta) = -M_{CBmax} \cdot sin(\theta \pm \tau) \qquad \textit{Equation 18.}$$

Where:

M_{CBmax}	maximal counterbalance torque [Nm or in-lbs.]
τ	phase angle of the counterbalances [° or rad]

In a real pumping unit, the crankshaft never rotates with a constant angular velocity. The changes in the velocity will cause the presence of rotary inertial torques in the system. The rotary inertial torques are more important for prime movers where the rotational speed can vary significantly hence for NEMA D or high slip prime movers and in case of fluctuating loads. If the speed variation is smaller than 15% of the average pumping speed than inertial torques will cause smaller errors than 10% in the torque calculations. (API, 1988.). The rotary inertial torque can be calculated using the following equation:

$$M_{ir}(\theta) = I_s \cdot \ddot{\theta} \qquad \textit{Equation 19.}$$

Where:

I_s	mass moment of inertia of the cranks and counter weights, referred to the crankshaft [kg·m^2]
$\ddot{\theta}$	crank angular acceleration [1/s^2]

The other inertial torque is the articulating torque arising in pumping unit components that have an alternating movement during the pumping cycle (the walking beam, the horsehead, etc.). The articulating torque acts always because the walking beam and related equipment make continuously alternating movement. The alternating torque can be calculated from the dynacard using the methods discussed by (Kis, 2013.). The articulating torques can be calculated theoretically using the following equation:

$$M_{ia}(\theta) = \frac{TF(\theta)}{A} \cdot I_b \cdot \ddot{\theta}_b \qquad \textit{Equation 20.}$$

Where:

A	the length plotted in Figure 15. [m] after *(Svinos, 1983.)*
I_b	mass moment of inertia of the parts under alternating movement [kg·m^2]
$\ddot{\theta}_b$	angular acceleration of the beam [1/s^2]

DOI: 10.14750/ME.2019.010

The mass moment of inertia of the alternating movement making equipment is sometimes given by the manufacturer. Only the angular acceleration of the beam should be calculated.

3.4.1 Reverse torque calculation method

If one wants to invent a new measurement system where the input parameters are measured in the electrical system, the conventional torque calculation direction should be reversed. The torque calculation is done normally based on the dynamometer measurement as described previously. The reverse calculation is a rarely used method and not all torque components are normally included in the investigation as presented by (Silva, et al., 2014).

The input data of the inversed calculation method are the following:

- motor torque vs. time and speed vs. time functions;
- pumping unit geometrical data and rotational direction;
- wrist pin's position and counterweight's mass, counterweight's geometrical arrangement and crank's geometrical arrangement;
- crank mass and dimensions;
- transmission ratio in the mechanical linkage system: gearbox' transmission ratio, V-belt sheave's diameters;
- mass moment of inertia to perform inertial torque calculations;
- a fix point or time in the cycle: either upstroke starting time or downstroke starting time – there is no polished rod position data available when inverse calculations are applied.

The calculation steps can be seen in Figure 21. The maximum counterbalance torque needed in Eq. 21. can be calculated using the method presented by (Bommer & Podi, 2012.). The needed data are the mass and geometrical arrangement of the counterweights as shown in Figure 22.

DOI: 10.14750/ME.2019.010

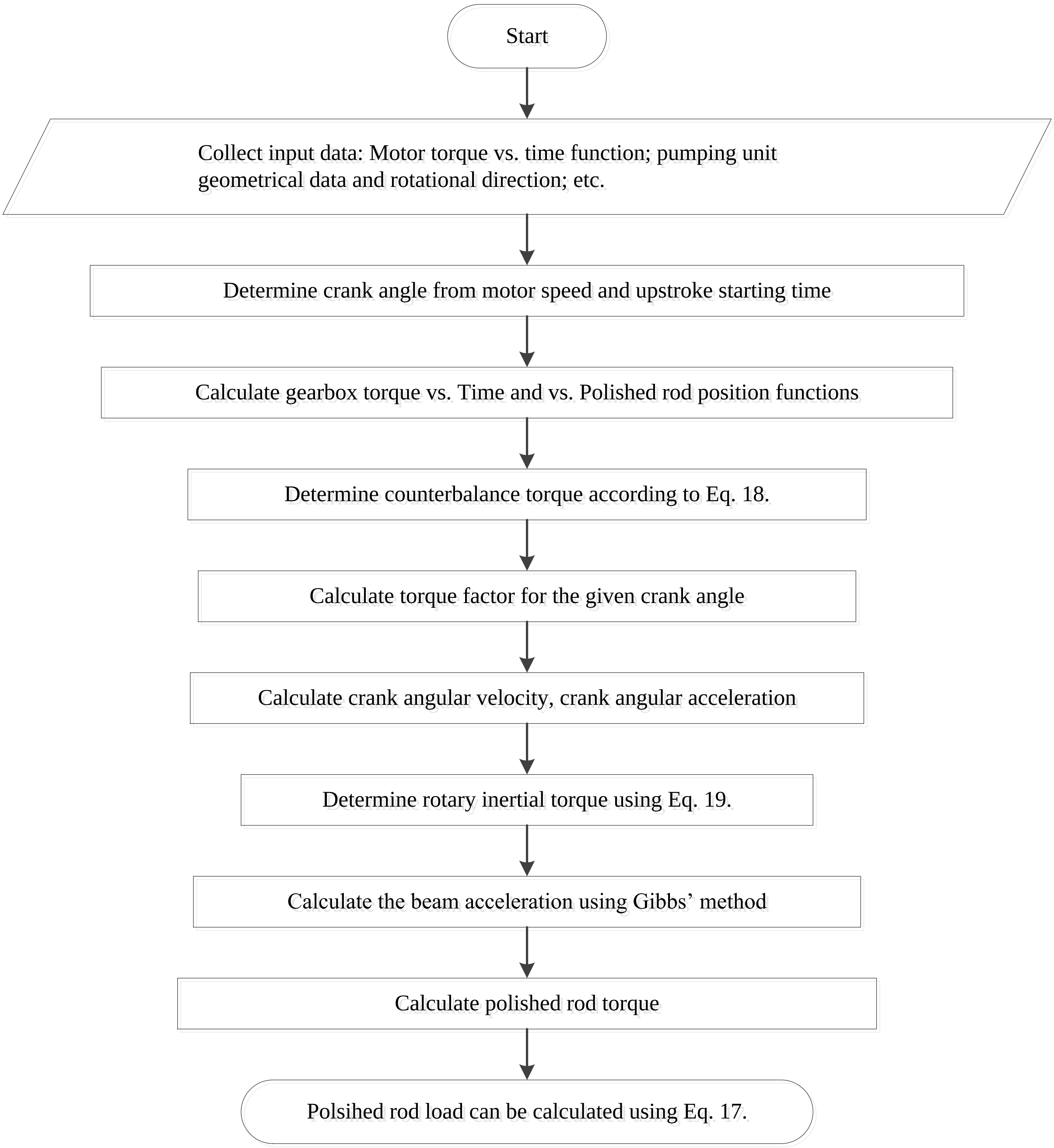

Figure 21. Inverse torque calculation procedure

The maximum counterbalance torque can be found from the following equation:

$$M_{CBmax} = M_{crank} + (M - D) \cdot N \cdot W \qquad \textit{Equation 21.}$$

Where:

M_{crank}	crank torque [Nm] or [in-lbs]
M, D	geometrical data after Fig. 22.
N	number of counterweights
W	mass of counterweights

The equation can be varied if more than one counterweight type is used or the M-D dimensions are different for the different counterweights. The torque factor and polished rod position at the given angle can be calculated using the pumping unit's geometrical arrangement: the calculation method is presented by (API, 1988.). The method is easy to follow; however many equations should be used. Those equations can be found in the original work and will be not presented here because of space limitations.

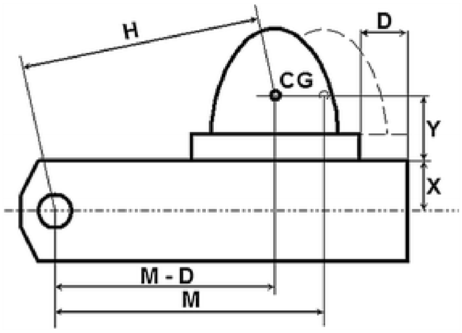

Figure 22. Geometrical arrangement of counterweights (Takács, et al., 2016.)

The easiest way to calculate the articulating torque is Gibbs' method (Gibbs, 2012.). He expressed the polished rod's position with the angle of the walking beam's centerline. Since the mechanical system in the sucker rod pumping unit is built with fixed connections the following formula can be applied (Gibbs, 2012.):

$$s(t) = A \cdot \theta_b(t) \qquad \textit{Equation 22.}$$

Where:

$s(t)$ polished rod position vs. time function

$\theta_b(t)$ angle vs. time function of the walking beam's centerline

The polished rod position vs. time function can be calculated from the crank angle using the pumping unit's geometrical arrangement. The angular acceleration of the walking beam can be calculated using the following equation after Eq. 22. rearrangement and differentiation:

$$\ddot{\theta_b} = \frac{1}{A}\ddot{s} \qquad \textit{Equation 23.}$$

Where:

$\ddot{s}$ polished rod acceleration

The differentiation can be performed using the five-point stencil method both for the beam acceleration and for the polished rod acceleration as well. The five-point method is a robust method if the input function's noise level is low.

If the measured function is highly fluctuating smoothing algorithms should be applied as well. An alternative solution could be the method presented by (Kis, 2013.). The aim of his method is the use of the Fourier-series. The original rough function can be smoothed using the Fourier-series - 10^{th} orders in the original work – and the differentiation can be easily performed using the Fourier-series equations. It offers a simple numerical solution to the problem.

The five-point stencil method uses more collected points and gives normally better results than Newton's method. The original equation of the five-point stencil method for the second derivative is the following:

$$f''(x) \approx \frac{-f(x+2h)+16f(x+h)-30f(x)+16(f(x-h)-f(f-2h)}{12h^2} \qquad \textit{Equation 24.}$$

Where:

$f(x)$	function's value at the given (time) point
h	sampling rate

The mass moment of inertia needed for the inertial torque calculations are not always published by the pumping unit producers. The mass moment of inertia of any equipment can be calculated using the following equation:

$$I = m \cdot r^2 \qquad \textit{Equation 25.}$$

Where:

I	mass moment of inertia of the equipment [kg·m^2]
m	mass of the given equipment [kg]
r	distance from the movement's shaft [m]

The correct solution of Eq. 25. needs integration but good approximation can be achieved measuring the counterbalance's center of gravity from the shaft.

The polished rod torque can be calculated using Eq. 16. and the polished rod load using Eq. 17.

DOI: 10.14750/ME.2019.010

4 ELECTRICAL MEASUREMENTS ON SUCKER ROD PUMPING UNITS

Electrical measurements are still optional only and they are not the main way of sucker rod pumping analysis. The basic sucker rod pumping analysis includes electrical measurements only for proper counterbalancing (Podio, et al., 1994.) and for efficiency calculations. The industry-standard dynamometer systems include electrical measurements only from the middle of the 90's. The biggest Hungarian oil company (and other companies in Hungary as well) applies electrical measurements only for proper counterbalancing and electrical measurements are not a part of the standard sucker rod pumped well analysis. The importance of electrical measurements could be improved using other author's novel techniques described in Chapter 2. or using the methods presented in this Thesis.

4.1 SPECIAL FEATURES OF ELECTRICAL MEASUREMENTS ON SUCKER ROD PUMPING UNITS

Sucker rod pump prime movers are usually connected to a 3-phase power system. Therefore, electrical measurements should include the measurement of the following basic parameters:

- 3-wire voltage (line or phase voltage depending on the network topology) and minimum 2 phase current measurement,
- power factor measurement for power demand determination.

The measurement system should be capable of continuous data acquisition and data recording. The sampling rate depends on the expectations and measurement goals. The conventional dynamometer measurement solution of an industry-standard manufacturer creates final data at a rate of 20 Hz. Higher sampling rate should be used if one wants to use special measurement solutions like (Silva, et al., 2014) who determined the surface dynamometer card from electrical measurements using the rotor slot harmonics analysis. They used a linearized induction motor performance curve: the torque curve in the operational range was linearized using the nameplate data and synchronous speed. They were able to produce the surface dynamometer diagram however they did not publish the overall errors. The induction motor's performance curve linearization works only in cases where the motor is oversized because in well-loaded units the motor can be temporarily overloaded resulting in higher loads than the nominal one. Thus the method cannot be adopted for all sucker rod pumping system analysis and motor models described in Chapter 2. should be used.

The measurement system presented in this chapter was developed to prove the usefulness of the methods presented in this Thesis. Special needs were determined by the application of the measurements:

- all 3-phase electrical data should be presented for further analysis,
- flexible measurement system is needed because of the unconventional measurement needs: speed measurement both at the motor's shaft and at the gearboxes' sheave,
- real-time data recording, data export capability,
- a system which is ready for high sampling rate measurements: high rate measurements are needed to provide the opportunity of combination of the presented methods in this Thesis and other authors, like (Silva, et al., 2014)
- low investment cost.

There was no available measurement system on the market meeting all previously mentioned expectations thus an alternative system had to be invented. There are available solutions for making 3-phase power analysis, but those systems cannot handle speed sensors. A modular, individually programmable unit had to be created to meet all expectations.

4.1.1 *MEASURING SYSTEM HARDWARE DEVELOPMENT*

The final goal of the work would be a method which can infer the dynamometer diagram from electrical measurement only - as discussed earlier. Therefore, a new electrical measurement system must be designed which is capable to deal with the required raw data and provides the proper accuracy. The data acquisition system should be able to measure all electrical parameters (voltage, current, phase angle) and to register them. A speed transducer is also required to prove the system's usefulness in the first stage, at the system validation period. The main objectives of the development are the following:

- the system must work in field conditions (low power requirements, robustness for the harsh environment),
- proper accuracy for the evaluation,
- low cost because of the limited resources with a maximum budget of $1,000 for the measurement system,
- easy access to the SRP system when preparing the measurement,
- the measurement must not have any effect on the well's production rate.

The first step of designing a new measurement system is always the determination of the measurement ranges. The system must be able to measure a three-phase system in three voltage ranges: 230 V/400 V/690 V. The current to be measured for smaller and normal motors is about a few tens of Amps while running and 5-7 times greater at starting conditions. A laptop's USB connector was chosen as the power source for the measuring system. That means a voltage of + 5 V and a max. available current of 500 mA for operating the measurement system. The low voltage power source was a tough limiting factor when selecting the components. All sensors and proposed electrical circuits must meet the basic safety regulations (galvanic isolation) and must be in accordance with the valid electrical standards. Sensors based on magnetic operation are preferred because of the effective galvanic isolation. The sensors, the data acquisition system and other parts of the system were selected according to these guidelines.

The data acquisition system is the "heart" of any measurement system and it is very important for the proper operation. The budget available had a strong influence on the DAQ selection. Seven channels are needed for the measurements: 3-3 for the three-phase voltage- and current measurements and one channel for the speed determination. The only power source used is the USB connector. The best match for our purposes was found in the MCCDAQ 1608 FS-Plus data acquisition system. Its specification is listed in the following (MCCDAQ Inc., 2014.):

- 8 analog input channels ((±10 V, ±5 V, ±2 V, and ±1 V can be selected in the software; 16 bit resolution), 8 digital I/O,
- simultaneous sampling (1 A/D converter per input),
- up to 400 kS/s overall throughput (100 kS/s max for any channel; 800 kS/s in burst mode but only for 32768 sample),
- 1 event counter,
- USB connection, no external power required,
- NI Labview compatible.

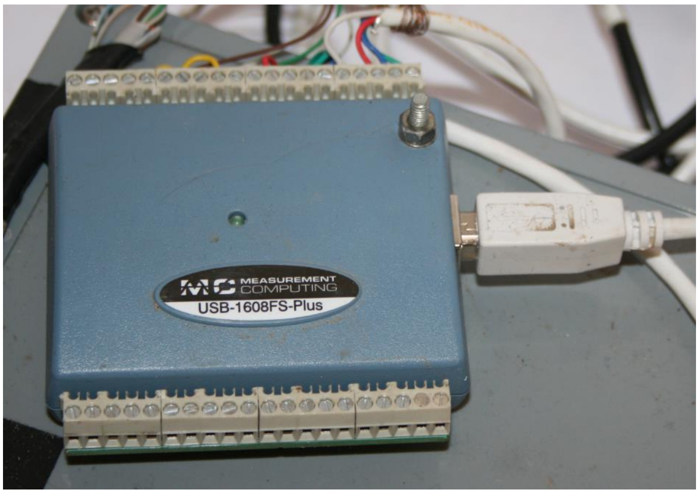

Figure 23. MCCDAQ USB 1608 FS-Plus data acquistion device

The theoretical accuracy of this device is ±0.04% according to the 16 bit resolution. This low cost measurement device seemed to be the best solution for our purposes.

Since LEM PR 200 sensors were already available for the measurement system the current sensor selection had a predetermined solution. The sensor can be seen in Figure 24.

DOI: 10.14750/ME.2019.010

Figure 24. LEM PR 200 sensor

The LEM PR 200 sensor's main parameters are the following based on the current probe's manual:

- non-intrusive current measurement using current probe,
- 20 A/200 A current range,
    - Lower value for small motors while running
    - Higher value for starting conditions
- power source: 9 V alkaline,
- accuracy: ±1 %.

Selection of the voltage sensor was a more complicated task because the voltage measurement had to be transformed into current signals. Different circuits should be prepared for the different voltage ranges. The only electrical current sensor available with the designed accuracy that can work at + 5 V is the Honeywell CSLW series sensor, the Honeywell CSLW40BM. Its main features are the following:

- hall-effect operational principle,
- supply voltage: 4.5-10.5 Vdc (ready for USB powered solutions); supply current: max. 9 mA,
- accuracy: ±1.5 %,
- needs additional sensing circuit,
- current range: ±40 mA.

When comparing the measurement current (~30 mA) with the normal operational current (~10 A) it can be seen that the built-in failure is only about 0.3 %. The sensor needs additional electrical circuit to set the measuring current always at about 30 mA. Use of special measuring resistances is needed, connected in series to the sensor. The measuring resistances have 1.5 % accuracy which is very responsible for those high resistance values. The selected measuring resistances and the actual measuring currents are summarized in Table 8.

Table 8. Measuring resistances and currents

Voltage range	Measuring resistance value	Peak measurement current
230 V_{eff}	10 kΩ	32,5 mA
400 V_{eff}	16 kΩ	35,4 mA
690 V_{eff}	28,2 kΩ	34,5 mA

The schematic of the electrical circuit is presented in Fig. 25. The switches (S1; S2; S3) are used to select the actual measuring line. The measuring wire can be connected to the board and to the data acquisition system using connectors. The measurement system can measure star and delta network configuration as well. The neutral point (referred as “N (high voltage)” in Figure 25. can be connected to the neutral line in wye network configuration and to the common reference line using the two-wattmeter method in delta network topology. Special attention should be given to the measurement ranges in delta connection because the measured voltages are line voltages.

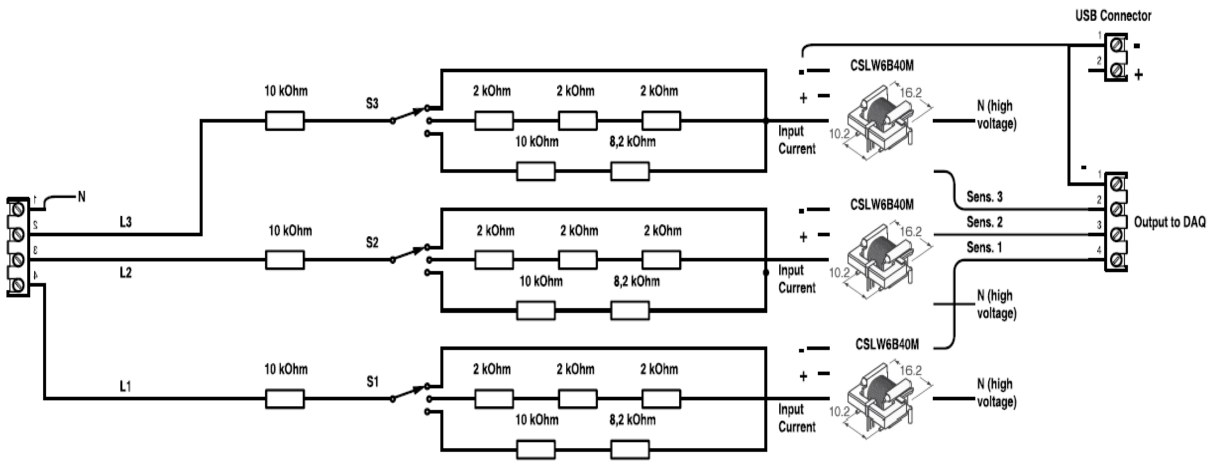

Figure 25. Measurement circuit for the different voltage ranges (star connection)

The invented voltage sensor is shown in Figure 26. The Voltage sensor consists of a box and flexible measurement cable can be used to connect the necessary terminals to the measurement points.

Figure 26. The voltage sensor with the selection buttons

The speed sensor is a simple photoelectric sensor (Omron EE-SY310) that produces one signal per reflection. The actual speed can be calculated by counting the signals. The most important features of the sensor are the following (OMRON, 2009):

- reflective type photo sensor;
- the wide supply voltage range (4.5-16 V DC) fits for the given purposes: the computer's USB port can drive the system or a 9 V alkaline when using more than one sensor;
- recommended sensing distance is 5 mm.

A reflective paper layer should be stuck to the gearbox's and motor's belt sheave and the sensor will be mounted on the motor and gearbox using a special, adjustable holder. The advantage of using a photoelectric sensor is the low current consumption, the easy installation of the reflective layer and the possibility to increase the speed measurement accuracy. The reflective paper contains a sticker and the cheap paper can be stuck on the required surface i.e. on the sheaves as well. The speed measurement accuracy can be increased using more stickers evenly distributed on the periphery of the sheaves. However, experience has shown that in real field conditions there is normally not enough space to stick more than one sticker on the shaft. The photoelectric sensor needs additional electrical circuit as well: one current limiter resistor connected in series to the photodiode and a sensing resistor to produce the necessary Voltage ramps in the measured signal. The resistors are sized according to the manufacturer's guidelines (OMRON, 2009).

DOI: 10.14750/ME.2019.010

4.1.2 DATA ACQUISITION SOFTWARE DEVELOPMENT

The software used to analyze the measurement results is probably more important than the hardware presented in Chapter 4.1.1. The software allows the user to detect signals and evaluate the measurement results. The software should guarantee a user-friendly and easy to use environment. The software should meet the following basic requirements:

- 3-phase electrical data should be measured, conditioned and recorded,
    - real-time data recording, data export capability,
    - effective values, power factor, real power should be calculated
    - tools for calibration are needed,
    - absolute timestamp to the measured points to make possible the comparison of the calculated data and dynamometer measurement done in the same time,
- evaluation section
    - the software should be able to convert electrical data into torque data
    - induction motor parameter estimation algorithm should be included as well,
    - well- and pumping unit data (API standardized list) should be available in the software.

The data acquisition system (MCCDAQ 1608 FS Plus) supports many programming languages, like C, C#, VB.net, Android, Labview. The correct selection of the original data acquisition software is important. All programming languages have some advantages and disadvantages as well. The final selection was the Labview programming environment.

The NI "Labview (Laboratory Virtual Instrument Engineering Workbench) is a graphical programming language that uses icons instead of lines or text to create applications" (National Instruments, 2014.). The Labview software uses "virtual instruments" which are responsible for one easy or complicated task, moreover, in-build express Vis can be found in the software to solve special problems. The graphical programing language is easy to use but heavily restricts and limits the programmer's freedom. The first implementation was to build the total system in Labview environment. The high sampling rate and the continuous saving- and analysis resulted computer-consuming algorithms which were impractical to run on a single notebook that is necessary at field conditions.

The final decision was to program the data acquisition system in Labview and to export the data into .txt files for further analysis. The resource demand of the software can be reduced using this solution because the data acquisition and evaluation is done at different times. The source code can be found in the Appendices in graphical form, divided into subsystems because unfortunately zooming does not work in the Labview environment. The operation of the software is explained using the flowchart presented in Figure 27.

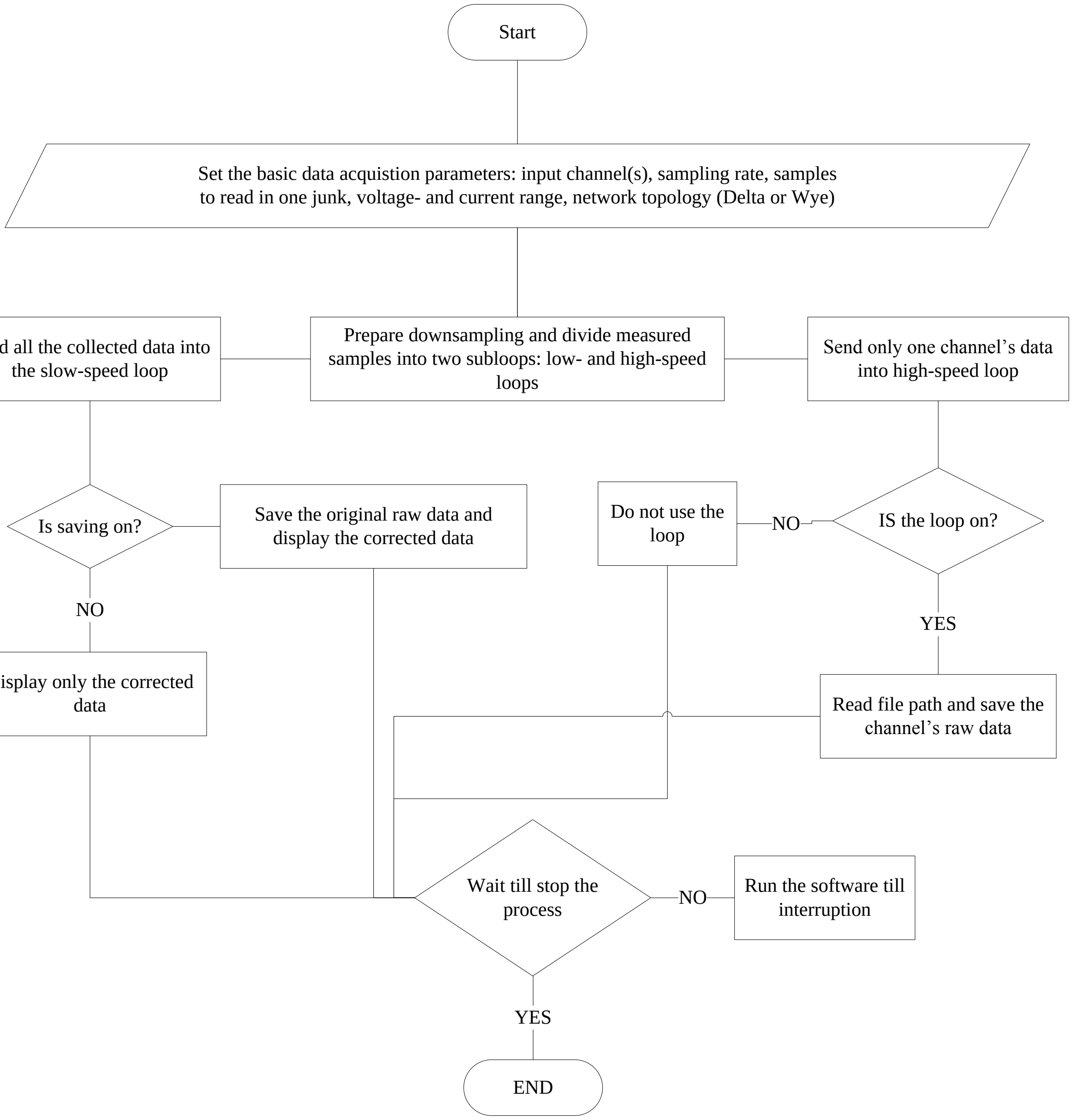

Figure 27. Flowchart of the data acquisition algorithm

The data acquisition parameters can be set in the first section of the software. The user can select the different input channels of the DAQ board. 8 channels are available: 3-3 channels for the voltage- and current measurement and 2 channels for the speed measurement. The sampling rate is important for the accuracy and robustness of the system. The basic rule of sampling theorem defines the minimal sampling frequency as the double of the highest frequency to be measured (Shannon's law in the English nomenclature). The correct voltage- and current range and network topology is important for the real-time display where the measurement setting can be checked while continuous measurement.

A special algorithm construction was chosen to ensure the capability of the high rate measurements: the producer-consumer pattern. There is a producer loop in this pattern that is responsible for the data collection and the data will be put in this loop into a special data type, into a queue. The data collection means the communication with the DAQ board. Different data can be selected to be sent into the queue. The queue contains the chosen measured data with time stamp. The production-consumer pattern provides the highest sampling rate because the data acquisition and basic processing tasks are done at different times and the computer's resources can be used at a higher level. The data are sent in basically 1000 sample long packages, but the length is software controlled as well. There can be more than one consumer loops making the signal processing faster. Two consumer loops and two different signals in two different queues were used for our purposes to produce a low speed loop (with data collected from all channels) and a high-speed loop (with data collected from only one current channel). The high-rate input signals are downsampled for the low-speed loop. The downsampling rate can be set by the user: only every i^{th} sample is sent to the queue and the rest will not be used. The collected data can be saved at a higher rate owing to the producer-consumer pattern on a relatively lower performance computer (a notebook).

The low-speed loop is used to save the data for later power- and performance analysis while the high-speed loop is used to measure the data for a potential rotor slot analysis. The data are saved into .txt files that can be used in different software for later analysis and the file path can be selected according the user's choice.

4.1.3 Data processing software development – the electrical section

The data analysis and evaluation are done using MS Excel software with the author's algorithms written in Excel VisualBasic. The Excel VisualBasic programming language has important advantages for data analysis: the Excel's spreadsheet-form for data storage can be used with the opportunity to write individual algorithms. The source code of the software can be found in the Appendices. It has four main parts: electrical analysis, speed determination, motor parameter estimator and torque calculator. The operational principles of the electrical measurements are discussed firstly and later the speed measurement. The motor parameter estimation and torque calculation were described in the previous chapters.

The data analysis can be performed after the data is imported into the spreadsheet file. The data just imported can be evaluated using a macro. The data analysis algorithm's flowchart can be seen in Figure 28. The sensors create voltage signals which should be converted into the appropriate unit. The measurement range is important in the signal conditioning section: different constants belong to the different measurement ranges both in case of current- and voltage measurement. The proposed software merges all algorithms and methods presented in this Thesis hence motor parameter estimator section, torque calculation section, surface dynamometer graph determination section. All measurement parameters and well data should be given in the software's input section containing the following information:

- motor nameplate data (current, power, power factor, starting current);
- well data (well name, well depth, production rate, annular pressure, fluid specific gravity, pumping unit);

DOI: 10.14750/ME.2019.010

- measurement information (measurement ranges, sampling rate, network configuration).

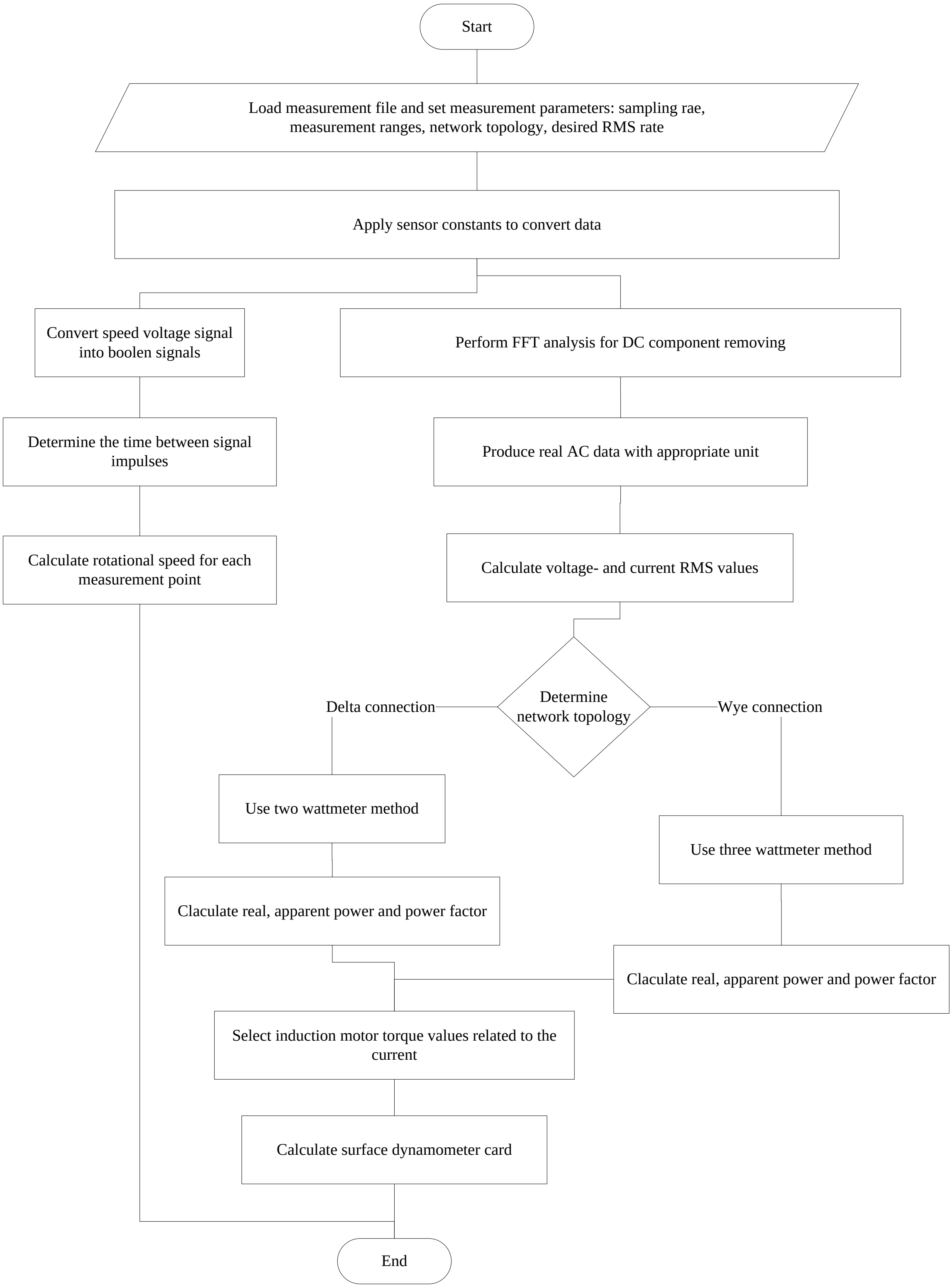

Figure 28. Data processing algorithm

The sensor used to measure the voltage signal (CSLW6B40M) applies ~+2.5 V as its reference voltage. The ~2.5 V is a DC offset noise in the measurement results that should be removed. The reference voltage changes with temperature, humidity, etc. and should be compensated. The current sensor (LEM PR 200) is equipped with zeroing equipment however the software can remove the DC component from the measured signal as well. The first section of the software can remove the DC component and calculate the RMS values of the measured voltage- and current signals.

The DC removal section's main idea is the usage of the Fast Fourier Transformation (FFT). The FFT can produce the frequency domain of a given signal and a built-in function is available in the MS Excel software to perform FFT analysis. The function can be run only from the spreadsheet hence the VBA code uses the cells to run the FFT analysis. The frequency domain contains the zero-frequency component as well and the actual DC offset can be removed using the just determined value. It is assumed that the DC offset is constant during one analysis (~1-5 minutes) and the value is recalculated only at the next measurement. The sensor constants can be applied when the DC component is removed from the signal. The final result is the clear AC sine waves of the current and voltage.

The root mean square values of the current and voltage need to be calculated because the RMS values should be used for apparent power calculation and for the motor torque calculation as well. RMS values are calculated using the following formula:

$$x_{RMS} = \sqrt{\frac{1}{n} \cdot \sum_{i=1}^{n} x_i^2} \qquad \textit{Equation 26.}$$

Where:

x_{RMS}	current- or voltage RMS value [A] or [V]
n	number of samples included in the RMS calculation
x	measured current- or voltage data [A] or [V]

The number of samples included in the RMS calculation can be set by the user in the software and the only restriction is that it should be an integer where the RMS frequency is divisible by the sampling rate. The network topology will set the course for the further calculations.

The three-wattmeter method is used to calculate the real power, apparent power and power factor in a 3 phase 4 wire network (star network topology). Each individual phase current and voltage is measured, and the total three-phase power is calculated as the sum of the measured power values and the power factor as the average of the three different power factors. The real power can be calculated as the average of the instantaneous power (National Instruments, 2014.):

$$P = \frac{\sum_{i=1}^{n} i_i \cdot u_i}{n} \qquad \textit{Equation 27.}$$

Where:

P	real 1-phase electrical power [W]
n	number of samples included in the power calculation
i	measured (raw) current value [A]

u measured (raw) voltage value [V]

The apparent power can be calculated as the average of the product of the RMS values (National Instruments, 2014.):

$$Q = \frac{\sum_{i=1}^{n} I_i \cdot U_i}{n} \qquad \textit{Equation 28.}$$

Where:

Q	1-phase apparent power [VAr]
n	number of samples included in the power calculation
I	effective current [A]
U	effective voltage [V]

The power factor can be calculated as the quotient of the real- and apparent power (Uray & Dr. Szabó, 1998):

$$PF = \frac{P}{Q} \qquad \textit{Equation 29.}$$

Where:

PF 1-phase power factor

The three-phase real power and apparent power is the sum of the three individual phase powers. The 3-phase power factor is the average of the three individual phase power factors.

The two-wattmeter method is used in delta network connection. Theoretically the three-wattmeter method could be used as well however it is impossible to perform a field measurement according to the three wattmeter-method: the phase current could be measured only inside the load. The two-wattmeter method measures the line current in two lines and the voltage between the third line and the given two lines. So, if the current is measured in L1 and L2 than the voltage should be measured between L1-L3 and L2-L3. The real (instantaneous) power can be calculated as the sum of the product of the measured current- and voltage values (Gatheridge, 2012.):

$$P_{3phase\Delta} = \frac{\sum_{i=1}^{n} i_{1i} \cdot u_{1i}}{n} + \frac{\sum_{i=1}^{n} i_{2i} \cdot u_{2i}}{n} \qquad \textit{Equation 30.}$$

Where:

$P_{3phase\Delta}$	real 3-phase electrical power [W]
n	number of samples included in the power calculation
i_1 and i_2	measured (raw) current in the two phases L1 and L2 [A]
u_1 and u_2	measured (raw) voltage between the reference phase (L3) and the measured phases (L1 and L2) [V]

The apparent power can be calculated similarly to the previous cases only a constant is changed in the equation (Gatheridge, 2012.):

$$Q_{3phase\Delta} = \frac{\sum_{i=1}^{n} I_{1i} \cdot U_{1i}}{n} + \frac{\sum_{i=1}^{n} I_{2i} \cdot U_{2i}}{n}$$ *Equation 31.*

Where:

$Q_{3phase\Delta}$	3-phase apparent power [VAr]
n	number of samples included in the power calculation
I_1 *and* I_2	effective current in the two phases L1 and L2 [A]
U_1 *and* U_2	effective voltage between the reference phase (L3) and the measured phases (L1 and L2) [V]

The power factor can be calculated as the quotient of the real- and apparent power, according to Eq. 29.

4.1.4 Data processing software development – the speed measurement section

The speed calculation is a different section in the algorithm from the electrical data processing. The speed sensor creates a signal at each revolution or according to the number of reflective layers. The time should be measured between the different impulses and then the rotational speed can be calculated. The field measurements have shown that the speed sensor created really low noise/signal ratio signals. The normal impulse amplitude was only a few millivolts. The reason of the bad quality signal was the 35 m long cable which was necessary to reach the wellhead from the switchbox. The low voltage power source, the long cable, the imperfect spacing of the reflective paper and the harsh environment while measuring caused high noise and hardly detectable impulses. The signal was derived to increase the status changing points detectability using the five-point stencil method according to the following equation:

$$f'(x) \approx \frac{-f(x+2h) + 8f(x+h) - 8(f(x-h) + f(f-2h)}{12h}$$ *Equation 32.*

Where:

$f(x)$	function's value at the given (time) point
h	sampling rate

After the signal conditioning the time is calculated between the first positive signs and the other will not be used. The actual speed can be calculated from the time difference. The first detection will contain no information because there is no reference point for the time calculation. The period length where the speed values will be averaged is fitted to the RMS section's cycle. The measurement result is a speed value for each current- and power sensing points ready for further usage in the sucker rod pump analysis.

DOI: 10.14750/ME.2019.010

5 INFERRING DYNAMOMETER DIAGRAMS BASED ON ELECTRICAL MEASUREMENTS

The conventional well supervision techniques were described in Chapter 3.2. The weaknesses of the commonly used procedures were explained as well. A new method was invented to overcome those weaknesses and to create a cheap and effective solution for everyday well supervision.

The well-supervising cost could be dramatically decreased using easier and cheaper equipment to analyze sucker rod pumped wells. Easier measurement could be electrical measurement only and the surface dynamometer card could be inferred from the electric measurements. The proposed model is the summary and conclusions of the research presented in this Thesis. The block diagram of the proposed techniques can be seen in Figure 29.

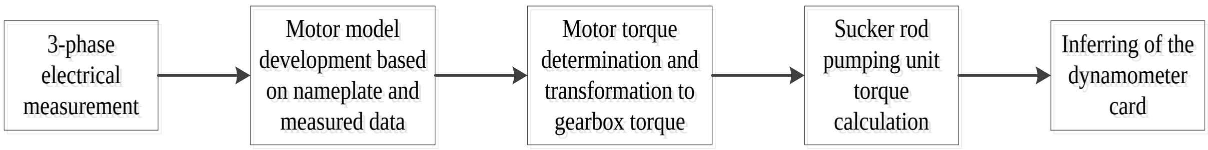

Figure 29. Proposed model milestones

The 3-phase electrical measurement can be done using power analyzer to measure current and power. The data should be available at a minimum rate of 15-25 Hz and ready for computer applications. A cost-effective measurement system was developed in Chapter 4. The conventional dynamometer measurement is done at 20 Hz data acquisition rate according to the Echometer company (Echometer, 2017.). Similar rates are satisfactory for any new measurement method as well. The actual final sampling rate should depend on the pumping speed: higher speeds need higher sampling frequency to infer the dynamometer diagram. The system can be easily, and cost effectively improved to a remote supervision system when using power analyzers ready for wireless communication (GPRS or similar).

Motor models can be developed according to Chapter 2. An accurate motor model is necessary to build such applications. The torque calculation procedure for reversed calculation direction is fully described in Chapter 3.4.1.

The inferred dynamometer card can be analyzed using conventional techniques. The author’s experience has shown that the basic shape of the dynamometer cards is identical to the original conventionally measured ones and the magnitude of the loads can be inferred as well. However, the most important result is the shape of the dynamometer card to detect any operational failures.

The proposed model was tested on operating sucker rod pumped wells to prove its usefulness. The field measurement procedure begins with data collection. All conventional data are needed as for the normal dynamometer measurement and some additional information as well. The motor -and electrical network data are necessary for the motor torque – and current characteristics.

The necessary well data are the followings for a thorough well analysis:

- well name for identification,
- liquid production rate, perforation depth, fluid specific gravity and dynamic liquid level for efficiency calculations,
- pumping unit data for the torque calculation:
    - API standard unit type,
    - rotational direction and pumping speed,
    - accurate counterbalance weight and position, stroke length,
    - gearbox data and transmission ratio,
    - structural unbalance and mass moment of inertia of rotary equipment and mass moment of inertia of alternating equipment.
- motor data for the given parameter estimation method,
- data acquisition system data:
    - sampling rate,
    - upstroke starting time,
    - number of samples to be analyzed.

Those data are hard to obtain in conventional, old installations like most of the stripper wells. Some data can be measured at the field, like the pumping unit geometrical arrangement and production parameters, however some other data must be estimated. Structural unbalance and mass moments should be basically published by the pumping unit manufacturers. Unfortunately, data on pumping units working in old installations are often unavailable. Such data should be estimated. The easiest way is to find a similar pumping unit available in published catalogs and use those in further calculations. Actual counterbalance weight should be assumed as well but measuring their dimensions makes estimations possible.

The upstroke (or downstroke) starting time is important for timing the data processing algorithm. The motor current data does not contain any significant sign for the pumping unit's position and the torque calculation can be done only if the actual crankshaft angles are known. The upstroke's starting time can be measured using a simple push-button in the measurement system (easiest solution) or using position transducer at the shaft. The speed measurement system described in Chapter 4.1.4. can be used for such purposes as well. The reflective layer should be mounted on the counterbalance and the position can be detected.

5.1 THE NEW MODEL'S APPLICATION

The field measurements started with data collection. There were always inaccessible data during the field tests. The only solution remained: the pumping unit's geometrical arrangement and the counterbalance position were measured, and the mass moment of inertias were taken from similar pumping unit catalog's data. Table 9. contains the necessary data for the further calculation in case of a 7-SZK7-3,5 pumping unit. The method was tested on more wells but only one will be discussed in detail to follow on the model's steps and prove its effectiveness.

Table 9. Pumping unit data (all abbreviations according to the conventional API standards)

Parameter	Value	Unit
Pumping unit type:	7-SZK7-3,5 C API code:347-176-138	
Rotational direction:	CCW	
Counterbalance weight:	750	kg
R position:	R3	
Counter balance position R1-R2-L1-L2	0.38	m
Stroke length:	243	cm
Speed:	6.7	SPM
Motor sheave diameter:	240	mm
Gearbox sheave diameter:	910	mm
Gearbox transmission ratio:	38.39	1:x
SU	149.930422	kg
Mass moment of inertia of rotary eq.	3901.7859	kg*m2
Mass moment of inertia of alternating equipment	4640.70964	kg*m2
A:	3.50012	m
Calculated stroke length:	243.8906115	
Overall transmission ratio:	145.5620833	1:x
Average motor RPM:	975.2659583	RPM
Counterbalance torque (without crank)	11400	Nm
Crank torque:	14346.68355	Nm
Maximal counterbalance torque	25746.68355	Nm
Crank effective length	1.8	m
Crank width	0.575	m
Crank height	0,2	m

The data collection should continue with the motor data. Table 10. contains the motor data. The 3-phase power analysis can help to find out the necessary but missing motor data as well. Starting current and magnetizing were measured as discussed in Chapter 2. It can be seen on the data that the motor was a normal 2-pole industrial Ex-prove motor. However, the pumping unit was an old installation and neither NEMA-code nor other additional data were available about the motor. The motor's speed-torque and speed-current characteristics were obtained using two different methods: using the linearization of the curves between the nominal data and the synchronous speed data (similar to the solution of (Silva, et al., 2014)) and using the accurate motor model presented in Chapter 2.4.3. The motor was an old construction and its nominal Voltage according to the nameplate is 380 V. But the motor is operated through a 400 V network, so the parameter estimation was done using the nominal Voltage and the actual speed and torque were calculated using the 400 V Voltage level.

DOI: 10.14750/ME.2019.010

Table 10. Motor nameplate data (complemented with measured data)

Motor parameter name	Value	Unit
Connection:	DELTA	
$U_{nameplate}$	380	V
$I_{nameplate}$	33	A
$P_{nameplate}$	16	kW
$\cos\varphi_{nameplate}$	0.81	
I_{start} (measured)	166	A
$I_{magnetizing}$ (measured)	15	A
$N_{nameplate}$	975	RPM
$\eta_{nameplate}$	91	%
Synchronous speed	1000	RPM

The measured power and current with the start-up procedure can be seen in Figure 30. The x-axis contains the sample numbers where one sample number equals 0.0625 sec (16 Hz sampling rate). It can be seen that the motor is drastically underloaded. The motor current reaches the nominal value only at the peak loads which leads probably to low efficiency.

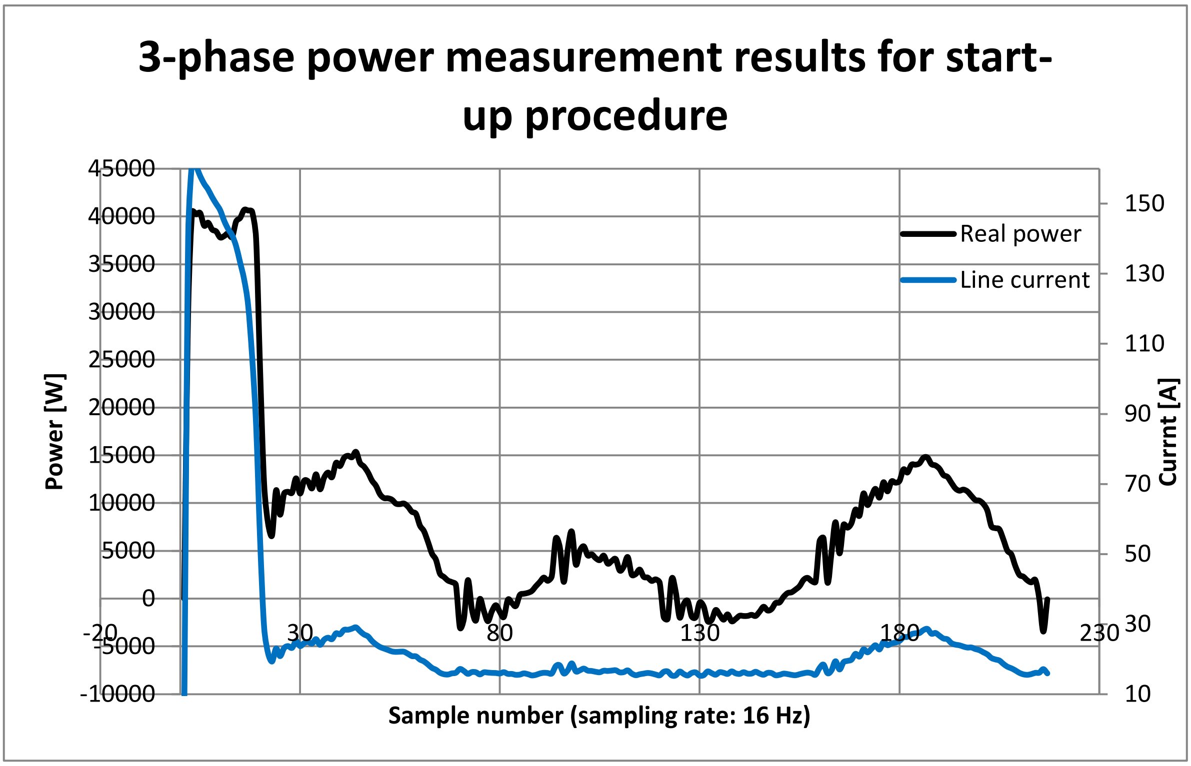

Figure 30. 3-phase power measurement results for start-up procedure and 2 cycles

Figure 31. shows the motor speed and torque for the same cycles, both the easy model (linearization between the nominal values and the synchronous value) and the complex motor model's calculation according to Chapter 2.4.3. are indicated.

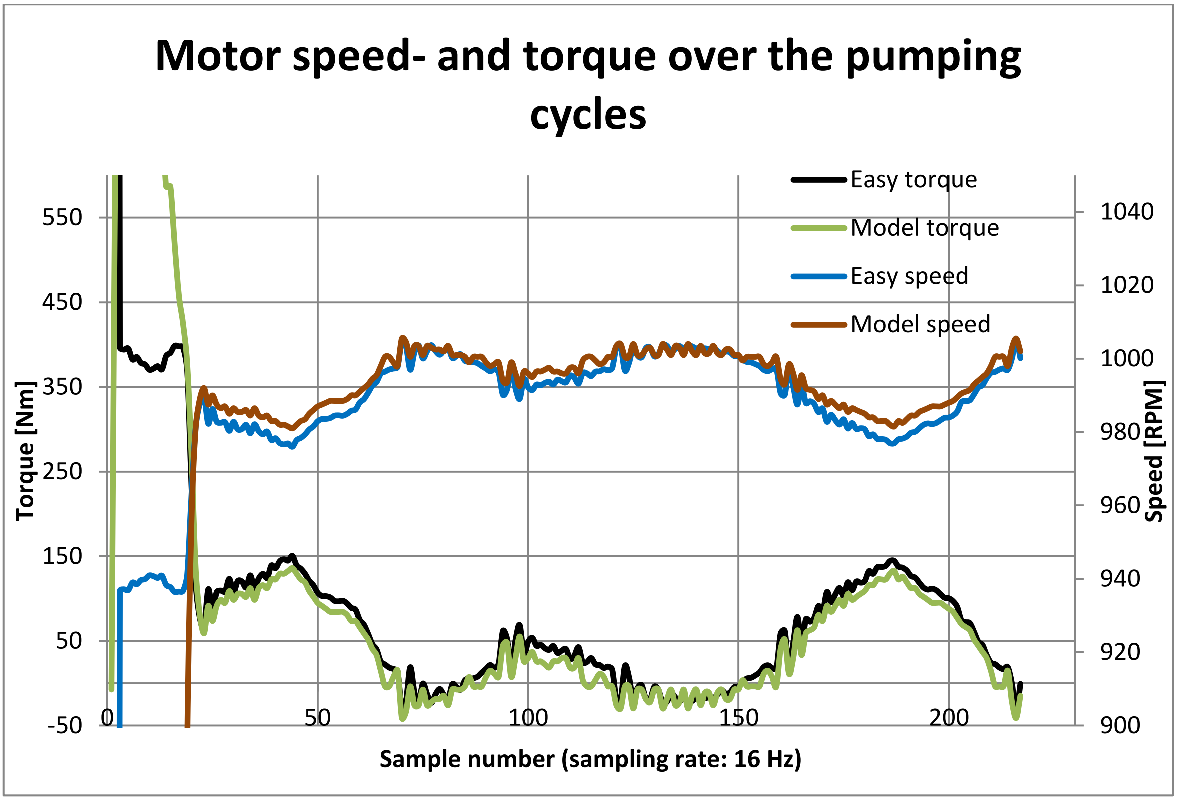

Figure 31. Motor speed and torque cycle

The speed values are assigned to the current values using a look-up table. The resolution if the look-up table was 0.5 rpm. The weaknesses of the easy solution used by (Silva, et al., 2014) can be seen at the starting procedure: smaller speed values than the nominal speed are inaccurate. The problem caused by this phenomenon is not as important in this case than by well-loaded motors: the motor was never overloaded in this well. However, the method presented by (Silva, et al., 2014) is not able to estimate the torque values at all working conditions. The use of the complex motor model has its advantages: the motor's torque can be inferred at any conditions. The big fluctuation on the speed- and torque is the result of the fluctuating current. The use of a smoothing process – Fourier-series - can overcome that problem.

The reversed torque calculation method described in Chapter 3.4.1. can be applied using the just calculated motor torque-time function. 90% surface system torque conversion efficiency was used for the calculations. The inertial effects were included in the calculation. Figure 32. shows the torque components during one pumping cycle.

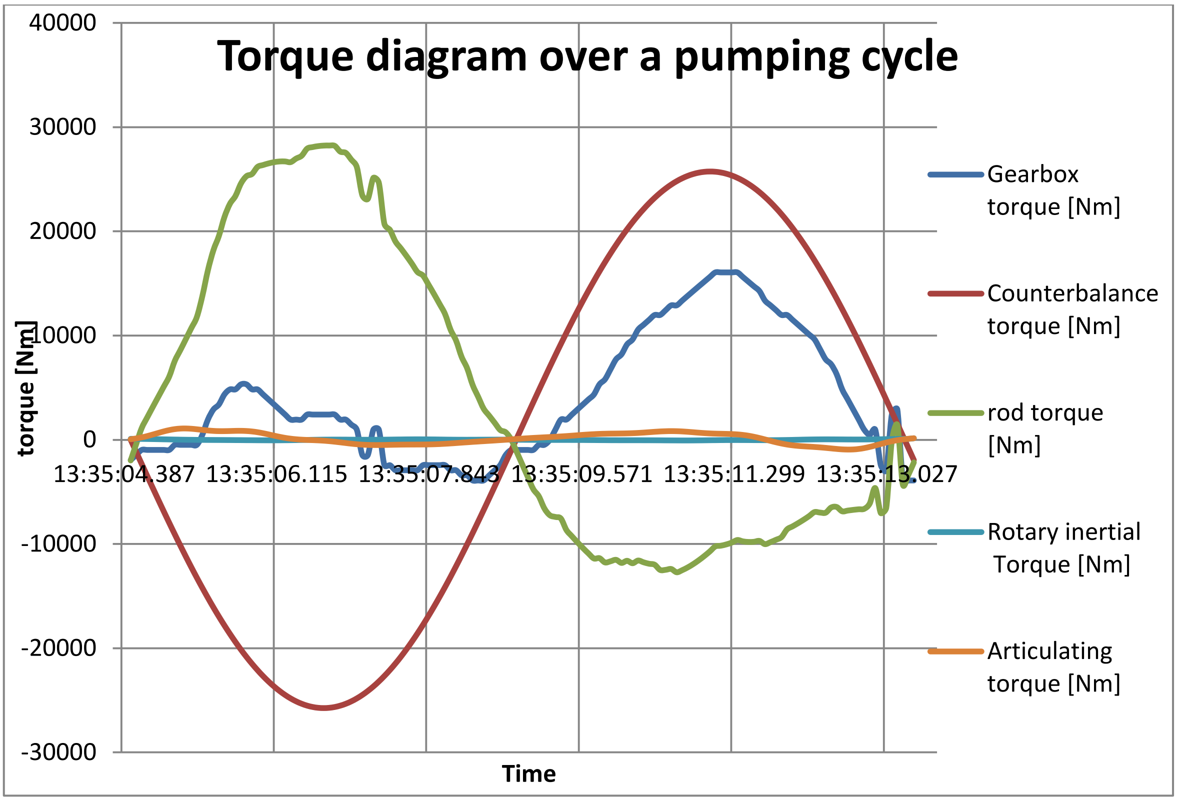

Figure 32. Torque diagram inferred using the new method with complex motor model

The dynamometer diagram can be obtained according to Eq. 17. from the rod torque-time function. The obtained dynamometer diagrams can be seen in Figure 34. The easy upstroke and downstroke refers to the simple, linearized motor model and the model upstroke and downstroke refer to the values obtained by the complex motor model. The shape of the dynamometer diagram is identical to the one measured using convention dynamometer measurements shown in Figure 33. The same result can be evaluated from the inferred and measured cards: travelling valve is malfunctioning. The cards are surface cards but the pump setting depth was not deep and because of the moderate pumping speed the dynamic effects are not so important in this well.

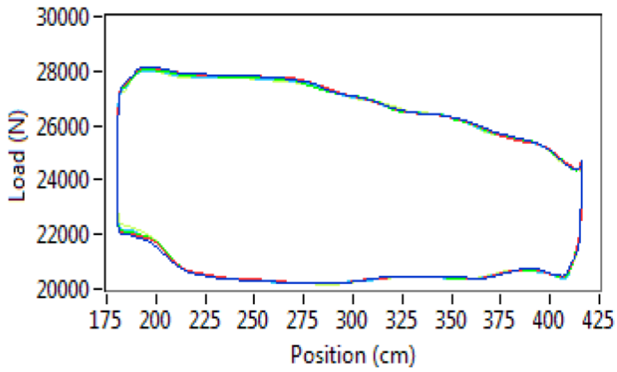

Figure 33. Conventionally measured dynamometer card

The complex motor model gave better results in the amplitude of the rod loads than the simple one. The most critical sections are the ends of the strokes: the torque factor tends to zero and according to Eq. 17. the torque factor is in the denominator in the reversed torque calculation. The mass moments of inertias were taken from similar pumping unit's catalog data that increases the inaccuracy at the end of the strokes as well. The same was obtained earlier by (Gibbs & Miller, 1997.) however, they neglected 30-35°crank angle close to the end of the strokes. Figure 34. shows a calculation where only the last 5° is not plotted! The new measurement and calculation methods generate more reliable and robust calculations than the previous attempts.

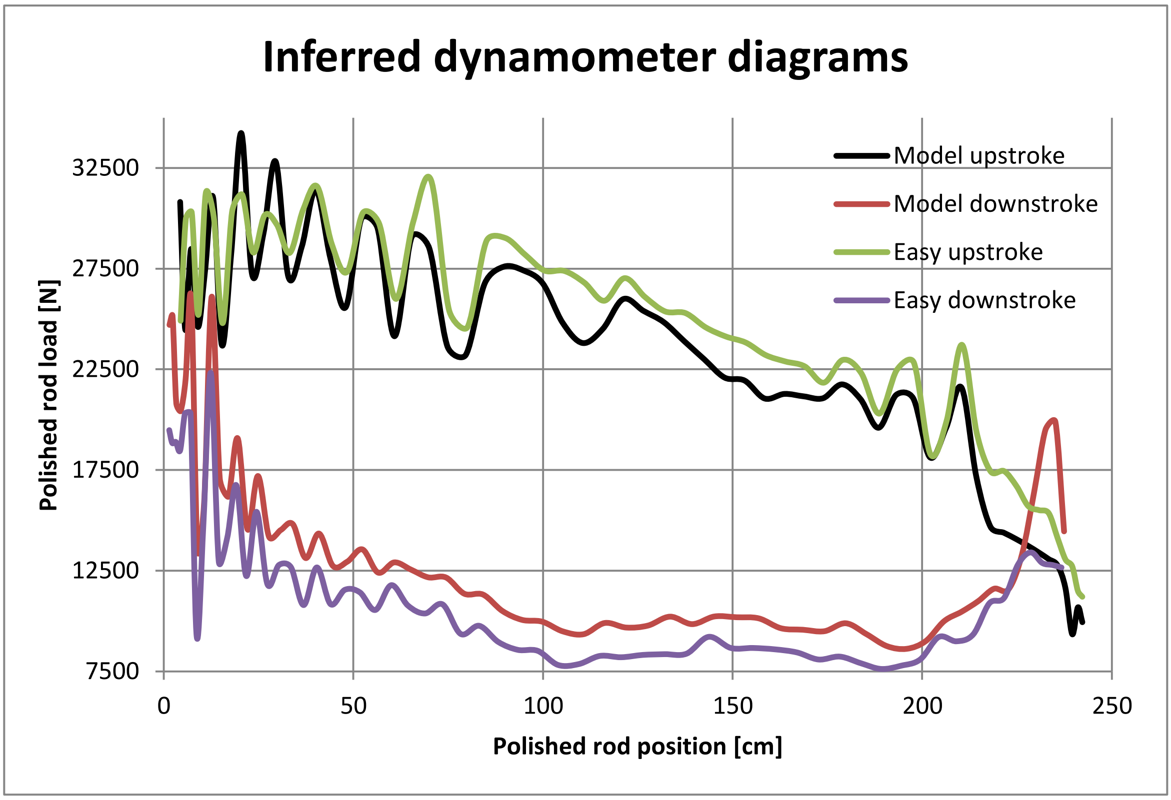

Figure 34. Inferred dynamometer cards

The inferred card's quality can be improved applying a smoothing filter at the main current function. A 10th order Fourier-function was used to remove the stochastically fluctuating section from the function. The smoothed dynamometer card obtained by the complex motor model can be seen in Figure 35. The figure shows good agreement with the conventionally measured dynamometer card.

The methods presented in the Thesis were applied in this chapter to a well's analysis and the results show the effectiveness of the developed calculations and motor model estimations.

DOI: 10.14750/ME.2019.010

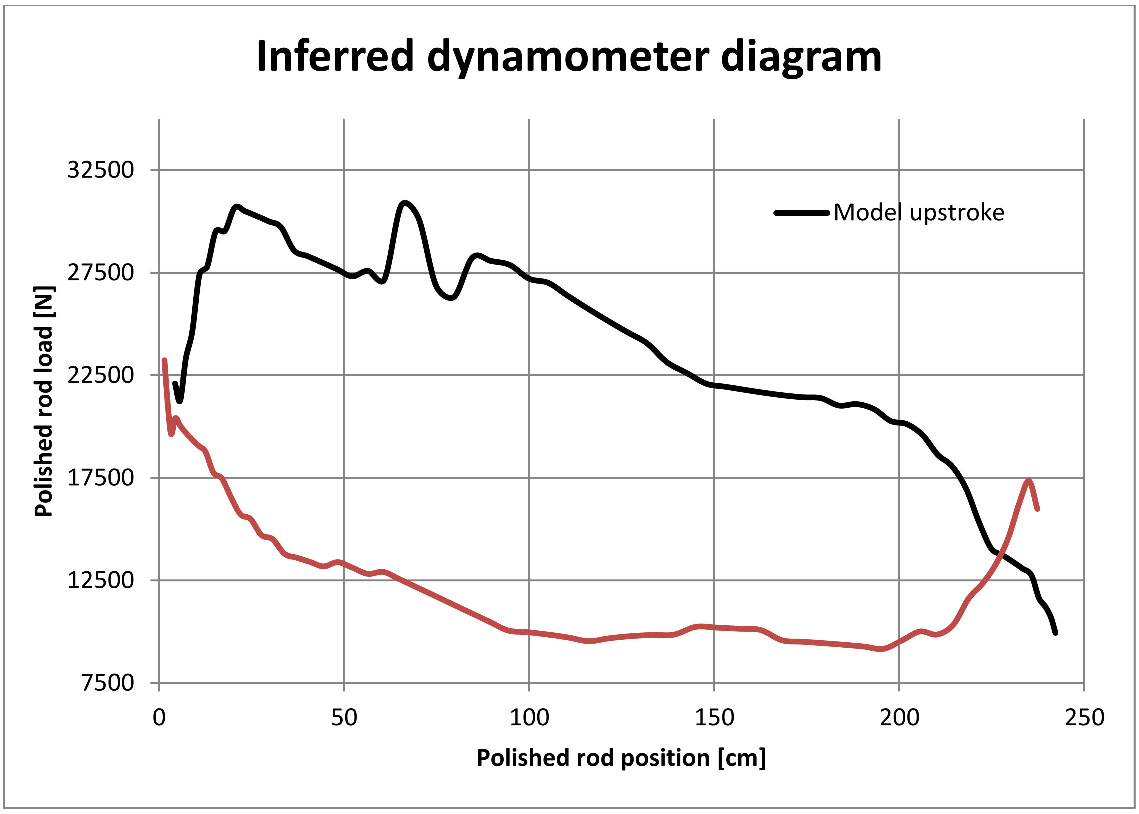

Figure 35. Dynamometer card calculated by the proposed model after data filtering

DOI: 10.14750/ME.2019.010

6 NEW SCIENTIFIC ACHIEVEMENTS

New scientific results found through the research are presented in this chapter. The theses are listed in the order of the appearance in the Thesis.

6.1 THESIS #1

I developed a new empirical correlation for high-slip motor efficiency determination. The empirical correlation is based on the analysis of 28 different high-slip motor's characteristic curves. The maximal efficiency of high-slip motors can be approximated using the following empirical equation:

$$\eta_{max} = 2.5779 \cdot ln(P_{ref}) + 61.124$$

Where P_{ref} is the mechanical power of the given motor referenced to a special speed between the nominal speed and the synchronous speed. The average absolute error of the equation was found to be 1.86% on the investigated motors.

6.2 THESIS #2

I developed a new method to determine the full speed-efficiency characteristics of electric motors. The method is based on using of the empirical correlation presented in the Chapter 6.1. Efficiency approximation using empirical correlation is important because the widely used parameter estimation algorithms (Pedra, 2008.) unfortunately cannot create a reliably one especially not for high slip motors.

The maximal efficiency value can be used to develop the full speed-efficiency characteristics approximating the first section (for lower speeds than the nominal speed) of the performance curve with a linear line crossing the nameplate data and determining the maximal efficiency speed

The maximal efficiency point-synchronous speed-efficiency region was divided into two subsections. The data analysis has shown that the speed-efficiency characteristics can be reconstructed using a given efficiency reduction. 16% reduction in efficiency was found at a speed of 1164 rpm for the investigated motors and a 50% reduction at a speed of 1187. The efficiency conditions of high-slip motors used in sucker rod pumping can be approximated using my empirical correlation. Previously only the measurements of those characteristics were available.

6.3 THESIS #3

A new method was developed for sucker rod pumping system's part efficiency determination that is more accurate than previous models (Echometer, 2017.). The method is based on the newly developed speed-efficiency motor characteristics. The speed-torque characteristics are presented using the motor model and parameter estimation described in Chapter 2.4.1. Then an efficiency value is assigned to all available measured results over the pumping cycle and the motor's average overall efficiency in one pumping cycle can be determined. Using my new method, all part efficiencies can be accurately computed when the motor's efficiency is calculated for a full period.

6.4 THESIS #4

I proved that similar parameter estimation methods which are conventionally used for NEMA-B motor parameter estimations can be modified to model the high-slip or NEMA-D motors. I proved that the magnetizing current can be used as a strong constraint instead of the breakdown torque in such calculations.

The parameter estimation procedure for NEMA D or high slip motors is different than for conventional industry-standard NEMA B motors. The equivalent circuit parameter estimators use different input parameters to identify the physical values of the given basic electric elements (Lindenmeyer, et al., 2001.). The breakdown torque plays an important role in those parameter determination procedures (Pedra, 2008.) however NEMA D or high-slip motors do not always have breakdown torque. The breakdown torque – as an important optimization limit - can be replaced by magnetizing current for conventional numerical optimization methods. The use of magnetizing current makes it possible to build a well-defined numerical problem for the parameter estimation optimization procedure, as described in Chapter 2.4.2.

6.5 THESIS #5

I created a new, CPSO-S-based algorithm for high-slip or NEMA-D motor parameter estimation. The algorithm is strong and robust, and I proved that it can successfully be used for general prediction of the asynchronous motor's speed-torque and speed-current characteristics. The method is presented in Chapter 2.4.3.

6.6 THESIS #6

I implemented the available torque calculation methods (Takács, et al., 2016.) for reverse torque calculation. The torque conditions in the sucker rod pumping system are calculated normally from the polished rod and the different gearbox-torque components are determined for system analysis. I proved that the calculation's direction can be changed, and the polished rod torque can be determined. The previous attempts to calculate into the inverse direction neglected the last 30-35° crankshaft rotation angles at the end and start of strokes causing only ~240° useful information. The reason behind this phenomenon is the torque factor: it is a denominator in the calculation thus the accuracy is limited at the end

DOI: 10.14750/ME.2019.010

of the strokes. My procedures can calculate over 330-340°crankshaft angles so the accuracy is highly increased.

6.7 THESIS #7

I proved that the dynamometer diagram can be inferred using my newly invented accurate motor model, the reversed torque calculation procedure and numerical calculations presented in this Thesis. The inferred dynamometer cards are ready for further applications like evaluation and pumping system failure detection.

6.8 THESIS #8

The dynamometer diagram based on basic electrical measurements has fluctuating curves which makes their evaluation complicated. I suggested to use a filtering algorithm (Fourier-series) to smooth the curves and the result is a much better understandable dynamometer diagram. All new scientific achievements and methods presented in this Thesis make it possible to build dynamometer measurement systems based only on electrical measurements. The use of this approach opens new opportunities in stripper well supervision.

DOI: 10.14750/ME.2019.010

7 SUMMARY

Rod pumping is a mature and well-known production method and the long history of rod pumping provided enough time for petroleum (and other mechanical) engineers to invent and optimize the technology. However, there are always new ways to improve the existing system. In this Thesis, the sucker rod pumping system was analyzed from a quite new point of view: from the motor's side. The energy flow in the system flows from the motor hence it is straightforward to find methods for describing the system from that direction. The conventional methods use dynamometer measurements and the system analysis is based on dynamometer card analysis. This Thesis presents solutions to describe the pumping unit's actual loads started from the motor's power source.

The research was done to prove that the system can be analyzed based only on electrical measurements. A comprehensive literature review in the field of asynchronous modeling was done first and new scientific achievements were presented. I invented a new empirical method for NEMA-D or high-slip motor efficiency prediction over the full speed range. I implemented the conventional induction motor parameter estimation methods for high-slip motors and showed that the conventional limiting factor, the breakdown torque can be replaced using a better limiting factor which fits to sucker rod pumping system measurements. I coded a new, robust algorithm for high slip motors and showed how to apply the algorithm for parameter estimation procedures.

The research's main goal was achieved, and dynamometer diagrams were developed based on electrical measurements only. The dynamometer diagram's shape is identical to the conventionally measured ones and the amplitude of the loads follows the measurements.

DOI: 10.14750/ME.2019.010

8 ÖSSZEFOGLALÁS

A himbás-rudazatos mélyszivattyúzás napjaink egyik vezető mesterséges kiemelési technológiája, a mesterséges kiemelési technológiával üzemeltett olajkutak több, mint 75%-a üzemel ezen az elven a világ olajmezőin. Ennek ellenére a kitermelt olaj mennyiségéből sokkal kisebb mértékben részesülnek, mivel az ilyen módon termeltetett kutak nagy része kicsi hozammal termel, ezért az üzemeltetési-, illetve felügyeleti költségek hatványozottan fontosak. A himbás-rudazatos mélyszivattyúzás gazdaságosságát a rendszerben jelen lévő energiafolyam alapvetően meghatározza. Az energia áramlása a villamos motortól indul, a gyakorlatban elterjedt módszerek azonban mégis a mechanikus oldalról közelítik meg a rendszer leírását, a dinamométeres diagramokat alapul véve a rendszerek vizsgálatához. Ezért alapvető célkitűzés volt a himbás-rudazatos mélyszivattyúzás energiaviszonyainak tisztázása, a rendszer üzemének leírása a motor kapcsaitól kezdődően a kitermelt fluidummal bezárólag.

A kutatás a himbás-rudazatos mélyszivattyúzásban használt háromfázisú aszinkron motorok leírásával kezdődött. Kifejlesztettem egy új, empirikus korreláción alapuló leírást a motorok hatásfokának meghatározására a teljes fordulatszám-tartományon. Bebizonyítottam, hogy a motorok paraméter-meghatározására alkalmazott szokványos eljárások nem alkalmazhatóak a nagy szlipű motorokhoz. Jellemzően ezeknél a motoroknál az indítónyomaték a billenőnyomaték, ami nem alkalmazható az optimalizálási eljárás megoldása során korlátozó feltételként. Ezért ehelyett a mágnesezési áram használatát javasoltam, ami himbás-rudazatos mélyszivattyús rendszerek esetén kedvező, hiszen a himbákon üzemeltetett motoroknál a ciklikusan változó terhelés generátoros üzemet is előidéz jó ellensúlyozás esetén, vagyis a mágnesezési áram mérhető. A számítások során bebizonyosodott, hogy a mágnesezési áram kiváló korlátozó feltétel a billenőnyomaték helyett.

Új saját eljárást dolgoztam ki az aszinkron motorok paraméter-meghatározására, CPSO-S algoritmuson alapul optimalizálási eljárással. A metódus 28 nagy szlipű motor jelleggörbéin volt tesztelve, és jó eredményeket adott. A pontos motor modell ismeretében a motor által felvett áramból a tengelyen leadott teljesítményt meghatároztam.

Ahhoz, hogy a motor tengelyén leadott nyomatékból meghatározzuk a simarúdon ébredő terhelés-idő függvényt, vagyis a dinamométer diagramot, még további ismeretek is szükségesek. A hagyományos nyomatékanalízis himbás-rudazatos mélyszivattyúzás esetén elsősorban az ellensúlynyomaték optimalizálására törekszik, ennek megfelelően a nyomaték meghatározási eljárások a simarúd nyomatékot használják kiinduló adatként. Szükséges volt az eljárások vizsgálata és illesztése a másik irányból, vagyis a motortól történő nyomatékszámításhoz. Ezt elvégeztem, és a szakirodalomban elérhető megoldások megfelelő adaptálásával ezt meg is valósítottam.

A végeredmény a simarúd terhelés-idő (esetleg elmozdulás) függvények, melyek már alkalmazhatóak a himbás-rudazatos mélyszivattyúzás üzemállapotának ellenőrzésére. A diagramokat sikeresen meghatároztam, melyek jellege a hagyományos mérési eljárással mért görbékhez hasonló. A terhelés nagyságrendje is hasonló pályán mozog, mint a valódi méréseknél, ezért a mérési eljárás gyakorlati használhatóságát is prezentáltam.

DOI: 10.14750/ME.2019.010

9 PUBLICATIONS PRESENTED IN THE THESIS' TOPIC

9.1 WRITTEN PUBLICATIONS

Á. Koncz: Simple calculation model for performance curves of electric motors used in sucker rod pumping service Doktoranduszok Fóruma: Műszaki Földtudományi Kar section edition. Miskolc, Hungary, 07.10.2013., pp. 51-56.

Á. Koncz: An Improved Prime Mover Parameter Estimation Process For Sucker Rod Pumping Units microCAD 2014, A1 section ENVIRONMENTAL Science: SUSTAINABLE NATIONAL RESOURCES MANAGEMENT SYMPOSIUM. Miskolc, Hungary, 10-11st 10.2014. University of Miskolc, 2014. Paper A/2-9. 8 p. ISBN: 978-963-358-051-6

Á. Koncz: A himbás-rudazatos mélyszivattyús berendezés részhatásfokainak vizsgálata Doktoranduszok Fóruma: Műszaki Földtudományi Kar section edition Miskolc, Hungary, 19-21st 10.2014. pp. 22-27.

G. Takács, L. Kis, Á. Koncz: The calculation of gearbox torque components on sucker-rod pumping units using dynamometer card data JOURNAL OF PETROLEUM EXPLORATION AND PRODUCTION TECHNOLOGIES 172: Paper 10.1007/s13202-015-0172-z. 10 p. (2015)

G. Takács, L. Kis, Á. Koncz: The Use of Dynamometer Data for Calculating the Torsional Load on Sucker-Rod Pumping Units Proceedings of the 62nd Southwestern Petroleum Short Course. Lubbock, USA, 20-23rd 04. 2015.pp. 176-183.

Á. Koncz: Innovative developments in sucker rod pumped well analysis The Publications of the MultiScience - XXIX. microCAD International Multidisciplinary Scientific Conference. Miskolc, Hungary, 09-10th 04.2015. University of Miskolc, 2015. Paper A7. ISBN:978-963-358-061-5

Á. Koncz: Difficulties of a low cost measurement system development for sucker rod pumped well analysis MŰSZAKI FÖLDTUDOMÁNYI KÖZLEMÉNYEK 85:(1) University of Miskolc, 2016.

DOI: 10.14750/ME.2019.010

9.2 Conference presentations, posters

Á. Koncz: Efficiency analysis of sucker rod pumping unit using new techniques East Meets West International Student Petroleum Congress & Career Expo. Kraków, Poland, 22-24th 04.2015. poster

Á. Koncz: Instrument development for sucker rod pumped well analysis, SPE European Regional Student Paper Contest, 2nd of June 2015. Budapest

Á. Koncz: Improvements in stripper well supervision, 31st International Oil and Gas Conference and Exhibition, 5-6th October 2017, Siófok

Á. Koncz: Simple calculation model for performance curves of electric motors used in sucker rod pumping service Doktoranduszok Fóruma Miskolc, Hungary, 07.10.2013.

Á. Koncz: An Improved Prime Mover Parameter Estimation Process For Sucker Rod Pumping Units microCAD 2014, A1 section ENVIRONMENTAL Science: SUSTAINABLE NATIONAL RESOURCES MANAGEMENT SYMPOSIUM. Miskolc, Hungary, 10-11st 10.2014.

Á. Koncz: A himbás-rudazatos mélyszivattyús berendezés részhatásfokainak vizsgálata Doktoranduszok Fóruma Miskolc, Hungary, 19-21st 10.2014.

Á. Koncz: Innovative developments in sucker rod pumped well analysis The Publications of the MultiScience - XXIX. microCAD International Multidisciplinary Scientific Conference. Miskolc, Hungary, 09-10th 04.2015.

Á. Koncz: Difficulties of a low cost measurement system development for sucker rod pumped well analysis Innovative technologies in the fluid production conference, 17th 06. 2015. Miskolc, Hungary

10 ABBREVIATIONS

- flowing bottomhole pressure: FBHP
- static reservoir pressure: SNHP
- loads in the polished rod: PRL
- wellhead pressure: WHP
- Particle Swarm Optimization: PSO
- CPSO-S: cooperative PSO-split
- Fast Fourier Transformation: FFT
- Alternating current: AC
- Direct current: DC
- Root mean square: RMS
- Water-oil ratio: WOR
- Polished rod horse power: PRHP
- Structural unbalance: SU
- constant multiplication factor between the stator- and rotor resistances: k_r
- constant multiplication factor between the stator- and rotor reactance: k_x

11 REFERENCES

Silva, W. L. et al., 2014. *Determining the surface dynamometer card of a pumping system from the torque curve of a three-phase induction motor.* Belo Horizonte, Brasilia, Anais do XX Congresso Brasileiro de Automática.

API, 1988.. *Specification for Pumping Units API Spec. 11E 15th ed..* Washington D.C., USA: API.

Bayoumi, E., 2010.. Parameter estimation of cage induction motors using cooperative bacterial foraging optimization. *Electromotion,* Volume 17, pp. 247-260.

Beckwith, R., 2014.. 155 Years of Artificial Lift. *SPE Journal of Petroleum Technology,* October(SPE-1014-0101-JPT).

Bigler, J. & Heston, S., 2013.. *Energy Efficiency Benefits of Maintaining Proper Belt Tension in an Air Handling Unit.* Fenner Drives white paper: Fenner Drives.

Bommer, P. M. & Podi, A. L., 2012.. *The beam lift handbook.* 1st edition ed. Austin: University of Texas at Austin.

Clerc, M. & Kennedy, J., 2002.. The Particle Swarm - Explosion, Stability, and Convergence in a Multidimensional Complex Space. *IEEE Transactions on Evolutionasy Computation,* 6.(1.), pp. 58-73..

Durham, M. O. & Lockerd, C. R., 1988.. Effect of Cyclic Loading on Motor Efficiency. *IEEE Transactions on Industry Applications,* 24.(6.), pp. 1153-1159..

Eberhardt, R. C. & Kennedy, J., 1995.. *A new optimizer using particle swarm theory.* Proceedings of the Sixth International Symposium on Micro Machine and Human Science held in Nagoya, Japan, IEEE.

Echometer, 2017.. *www.echometer.com.* [Online] Available at: http://echometer.com/products/Wireless/Tabid/145/Default.aspx [Accessed 29. 01. 2017.].

eProduction Solutions Inc., 2014.. *Value of Rod Pump Control TWP-003. Rev. 0..* [Online] Available at: https://www.yumpu.com/en/document/view/8764886/value-of-rod-pump-control-ep-solutionscom
[Accessed 03. 07. 2017.].

Gatheridge, B., 2012.. *Fundamentals of electrical power measurement.* web seminar: Yokogawa Corporation of America.

Gault, R. H., 1987.. Designing a Sucker-Rod Pumping System for Maximum Efficiency. *SPE Production Engineering,* 2.(4.).

Giangacomo, L. A. & Hill, D. R., 1999.. *Optimizing pumping well efficiency with smart fluid-level controller technology.* SPE Mid-Continent Operations Symposium held in Oklahoma City, Oklahoma, USA SPE 52210, SPE.

Gibbs, S. G., 2012.. *Rod pumping: Modern Methods of Design, Diagnosis and Surveillance.* Ashland: BookMasters Inc..

Gibbs, S. G. & Miller, D. L., 1997.. Inferring power consumption and electrical performance from motor speed in oil-well pumping units. *IEEE Transactions on Industry Applications,* 33.(1.).

Graf, R. F., 1999.. *Modern Dictionary of Electronics.* 7th ed. Boston, Oxford, Auckland, Johannesburg, Melbourne, New Delhi: Newnes.
Haque, M. H., 1993. Estimation of three-phase induction motor parameters. *Electric Power Systems Research,* Volume 26, pp. 187-193.
Hubble, E., 2011.. *Maximizing power transmission.* Van Meter Inc. presentation: Van Meter Inc..
Hughes, A., 2006. *Electric Motors and Drives Fundamentals, Types and Applications Third Edition.* Amsterdam, Boston, Heidelberg, London, New York, Oxford, Paris, San Diego, San Fransisco, Singapore, Sydney, Tokyo: Elsevier - Newnes.
Kilgore, J. J. & Tripp, H. A., 1991.. *Walking beam pumping unit system efficiency measurements.* 66th Annual Technical Conference and Exhibition of the Society of Petroleum Engineers held in Dallas, Texas, USA SPE-22788, SPE.
Kis, L., 2013.. *Calculation of the gearbox torque including inertia effects.* Doktoranduszok Fúruma, Miskolc, University of Miskolc.
Kral, C., Haumer, A. & Grabner, C., 2009.. *Consistent Induction Motor Parameters for the Calculation od Partial Load Efficiencies.* World Congress on Egineering, held in London, UK, WCE.
Lindenmeyer, D., Dommel, H., Moshref, A. & Kundur, P., 2001.. An induction motor parameter estimation method. *Elsevier Electrical Power and Energy Systems,* Volume 23., pp. 251-262..
Lufkin Industries Inc., 2015.. *www.lufkin.com.* [Online] Available at: 15. http://www.lufkin.com/index.php/products-a-services/oilfield/automation/beam-pumping-units/rod-pump-controller
[Accessed 28. 01. 2015.].
MCCDAQ Inc., 2014.. *MCCDAQ USB 1608FS-PLUS User's manual.* s.l.:s.n.
McCoy, J. N., 1969.. *Analyzing Well Performance.* 20th Annual Technical Meeting of the Petroleum Society of CIM, held in Edmonton, Alberta, Canada PETSOC-69-04-05, SPE.
McCoy, J. N., 1974.. *Acoustic Velocities for Natural Gas.* SPE-5251-MS: SPE.
McCoy, J. N., Huddleston, K. L. & Drake, B., 1985.. *Acoustic Static Bottomhole Pressures.* SPE Production Operations Symposium, held in Oklahoma City, Oklahoma, USA SPE 13810, SPE.
McCoy, J. N., Rowlan, O. L. & Podio, A. L., 2002.. *Advanced Techniques for Acoustic Liquid Level Determination.* Canadian International Petroleum Conference, held in Calgary, Alberta, Canada PETSOC-2002-153, SPE.
National Instruments, 2014.. *LabView Help.* Labview 2014.: National Instruments.
Neely, A. B., Opal, K. E. & Tripp, H. A., 1989.. *Power savings and load reductions on sucker rod pumping wells.* 64th Annual Technical Conference and Exhibition of the Society of Petroleum Engineers held in San Antonio, Texas, USA SPE-19715-MS, SPE.
NEMA, 2017.. *NEMA MG 10-2017.*. Rosslyn, Virginia: NEMA Standards Publication.
NSWC, 2011.. *Handbook of Reliability Prediction Procedures for Mechnaical Equipment.* Naval Surface Warfare Center Carderock Division, Logistics Technology Support: NSWC.
OMRON, 2009. *Micro Sensing Device Data Book.* Kyoto, Japan: OMRON Industrial Automation Company.

Pedra, J., 2008.. On the Determination of Induction Motor Parameters From Manufacturer Data for Electromagnetic Transient Programs. *IEEE Transactions on Power Systems,* 23.(4.), pp. 1709-1718..

Pedra, J. & Córcoles, F., 2004.. Estimation of induction motor double-cage model parameters from manufacturer data. *IEEE Transactions on Energy Conversion,* 19.(2.).

Podio, A. L., McCoy, J. N. & Collire, F., 1994.. *Analysis of beam pump system efficiency from real-time meassurement of motor power.* III. Latin American/Caribbean Petroleum Engineering Conference, Buenos Aires, SPE.

Puranen, J., 2006. Induction Motor Versus Permanent Magnet Synchronous Motor in Motion Control Applications: a Comparative Study - a PhD Thesis. *Acta Universitatis Lappeenrantaensis,* Volume 249, pp. 1-147..

Rowlan, O. L. & McCoy, J. N., 2007.. *Overview of Beam Pump Operations.* SPE Annual Technical Conference and Exhibition held in Anaheim, California, USA 11-14. November 2007. SPE 110234, SPE.

Sakhtivel, V. P., Bhuvaneswari, R. & Sibramanian, S., 2010.. An improved particle swarm optimization for induction motor parameter determination. *International Journal of Computer Applications,* 1.(2.), pp. 62-67..

SPE, 2015.. *Petrowiki.* [Online] Available at: http://petrowiki.org/Artificial_lift [Accessed 22. 01. 2015.].

Stefopoulos, G. K. & Mliopoulos, A. P. S., 2007.. *numerical Parameter Estimation Procedure for Three Phase Induction Motor Models.* Power Tech Conference, held in Lausanne, Switzerland, IEEE.

Svinos, J. G., 1983.. *Exact kinematic analysis of pumping units.* SPE Annual Technical Conference and Exhibition, held in San Fransisco, California, USA - SPE 012201-MS, SPE.

Takács, G., 2010.. *Ways to obtain optimum power efficiency of artificial lift installations.* SPE Oil and Gas India Conference and Exhibition held in Mumbai, India SPE-126544-MS, SPE.

Takács, G., 2015.. *Sucker-Rod Pumping Handbook.* USA: Elsevier.

Takács, G., Kis, L. & Koncz, Á., 2016.. The calculation of gearbox torque components on sucker-rod pumping units using dynamometer card data. *Journal of Petroleum Exploration and Production Technology,* 6.(1.), pp. 101-110..

Uray, V. & Dr. Szabó, S., 1998. *Elektrotechnika.* Budapest: Nemzeti Tankönyvkiadó Rt..

van den Bergh, F., 2001.. *An Analysis of Particle Swarm Optimizers - a PhD Thesis.* Pretoria: University of Pretoria.

Wikipedia, 2017.. *www.wikipedia.de.* [Online] Available at: https://de.wikipedia.org/wiki/Drehstrom-Asynchronmaschine [Accessed 23. 06. 2017.].

Wilamowsky, B. & Kaynak, O., 2000.. Oil well diagnosis by sensing terminal characteristics of the induction motor. *IEEE Transactions on Insudtrial Eelctronics,* 47.(5.).

DOI: 10.14750/ME.2019.010

12 APPENDICES

12.1 SOURCE CODE OF PARAMETER ESTIMATION FOR NEMA D OR HIGH SLIP MOTORS – METHOD 1.

```
function [ y ] = double_cage_k_arany( U,Pmfl,cosfi,Imagn,nfl,Imind,Mmind,Imfl,kr,kx )
%program a két kalickás motor paramétereinek meghatározására.
%bemenő értékek:  névleges teljesítmény, névleges cos fi, mágnesező áram,
%névleges feszültség. visszatérő értékek:Xs,Xm,Rr
%póluspárszám, hálózati frekvencia meghatározása
kezdoertek=single_cage_v2_rs_nelkul(U,Pmfl,cosfi,Imagn,Imfl,nfl,kr,kx);
fi=acos(cosfi);
Qmfl=(Pmfl/cosfi)*sin(fi);
p=3;
f=60;
omega=2*pi*f;
ns=120*f/(2*p);
sfl=(ns-nfl)/ns;
%szimbolikus változók létrehozása
syms Rr1 Rr2 Xs X1 Xm Rc Isreal Isim Irreal Irim M P Q s I1real I1im I2real I2im Irreal
Irim Zr1real Zr1im Zr2real Zr2im;
%belső kalicka impedanciája
Zr1real=Rr1/s;
Zr1im=X1;
%külső kalicka impedanciája
Zr2real=Rr2/s;
Zr2im=kx*Xs;
%eredő rotor impedancia számítása,rotor impedancia valós és képzetes része:
Zrreal=komplextortvalos(1,0,komplextortvalos(1,0,Zr1real,Zr1im)+komplextortvalos(1,0,
Zr2real,Zr2im),komplextortkepzetes(1,0,Zr1real,Zr1im)+komplextortkepzetes(1,0,Zr2real,
Zr2im));
Zrim=komplextortkepzetes(1,0,komplextortvalos(1,0,Zr1real,Zr1im)+komplextortvalos(1,
0,Zr2real,Zr2im),komplextortkepzetes(1,0,Zr1real,Zr1im)+komplextortkepzetes(1,0,Zr2rea
l,Zr2im));
%mágnesező + vasveszteség eredő számítása
Zmreal=komplextortvalos(1,0,komplextortvalos(1,0,Rc,0)+komplextortvalos(1,0,0,Xm),ko
mplextortkepzetes(1,0,Rc,0)+komplextortkepzetes(1,0,0,Xm));
Zmim=komplextortkepzetes(1,0,komplextortvalos(1,0,Rc,0)+komplextortvalos(1,0,0,Xm),
komplextortkepzetes(1,0,Rc,0)+komplextortkepzetes(1,0,0,Xm));
%párhuzamosan kapcsolt impedanciák eredője
Zrmreal=komplextortvalos(1,0,komplextortvalos(1,0,Zrreal,Zrim)+komplextortvalos(1,0,Z
mreal,Zmim),komplextortkepzetes(1,0,Zrreal,Zrim)+komplextortkepzetes(1,0,Zmreal,Zmi
m));
```

```
Zrmim=komplextortkepzetes(1,0,komplextortvalos(1,0,Zrreal,Zrim)+komplextortvalos(1,0,Zmreal,Zmim),komplextortkepzetes(1,0,Zrreal,Zrim)+komplextortkepzetes(1,0,Zmreal,Zmim));
%komplex feszültség meghatározása Uv=U+0*1i szerint
%sztátor áram számítása
Isreal(Rr1,Rr2,Xm,Xs,Rc,s)=komplextortvalos(U,0,kr*Rr1+Zrmreal,Xs+Zrmim);
Isim(Rr1,Rr2,Xm,Xs,Rc,s)=komplextortkepzetes(U,0,kr*Rr1+Zrmreal,Xs+Zrmim);
%forgórész áram számítása
Irreal(Rr1,Rr2,Xm,Xs,Rc,s)=-komplexszorzasvalos(Isreal,Isim,komplextortvalos(Zmreal,Zmim,Zrreal+Zmreal,Zrim+Zrim),komplextortkepzetes(Zmreal,Zmim,Zrreal+Zmreal,Zrim+Zrim));
Irim(Rr1,Rr2,Xm,Xs,Rc,s)=-komplexszorzaskepzetes(Isreal,Isim,komplextortvalos(Zmreal,Zmim,Zrreal+Zmreal,Zrim+Zrim),komplextortkepzetes(Zmreal,Zmim,Zrreal+Zmreal,Zrim+Zrim));
%belső kalicka áram
I1real=komplexszorzasvalos(Irreal,Irim,komplextortvalos(Zr2real,Zr2im,Zr1real+Zr2real,Zrim+Zr2im),komplextortkepzetes(Zr2real,Zr2im,Zr1real+Zr2real,Zrim+Zr2im));
I1im=komplexszorzaskepzetes(Irreal,Irim,komplextortvalos(Zr2real,Zr2im,Zr1real+Zr2real,Zrim+Zr2im),komplextortkepzetes(Zr2real,Zr2im,Zr1real+Zr2real,Zrim+Zr2im));
%külső kalicka áram
I2real=komplexszorzasvalos(Irreal,Irim,komplextortvalos(Zr1real,Zr1im,Zr1real+Zr2real,Zrim+Zr2im),komplextortkepzetes(Zr1real,Zr1im,Zr1real+Zr2real,Zrim+Zr2im));
I2im=komplexszorzaskepzetes(Irreal,Irim,komplextortvalos(Zr1real,Zr1im,Zr1real+Zr2real,Zrim+Zr2im),komplextortkepzetes(Zr1real,Zr1im,Zr1real+Zr2real,Zrim+Zr2im));
%nyomaték számítása --> 1. egyenlet
M(Rr1,Rr2,X1,Xm,Xs,s)=(3*p/omega)*(((I1real*I1real+I1im*I1im)*(Rr1/s))+((I2real*I2real+I2im*I2im)*(Rr2/s)));
%teljesítmény számítása  --> 2. egyenlet
P(Rr1,Rr2,X1,Xm,Xs,s)=M*(omega/p)*(1-s);
%reaktáns teljesítmény számítása, negatív előjel!!!!  --> 3. egyenlet
Q(Rr1,Rr2,X1,Xm,Xs,s)=3*komplexszorzaskepzetes(U,0,Isreal,-Isim);
sm=0.0000001;
%sztátor áram számítása -->4.egyenlet (mágnesező áram),5. egyenlet (induló)
Ist(Rr1,Rr2,X1,Xm,Xs,s)=sqrt(Isreal*Isreal+Isim*Isim);
%változók kicserélése az fsolve számára használható vektorrá. Egyenletek
%összeállítása: azért kétszer, hogy a kx is behelyettesíthető legyen
%cosfifg(Rr1,Rr2,X1,Xm,Xs,s)=Isreal/Isim;
Pfl1=subs(P,{'Rr1','Rr2','Xm','Xs','X1','Rc','s'},{'(abs(x(1)))','((abs(x(1)))+(abs(x(2))))','(abs(x(3)))','(abs(x(4)))','(kx*abs(x(4))+abs(x(5)))','(abs(x(6)))',sfl});
Qfl1=subs(Q,{'Rr1','Rr2','Xm','Xs','X1','Rc','s'},{'(abs(x(1)))','((abs(x(1)))+(abs(x(2))))','(abs(x(3)))','(abs(x(4)))','(kx*abs(x(4))+abs(x(5)))','(abs(x(6)))',sfl});
Ims1=subs(Ist,{'Rr1','Rr2','Xm','Xs','X1','Rc','s'},{'(abs(x(1)))','((abs(x(1)))+(abs(x(2))))','(abs(x(3)))','(abs(x(4)))','(kx*abs(x(4))+abs(x(5)))','(abs(x(6)))',sm});
```

DOI: 10.14750/ME.2019.010

```
Mind1=subs(M,{'Rr1','Rr2','Xm','Xs','X1','Rc','s'},{'(abs(x(1)))','((abs(x(1)))+(abs(x(2))))','(
abs(x(3)))','(abs(x(4)))','(kx*abs(x(4))+abs(x(5)))','(abs(x(6)))',1});
Iind1=subs(Ist,{'Rr1','Rr2','Xm','Xs','X1','Rc','s'},{'(abs(x(1)))','((abs(x(1)))+(abs(x(2))))','(a
bs(x(3)))','(abs(x(4)))','(kx*abs(x(4))+abs(x(5)))','(abs(x(6)))',1});
Ifl1=subs(Ist,{'Rr1','Rr2','Xm','Xs','X1','Rc','s'},{'(abs(x(1)))','((abs(x(1)))+(abs(x(2))))','(ab
s(x(3)))','(abs(x(4)))','(kx*abs(x(4))+abs(x(5)))','(abs(x(6)))',sfl});
%cosfi1=subs(cosfifg,{'Rr1','Rr2','Xm','Xs','X1','s'},{'(abs(x(1)))','((abs(x(1)))+(abs(x(2))))'
,'(abs(x(3)))','(abs(x(4)))','(kx*abs(x(4))+abs(x(5)))',1});
Pfl=subs(Pfl1,{'kx'},{kx});
Qfl=subs(Qfl1,{'kx'},{kx});
Ims=subs(Ims1,{'kx'},{kx});
Mind=subs(Mind1,{'kx'},{kx});
Iind=subs(Iind1,{'kx'},{kx});
Ifl=subs(Ifl1,{'kx'},{kx});
%cosfih=subs(cosfi1,{'kx'},{kx});
%hibafüggvény előállítása, ezt kell majd minimalizálni
%(cosfimind-cosfih)/cosfimind
hiba0=[(Pmfl-Pfl)/Pmfl;(Qmfl-Qfl)/Qmfl;((Imagn-Ims)/Imagn);((Mmind-
Mind)/Mmind);2*((Imind-Iind)/Imind);((Imfl-Ifl)/Imfl)];
%a vectorize eredményül char-t ad, ezt kell function handle-é alakítani.
hiba1=vectorize(hiba0);
%a hiba1 char típusú változó hosszának meghatározása, hogy a felesleges
%karaktereket törölni lehessen
a=size(hiba1);
%fölösleges elemek törlése
hiba1(a(2))=[];
for z=1:7
   hiba1(1)=[];
end
%a char formátum átalakítása függvényformátummá, hogy az str2func be tudja
%olvasni
hiba2=['@(x) ' hiba1(1:end)];
hiba=str2func(hiba2);
%az optimalizálás kezdőértékének a megadása
x0(1)=kezdoertek(1);
x0(2)=4*(kezdoertek(1));
x0(3)=kezdoertek(2);
x0(4)=kezdoertek(3);
x0(5)=1.2*x0(4)-kx*x0(4);
x0(6)=kezdoertek(4);
options = optimoptions('fsolve','MaxFunEvals',8000,'MaxIter',3000);
[x]=fsolve(hiba,x0,options);
y(1)=abs(x(1));
y(2)=abs(x(1))+abs(x(2));
```

```
y(3)=abs(x(3));
y(4)=abs(x(4));
y(5)=kx*(abs(x(4)))+abs(x(5));
y(6)=abs(x(6));
y(7)=sum(abs(hiba(x)));
end
```

12.2 Source code of parameter estimation for high slip motors using the CPSO-S algorithm

```
Sub CPSO_S_egykalickas()
'program a 7 paraméteres, 5 ismeretlenes Pedra modell számításaira
Dim U, f, Imind, Pmfl, cosfi, Imagn, nfl, mmind, Imfl As Double

'U = InputBox("A következő párbeszádpanelek a motor alapadatait kérik be. Add meg a motor névleges feszültségét![V]", "Adatok beadása", 0)
U = Cells(1, 8)
'Imind = InputBox("Add meg a motor indítási áramát [A]!", "Adatok beadása", 0)
Imind = Cells(2, 8)
'Pmfl = InputBox("Add meg a motor névleges teljesítményét!", "Adatok beadása", 0)
Pmfl = Cells(3, 8)
'cosfi = InputBox("Add meg a motor névleges teljesítménytényezőjét!", "Adatok beadása", 0)
cosfi = Cells(4, 8)
'cosfiind = InputBox("Add meg a motor indukásakor a teljesítménytényezőt!", "Adatok beadása", 0)
cosfiind = Cells(5, 8)
'Imagn = InputBox("Add meg a motor mágnesező áramát)!", "Adatok beadása", 0)
Imagn = Cells(6, 8)
'nfl = InputBox("Add meg a motor névleges fordulatszámát!", "Adatok beadása", 0)
nfl = Cells(7, 8)
'mmind = InputBox("Add meg a motor indulónyomatékát [Nm](ha nem ismert, Nema D motor esetén Mnévleges*2,75)!", "Adatok beadása", 0)
mmind = Cells(8, 8)
'Imfl = InputBox("Add meg a motor névleges áramát!", "Adatok beadása", 0)
Imfl = Cells(9, 8)
'etafl = InputBox("Add meg a motor névleges hatásfokát (tizedes formában, nem százalékkal!)!", "Adatok beadása", 0)
etafl = Cells(10, 8)
p = Cells(11, 8)
f = Cells(12, 8)
Qmfl = Pmfl / cosfi
omega = 2 * 3.14159265358979 * f
ns = 120 * f / (2 * p)
```

DOI: 10.14750/ME.2019.010

```
sfl = (ns - nfl) / ns
'Rr1;Rr2;Xm;Xs;X1
'a változók korlátozó feltételei

ReDim Min(6) As Double
Min(1) = 0.000001
Min(2) = 0.000001
Min(3) = 0.000001

Dim max(6) As Double
max(1) = 1000
max(2) = 1000
max(3) = 100

'PSO változók'
Dim numberparticles As Integer
numberparticles = 50
Dim numberIterations As Double
Dim iteration As Double
' megoladandó feladat dimenziója
Dim Dimenzio As Integer
Dimenzio = 3
Dim bestglobalfitness As Double
bestglobalfitness = 2147483647
'maximális sebesség, ha szükség lenne rá
minV = -0.57
maxV = 0.57
'a swarm változóban lesznek tárolva a PSO adatai. az array megadási módja: (sor,oszlop)
'A változók sorrendje a tömbben, oszlop szerint:Rr1;Rr2;Rc;Xm;Xs;X1
ReDim swarm(numberparticles, Dimenzio) As Double
'saját legjobb pozíció tárolása az új sebesség meghatározása miatt
ReDim personalbest(numberparticles, Dimenzio) As Double
ReDim globalbest(Dimenzio) As Double
'fitness tároló tömb létrehozása
ReDim fitness(numberparticles, Dimenzio) As Double
Dim fg As Double
'kell átmeneti tároló vektor a context vektornak
ReDim bvektor(Dimenzio) As Double
'véletlen első sebesség tárolása
ReDim randomvelocity(numberparticles, Dimenzio), newvelocity(numberparticles, Dimenzio)
'inercia változók megadása. először a kognitív/helyi súlyozás, majd a globális, majd a véletlenszerű
Dim w As Double
```

```
w = 0.72
Dim c1 As Double
c1 = 1.49
Dim c2 As Double
c2 = 1.49
Dim ran1, ran2 As Double
Dim z As Integer
z = 0
'az inicializálás megtörtént, jöhet a PSO maga. A kr és kx értékeket 0,2-ről indítva 1,6-ig 0,2-es
'lépésközökkel kellene meghatározni
For kr = 0.4 To 1.6 Step 0.3
   For kx = 0.3 To 1.8 Step 0.3
      'kezdő érték meghatározása, iránymutatásul az optimalizációhoz. Az ezzel kapott értékek: Rr,Xm,Xs.
      numberIterations = 50000
      iteration = 0
      indulas = alapkezdoertek(Pmfl, U, sfl, cosfi)
      swarm(0, 1) = indulas(0)
      swarm(0, 2) = indulas(1)
      swarm(0, 3) = indulas(2)
      'az első iterációs lépcsőnél ez lesz a bestglobal érték
      For dz = 1 To Dimenzio
         globalbest(dz) = 100
      Next dz
      'a többi elem véletlenszerű legyártása dz=0 ha van kezdőérték
      For dz = 1 To numberparticles
         For dzs = 1 To Dimenzio
            Randomize
            swarm(dz, dzs) = ((max(dzs) - Min(dzs)) * Rnd + Min(dzs))
         Next dzs
      Next dz
      'a personalbest egyelőre a generált érték
      personalbest = swarm
      'ki kell számolni a fitness értékeket, hogy később legyen mihez viszonyítani. A kezdőértékkel számolt értékek alapján megy a context vektor.
      ReDim bvektor(Dimenzio) As Double
      For dz = 0 To numberparticles
         For dzs = 1 To Dimenzio
            bvektor = globalbest
            bvektor(dzs) = swarm(dz, dzs)
            fg = 0
            'segédszámítások
```

```
            nevlertekek = egykalickas_szamitasok(bvektor(1), bvektor(2), bvektor(3), kr, kx, sfl, U, p, omega)
            indertekek = egykalickas_szamitasok(bvektor(1), bvektor(2), bvektor(3), kr, kx, 1, U, p, omega)
            magnertekek = egykalickas_szamitasok(bvektor(1), bvektor(2), bvektor(3), kr, kx, 0.0001, U, p, omega)
            fg = ((nevlertekek(3) - Pmfl) / Pmfl) ^ 2 + ((magnertekek(1) - Imagn) / Imagn) ^ 2 + ((indertekek(1) - Imind) / Imind) ^ 2 + ((nevlertekek(1) - Imfl) / Imfl) ^ 2
            fitness(dz, dzs) = fg
        Next dzs
    Next dz
    bestglobalfitness = fitness(0, 1)
    bestownfitness = fitness
    'véletlen első sebességet kell gyártani, kis értékekkel
    For dz = 1 To numberparticles
        For dzs = 1 To Dimenzio
            Randomize
            randomvelocity(numberparticles, Dimenzio) = Rnd
        Next dzs
    Next dz
    'az aux nevű változók mindig az előző állapot tárolására szolgálnak
    auxvelocity = randomvelocity
    'iterálás programozása
    Do While iteration < numberIterations
        auxposition = swarm
        For dz = 1 To numberparticles
            For dzs = 1 To Dimenzio
                Randomize
                ran1 = Rnd()
                Randomize
                ran2 = Rnd()
                newvelocity(dz, dzs) = (w * auxvelocity(dz, dzs)) + (c1 * ran1 * (personalbest(dz, dzs) - swarm(dz, dzs))) + (c2 * ran2 * (globalbest(dzs) - swarm(dz, dzs)))
                swarm(dz, dzs) = auxposition(dz, dzs) + newvelocity(dz, dzs)
                auxvelocity(dz, dzs) = newvelocity(dz, dzs)
                If swarm(dz, dzs) <= 0 Then
                    swarm(dz, dzs) = 0.000001
                End If
                If swarm(dz, dzs) > 10000 Then
                    swarm(dz, dzs) = 9000
                End If
                bvektor = globalbest
                bvektor(dzs) = swarm(dz, dzs)
                fg = 0
```

```
            'segédszámítások
            nevlertekek = egykalickas_szamitasok(bvektor(1), bvektor(2), bvektor(3), kr, kx, sfl, U, p, omega)
            indertekek = egykalickas_szamitasok(bvektor(1), bvektor(2), bvektor(3), kr, kx, 1, U, p, omega)
            magnertekek = egykalickas_szamitasok(bvektor(1), bvektor(2), bvektor(3), kr, kx, 0.0001, U, p, omega)
            fg = ((nevlertekek(3) - Pmfl) / Pmfl) ^ 2 + ((magnertekek(1) - Imagn) / Imagn) ^ 2 + ((indertekek(1) - Imind) / Imind) ^ 2 + ((nevlertekek(1) - Imfl) / Imfl) ^ 2
            fitness(dz, dzs) = fg
            If fitness(dz, dzs) < bestownfitness(dz, dzs) Then
               bestownfitness(dz, dzs) = fitness(dz, dzs)
               personalbest(dz, dzs) = swarm(dz, dzs)
            End If
            If fitness(dz, dzs) < bestglobalfitness Then
               bestglobalfitness = fitness(dz, dzs)
               globalbest(dzs) = swarm(dz, dzs)
            End If
            iteration = iteration + 1
         Next dzs
      Next dz
   Loop
   Cells(14, 2) = "A módszer számítási eredményei"
   Cells(15, 2) = "kr"
   Cells(16, 2) = "kx"
   Cells(17, 2) = "Rr"
   Cells(18, 2) = "Xm"
   Cells(19, 2) = "Xs"
   'Cells(20, 2) = "Xs"
   'Cells(21, 2) = "X1"
   Cells(22, 2) = "A hibafüggvény minimum értéke:"
   Cells(15, 3 + z) = kr
   Cells(16, 3 + z) = kx
   Cells(17, 3 + z) = globalbest(1)
   Cells(18, 3 + z) = globalbest(2)
   Cells(19, 3 + z) = globalbest(3)
   'Cells(20, 3 + z) = globalbest(4)
   'Cells(21, 3 + z) = globalbest(5) + globalbest(4) / kx
   Cells(22, 3 + z) = bestglobalfitness
   z = z + 1
 Next kx
Next kr

End Sub
```

DOI: 10.14750/ME.2019.010

12.2.1 ADDITIONAL FUNCTIONS USED FOR CPSO-S OPTIMIZATION

```
Function acos(x) As Double

   acos = Atn(-x / Sqr(-x * x + 1)) + 2 * Atn(1)

End Function
Function ketkalickas_7parameteres(Rr1, Rr2, Xm, Xs, X1, kr, kx, s, U, p, omega)

      X2 = Xs * kx
      Rs = kr * Rr1
      'Rotor impedancia:
      Zrreal = (((Rr1 / s) * (Rr2 / s) - X1 * X2) * ((Rr1 / s) + (Rr2 / s)) + (X1 * (Rr2 / s) +
X2 * (Rr1 / s)) * (X1 + X2)) / (((Rr1 / s) + (Rr2 / s)) ^ 2 + (X1 + X2) ^ 2)
      Zrim = ((X1 * (Rr2 / s) + X2 * (Rr1 / s)) * ((Rr1 / s) + (Rr2 / s)) - ((Rr1 / s) * (Rr2 / s)
- X1 * X2) * (X1 + X2)) / (((Rr1 / s) + (Rr2 / s)) ^ 2 + (X1 + X2) ^ 2)
      'Eredő impedancia:
      Zreal = Rs + ((-Xm * Zrim) * (Zrreal) + (Xm * Zrreal) * (Xm + Zrim)) / ((Zrreal) ^ 2
+ (Xm + Zrim) ^ 2)
      Zim = Xs + ((Xm * Zrreal) * (Zrreal) - (-Xm * Zrim) * (Xm + X2)) / ((Zrreal) ^ 2 +
(Xm + Zrim) ^ 2)
      'Sztátor áram: (I=U/Z)
      Isreal = (U * Zreal) / (Zreal * Zreal + Zim * Zim)
      Isim = (-U * Zim) / (Zreal * Zreal + Zim * Zim)
      'Rotor áram:
      Irreal = ((Isreal * 0 - Isim * Xm) * (Zrreal + 0) + (Isim * 0 + Isreal * Xm) * (Zrim +
Xm)) / ((Zrreal + 0) ^ 2 + (Zrim + Xm) ^ 2)
      Irim = ((Isim * 0 + Isreal * Xm) * (Zrreal + 0) - (Isreal * 0 - Isim * Xm) * (Zrim +
Xm)) / ((Zrreal + 0) ^ 2 + (Zrim + Xm) ^ 2)
      '1-es rotor ág árama:
      I1real = ((Irreal * (Rr2 / s) - Irim * X2) * ((Rr1 / s) + (Rr2 / s)) + (Irim * (Rr2 / s) +
Irreal * X2) * (X1 + X2)) / (((Rr1 / s) + (Rr2 / s)) ^ 2 + (X1 + X2) ^ 2)
      I1im = ((Irim * (Rr2 / s) + Irreal * X2) * ((Rr1 / s) + (Rr2 / s)) - (Irreal * (Rr2 / s) -
Irim * X2) * (X1 + X2)) / (((Rr1 / s) + (Rr2 / s)) ^ 2 + (X1 + X2) ^ 2)
      '2-es rotor ág árama:
      I2real = ((Irreal * (Rr1 / s) - Irim * X1) * ((Rr1 / s) + (Rr2 / s)) + (Irim * (Rr1 / s) +
Irreal * X1) * (X1 + X2)) / (((Rr1 / s) + (Rr2 / s)) ^ 2 + (X1 + X2) ^ 2)
      I2im = ((Irim * (Rr1 / s) + Irreal * X1) * ((Rr1 / s) + (Rr2 / s)) - (Irreal * (Rr1 / s) -
Irim * X1) * (X1 + X2)) / (((Rr1 / s) + (Rr2 / s)) ^ 2 + (X1 + X2) ^ 2)

      nyomatek = (3 * p / omega) * (((Rr1 / s * ((I1im) ^ 2 + (I1real) ^ 2)) + (Rr2 / s *
((I2im) ^ 2 + (I2real) ^ 2))))
      I = Sqr(Isreal * Isreal + Isim * Isim)
      reakt_telj = -3 * Isim * U
```

```
teljesitmeny = nyomatek * omega / p * (1 - s)
Dim solution(5) As Double
'Delta connection
solution(1) = I * Sqr(3)
solution(2) = reakt_telj
solution(3) = nyomatek
solution(4) = teljesitmeny
ketkalickas_7parameteres = solution

End Function
```

12.3 SOURCE CODE OF THE DATA ACQUISITION SOFTWARE

12.3.1 INPUT SELECTION, DAQ TIMING SECTION

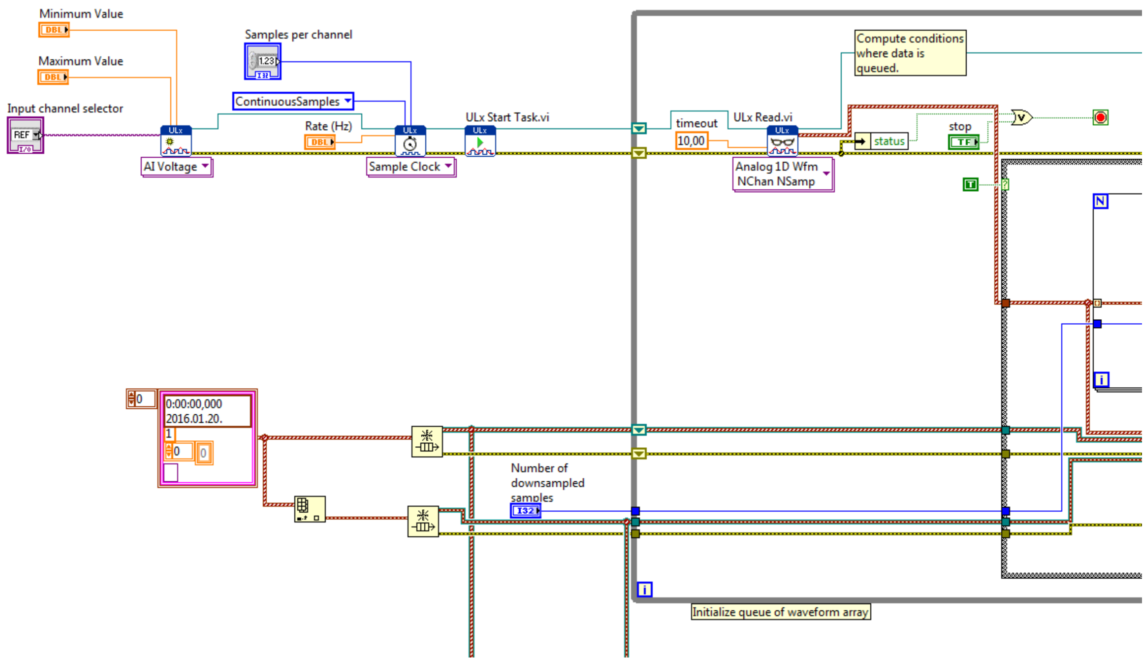

12.3.2 Downsampling, queue initialization

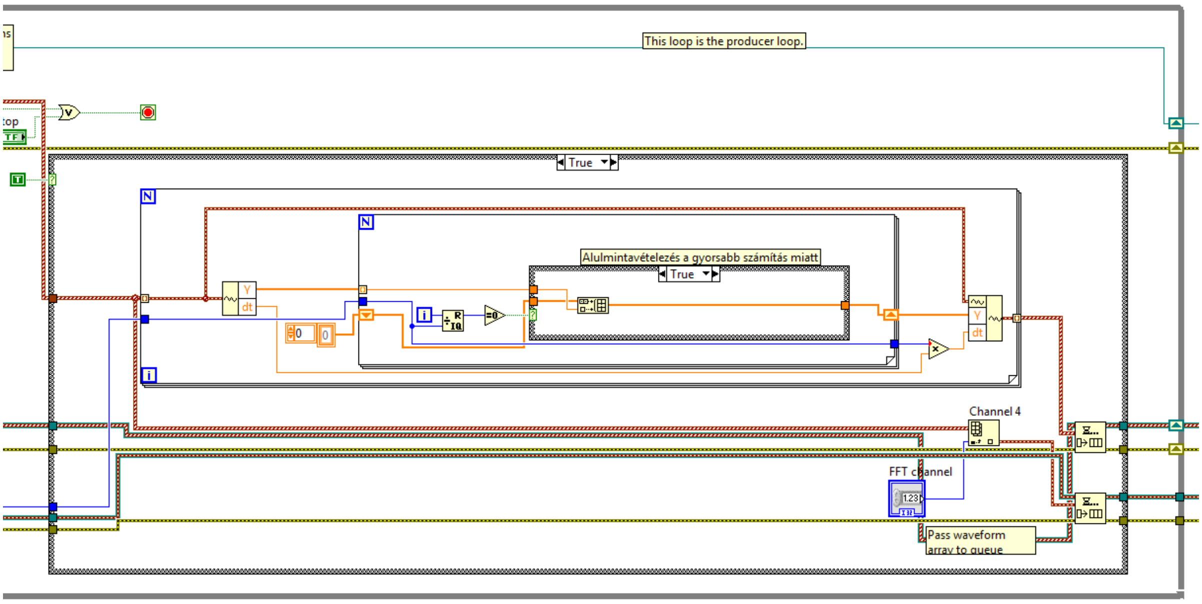

12.3.3 Main consumer loops: low speed and high-speed loops

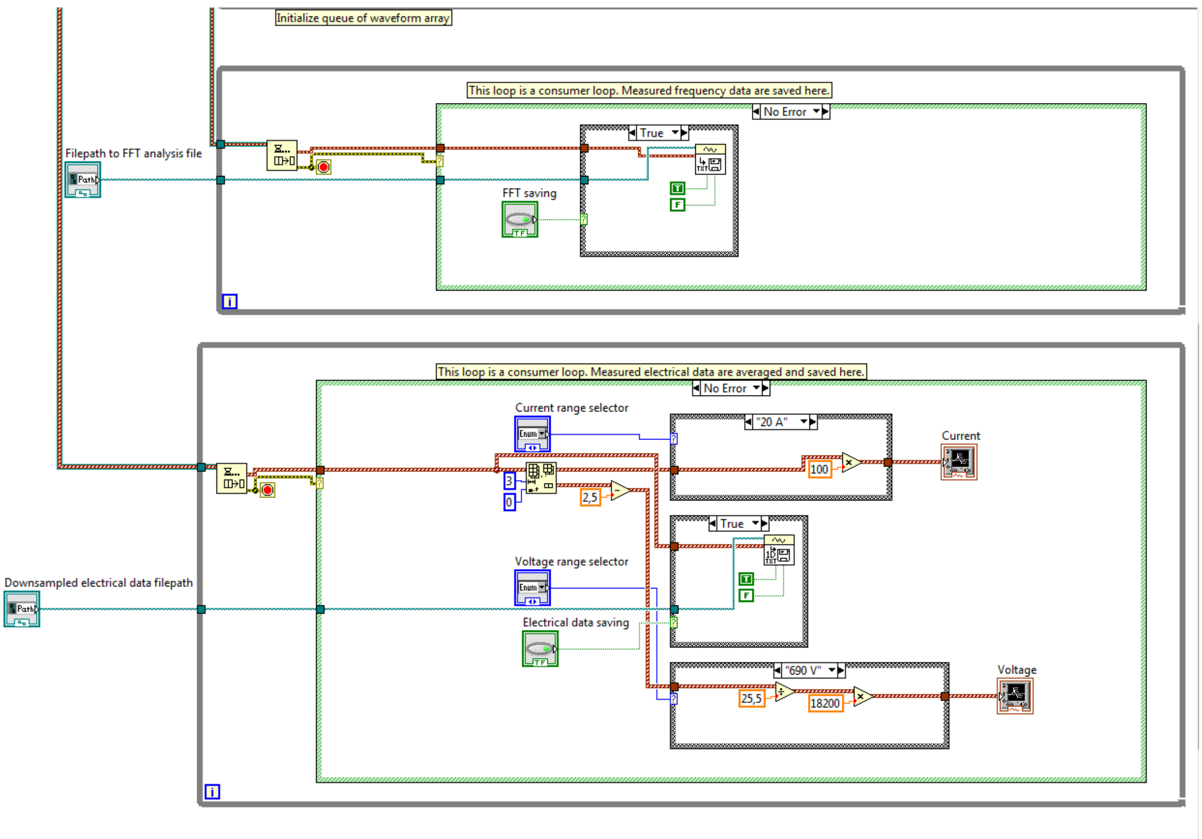

12.3.4 DAQ SOFTWARE CONTROL PANEL

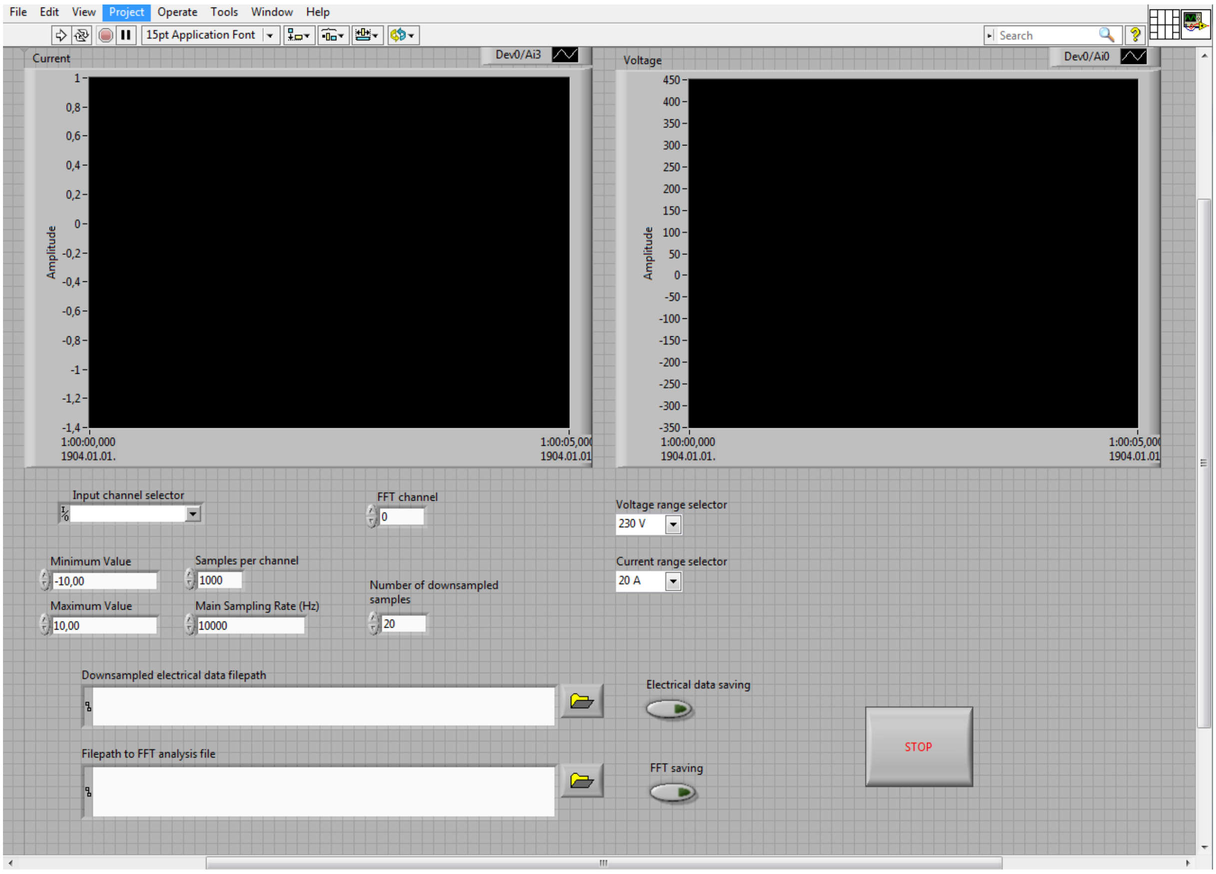

DOI: 10.14750/ME.2019.010

12.4 Source code of data processing algorithm

```
Sub Measurement_analysis()

' Keyboard shortcut: Ctrl+m


'Basic input data. They are needed for the further analysis

    Dim n, srate, rmsrate As Integer

    Dim connectiontype As String

    n = Cells(9, 11)

    srate = Cells(10, 11)

    connectiontype = Cells(11, 11)

    rmsrate = Cells(12, 11)

'reading voltage and current constants

    Dim uconst, iconst As Double

    uconst = Cells(2, 11)

    iconst = Cells(3, 11)


'Data reading

    Dim rawdata() As Variant

    rawdata() = Range(Cells(2, 2), Cells(1 + n, 9))


'Voltage & current waveform conditioning. The DC offset should be removed from the Voltage measurement results because of the

'sensor's behavoiur. The current sensor is equipped with DC removing feature however the software will do it as well.

'The DC offset will be determined based on the user defined number of measured data, using the DC

'component of an FFT analysis. The sensor constants will be apllied in this section as well

    Dim k As Integer
```

```
    Dim offset  As Double

    ReDim acdata(1 To n, 1 To 6) As Variant

    k = InputBox("Number of elements involved in the FFT analysis:", "Measurement
analysis data input", 0)

    Dim FFT() As Variant

    ReDim FFTstore(1 To k, 1 To 6) As Variant

    For i = 1 To 6

'original data will be used for the FFT

'FFT analysis

        Application.Run "ATPVBAEN.XLAM!Fourier", ActiveSheet.Range(Cells(2, 1 + i),
Cells(1 + k, 1 + i)) _

        , Cells(1, 50), False, False

'Data should be read from the storage place

        FFT() = Range(Cells(1, 50), Cells(1 + k, 50))

'offset equals the 0 Hz component divided by the element number

        offset = FFT(1, 1) / k

'FFT results will be stored for future usage

        For j = 1 To k

            FFTstore(j, i) = FFT(j, 1)

        Next j 'measured data correction, applying sensor constant as well

        If i < 4 Then

            For j = 1 To n

                acdata(j, i) = (rawdata(j, i) - offset) * uconst

            Next j

        Else

'Current waveform conditioning. Sensor constant wil be used.acdata stores the Voltage and
Amperage data.

            For j = 1 To n
```

```
            acdata(j, i) = (rawdata(j, i) - offset) * iconst
            Next j
        End If
'temporary stored cells cleaning
        Range(Cells(1, 50), Cells(1 + k, 50)).Clear
    Next i


'power calculation methods for different network connections. Three Wattmeter method is used for Wye connection.
    If connectiontype = "WYE" Then
    '----------------------WYE Connection----------------------------------
'Voltage and current RMS calculation taking into account the desired rate.
'Cycle length determination
        Dim cycle As Integer
        cycle = srate / rmsrate
'number of RMS values
        Dim analyzedpoints As Integer
        analyzedpoints = n \ cycle
'RMS determination
        Dim sum As Double
        ReDim rms(1 To analyzedpoints, 1 To 6) As Variant
        For i = 1 To analyzedpoints     'performing RMS calculation for all analyzed point result
            For j = 1 To 6              'number of channels (columns in acdata) for RMS calculation
                sum = 0
                For k = 1 To cycle      'for the cycle averaging
                    sum = sum + acdata((i - 1) * cycle + k, j) ^ 2
```

```
            Next k
            rms(i, j) = Sqr(sum / cycle)
        Next j
    Next i
'Apparent power calculation in WYE connection
    ReDim q(1 To analyzedpoints, 3) As Double
    For i = 1 To analyzedpoints
        For j = 1 To 3
            q(i, j) = rms(i, j) * rms(i, j + 3)
        Next j
    Next i
'Real (instantaneous) power calculation in WYE connection
    ReDim p(1 To analyzedpoints, 3) As Double
    For i = 1 To analyzedpoints
        For j = 1 To 3
            sum1 = 0
            For k = 1 To cycle
                sum1 = sum1 + acdata((i - 1) * cycle + k, j) * acdata((i - 1) * cycle + k, j + 3)
            Next k
            p(i, j) = -sum1 / cycle
        Next j
    Next i
'Power factor calulation
    ReDim PF(1 To analyzedpoints, 3) As Double
    For i = 1 To analyzedpoints
        For j = 1 To 3
            PF(i, j) = p(i, j) / q(i, j)
```

```
        Next j
    Next i
'Time will be calculated in the worksheet using the t0 value and the new frequency
(rmsrate)
'Display the calculated data. First conditioned AC data.
    For i = 1 To n
        For j = 1 To 6
            Cells(i + 1, 11 + j) = acdata(i, j)
        Next j
    Next i
'RMS values
    For i = 1 To analyzedpoints
        For j = 1 To 6
            Cells(i + 1, 19 + j) = rms(i, j)
        Next j
    Next i
'power & power factor values per phase
    For i = 1 To analyzedpoints
        For j = 1 To 3
            Cells(i + 1, 25 + j) = p(i, j)
            Cells(i + 1, 28 + j) = q(i, j)
            Cells(i + 1, 31 + j) = PF(i, j)
        Next j
    Next i
'3-phase data
    ReDim p3phase(analyzedpoints, 1), q3phase(analyzedpoints, 1),
PF3phase(analyzedpoints, 1) As Variant
    For i = 1 To analyzedpoints
```

```
            p3phase(i, 1) = p(i, 1) + p(i, 2) + p(i, 3)
            q3phase(i, 1) = q(i, 1) + q(i, 2) + q(i, 3)
            PF3phase(i, 1) = (PF(i, 1) + PF(i, 2) + PF(i, 3)) / 3
            Cells(i + 1, 35) = p3phase(i, 1)
            Cells(i + 1, 36) = q3phase(i, 1)
            Cells(i + 1, 37) = PF3phase(i, 1)
        Next i
    Else
        '------------------------DELTA connection ----------------------------
'Two Wattmeter method will be used for the calculation.
'Line Voltage should be calculate. Line3 will be used as the common reference.
'Voltage and current RMS calculation takes into account the desired rate.
'Cycle length determination
        cycle = srate / rmsrate
'number of RMS values
        analyzedpoints = n \ cycle
'Line Voltage determination
        ReDim acdatadelta(1 To n, 1 To 4) As Variant
        For i = 1 To n
            acdatadelta(i, 1) = acdata(i, 1)
            acdatadelta(i, 2) = acdata(i, 2)
            acdatadelta(i, 3) = acdata(i, 4)
            acdatadelta(i, 4) = acdata(i, 5)
        Next i
'RMS determination
        ReDim rms(1 To analyzedpoints, 1 To 4) As Variant
```

DOI: 10.14750/ME.2019.010

```
        For i = 1 To analyzedpoints     'performing Voltage + current RMS calculation for all
analyzed point result
          For j = 1 To 4              'number of channels (columns in acdata) for RMS
calculation
            sum = 0
            For k = 1 To cycle      'for the cycle averaging
              sum = sum + acdatadelta((i - 1) * cycle + k, j) ^ 2
            Next k
            rms(i, j) = Sqr(sum / cycle)
          Next j
        Next i
'Apparent power calculation in DELTA connection
        ReDim q(1 To analyzedpoints, 2) As Double
        For i = 1 To analyzedpoints
          For j = 1 To 2
            q(i, j) = Sqr(3) / 2 * rms(i, j) * rms(i, j + 2)
          Next j
        Next i
'Real (instantaneous) power calculation in DELTA connection
        ReDim p(1 To analyzedpoints, 2) As Double
        For i = 1 To analyzedpoints
          For j = 1 To 2
            sum1 = 0
            For k = 1 To cycle
              sum1 = sum1 + (acdatadelta((i - 1) * cycle + k, j)) * acdatadelta((i - 1) * cycle
+ k, j + 2)
            Next k
            p(i, j) = -sum1 / cycle
```

```
        Next j
    Next i
'Power factor calulation
    ReDim PF(1 To analyzedpoints, 2) As Double
    For i = 1 To analyzedpoints
        For j = 1 To 2
            PF(i, j) = p(i, j) / q(i, j)
        Next j
    Next i
'Time will be calculated in the worksheet using the t0 value and the new frequency
(rmsrate)
'Display the calculated data. First conditioned AC data.
    For i = 1 To n
        For j = 1 To 6
            Cells(i + 1, 11 + j) = acdata(i, j)
        Next j
    Next i
'RMS values
    For i = 1 To analyzedpoints
        For j = 1 To 2
            Cells(i + 1, 19 + j) = rms(i, j)
            Cells(i + 1, 22 + j) = rms(i, j + 2)
        Next j
    Next i
'power & power factor values per phase
    For i = 1 To analyzedpoints
        For j = 1 To 2
```

```
            Cells(i + 1, 25 + j) = p(i, j)
            Cells(i + 1, 28 + j) = q(i, j)
            Cells(i + 1, 31 + j) = PF(i, j)
        Next j
    Next i
'3-phase data
    ReDim p3phase(analyzedpoints, 1), q3phase(analyzedpoints, 1),
PF3phase(analyzedpoints, 1) As Variant
    For i = 1 To analyzedpoints
        p3phase(i, 1) = p(i, 1) + p(i, 2)
        q3phase(i, 1) = q(i, 1) + q(i, 2)
        PF3phase(i, 1) = (PF(i, 1) + PF(i, 2)) / 2
        Cells(i + 1, 35) = p3phase(i, 1)
        Cells(i + 1, 36) = q3phase(i, 1)
        Cells(i + 1, 37) = PF3phase(i, 1)
    Next i
  End If
'--------------------------Speed determination section.-----------------------------------------
'First convert Voltage to boolen variables.
  ReDim speedboolen(1 To n, 1 To 2) As Integer
  For i = 1 To n
    For j = 1 To 2
        If rawdata(i, 6 + j) > 1.5 Then
            speedboolen(i, j) = 1
            Else
            speedboolen(i, j) = 0
        End If
```

```
    Next j
  Next i
'Count the status changing points & store the actual indexes, different for the two channels
  ReDim indexstore1(1 To n, 1 To 1) As Variant
  ReDim indexstore2(1 To n, 1 To 1) As Variant
  Dim aux As Double
  aux = 1
  For i = 1 To n - 1
    If speedboolen(i, 1) = speedboolen(i + 1, 1) Then      'channel 7 calculation
    Else
      indexstore1(aux, 1) = i + 1
      aux = aux + 1
    End If
  Next i
  aux = 1
  For i = 1 To n - 1
    If speedboolen(i, 2) = speedboolen(i + 1, 2) Then      'channel 8 calculation
    Else
      indexstore2(aux, 1) = i + 1
      aux = aux + 1
    End If
  Next i
'Removing empty elements from the array and index number determination for the
variables
  Dim numb1, numb2 As Integer
  numb1 = numb2 = 0
  For i = 1 To n
```

```
        If IsEmpty(indexstore1(i, 1)) = False Then
            numb1 = numb1 + 1
        End If
        If IsEmpty(indexstore2(i, 1)) = False Then
            numb2 = numb2 + 1
        End If
    Next i
    ReDim newindexstore1(1 To numb1, 1) As Variant
    ReDim newindexstore2(1 To numb2, 1) As Variant
    For i = 1 To numb1
        newindexstore1(i, 1) = indexstore1(i, 1)
    Next i
    For i = 1 To numb2
        newindexstore2(i, 1) = indexstore2(i, 1)
    Next i
'Time difference determination between sensing points and conversation into revolution/minute
'The speed data are stored in an array having a dimension equal to the original measured point number.
'Array elements between sensing points will be the next available speed measurement result
'---------------------------For channel 7:-------------------------------------------
    ReDim speed1(numb1) As Variant
    ReDim speed2(numb2) As Variant
    ReDim interspeed1(n, 1) As Variant
    For i = 1 To numb1 / 2 - 2
        If i = 1 Then               'speed value is 0 till the first detection
            For j = 1 To newindexstore1(1, 1)
```

```
            interspeed1(j, 1) = 0
         Next j
      End If
      speed1(i) = 60 / (((newindexstore1(2 * i + 1, 1) + newindexstore1(2 * i + 2, 1)) / 2 -
(newindexstore1(2 * i, 1) + newindexstore1(2 * i - 1, 1)) / 2) * 1 / srate)
      For j = newindexstore1(2 * i - 1, 1) To newindexstore1(2 * i + 1, 1)
         interspeed1(j, 1) = speed1(i)
      Next j
   Next i
'The calculated speed values should be adopted to the RMS time points. The speed will be
the avarerage speed in the given cycle
   ReDim finalspeed1(n, 1) As Variant
   For i = 1 To analyzedpoints
      sum = 0
      For k = 1 To cycle      'for the cycle averaging
         sum = sum + interspeed1((i - 1) * cycle + k, 1)
      Next k
      finalspeed1(i, 1) = sum / cycle
   Next I         '---------------------------For channel 8:-----------------------------------------
   ReDim interspeed2(n, 1) As Variant
   For i = 1 To numb2 / 2 - 2
      If i = 1 Then             'speed value is 0 till the first detection
         For j = 1 To newindexstore2(1, 1)
            interspeed2(j, 1) = 0
         Next j
      End If
      speed2(i) = 60 / (((newindexstore2(2 * i + 1, 1) + newindexstore2(2 * i + 2, 1)) / 2 -
(newindexstore2(2 * i, 1) - newindexstore2(2 * i - 1, 1)) / 2) * 1 / srate)
```

```
        For j = newindexstore2(2 * i - 1, 1) To newindexstore2(2 * i + 1, 1)
            interspeed2(j, 1) = speed2(i)
        Next j
    Next i
'The calculated speed values should be adopted to the RMS time points. The speed will be the avarerage speed in the given cycle
    ReDim finalspeed2(n, 1) As Variant
    For i = 1 To analyzedpoints
        sum = 0
        For k = 1 To cycle      'for the cycle averaging
            sum = sum + interspeed2((i - 1) * cycle + k, 1)
        Next k
        finalspeed2(i, 1) = sum / cycle
    Next i
'data output to spreadsheet
        For i = 1 To analyzedpoints
            Cells(i + 1, 38) = finalspeed1(i, 1)
            Cells(i + 1, 39) = finalspeed2(i, 1)
        Next i
End Sub
```